CHALMERS

Assessing vibrational behavior of uncertain dynamic systems

Master of Science Thesis in the International Master's Programme Sound and Vibration

ANDERS LINDBERG

Department of Civil and Environmental Engineering
Division of Applied Acoustics
Vibroacoustics Group
CHALMERS UNIVERSITY OF TECHNOLOGY
Göteborg, Sweden 2010
Master's Thesis 2010:150

MASTER'S THESIS 2010:150

Assessing vibrational behavior of uncertain dynamic systems

Anders Lindberg

Department of Civil and Environmental Engineering
Division of Applied Acoustics, Vibroacoustics Group
CHALMERS UNIVERSITY OF TECHNOLOGY
Göteborg, Sweden 2010

Assessing vibrational behavior of uncertain dynamic systems

© Anders Lindberg 2009-2010
Supervisor Patrik Andersson, Applied Acoustics

Master's Thesis 2010:150

Department of Civil and Environmental Engineering
Division of Applied Acoustics, Vibroacoustics Group
Chalmers University of Technology
SE-41296 Göteborg
Sweden

Tel. +46-(0)31 772 1000

Reproservice / Department of Civil and Environmental Engineering
Göteborg, Sweden 2010

Abstract

Inherent uncertainty causes dynamic response of apparent identical structures to differ. In industrial applications discrepancies have been demonstrated for automotive vehicles. The solution is to evaluate design robustness and worst-case response, which demands that modeling and data uncertainties are incorporated. The emphasize of this thesis is on simple dynamic systems exposed to different amounts of global and local endogenous uncertainty.

To investigate structural uncertainty a traveling wave model was developed. Subsystems, were steady-state longitudinal motion occur, are modeled as piecewise homogeneous beams. Material, geometrical and boundary properties were assigned by statistical distributions or stochastic processes. Especially, Markov jump processes were used to generate local perturbations and an uniform distribution was used to generate global properties. Subsystem couplings were modeled by a spring impedance.

The results show that global uncertainty causes shifting and scaling of individual modes which impact the low-frequency response, the observed effects conform to response changes of a mass-spring system for the fundamental resonance in a homogeneous longitudinal rod. As the wavelength shortens phenomena related to local uncertainty, which is primarily due to partition impedance mismatch, are pronounced. Consequently; response discrepancies at high-frequencies compared to the nominal behavior is observed. A hypothesis is that localization and non-sinusoidal mode shapes can explain these results; however confirmation of this hypothesis demands further work, and is beyond the scope of this work.

Effects of varies kind and magnitude of uncertainty have been demonstrated. The model indicate that material and geometrical endogenous uncertainty has a large influence on overall system response.

Keywords: Linear time-invariant stochastic systems, disordered subsystems, local and global uncertainty, endogenous uncertainty, structural uncertainty, wave approach, jump processes, longitudinal wave propagation

Acknowledgments

I am grateful for the privilege to study at Chalmers and to all students and student organizations that made my five years in Göteborg enjoyable. Especially, I would want to thank those who studied the master's programme Sound and Vibration with me as well as the student organization and members of VIRUS.

I would like to thank the staff at the division of Applied Acoustics for all help and encouragement. I would not have managed my master's degree without my supervisor whom supported me when the project went poorly and allowed me too proceed in my own way; thank you Patrik.

Finally, I would like to thank my family and friends for all support.

Notation and abbreviations

Due to this thesis interdisciplinary nature and in order to get coherent equations are custom notation used. Complex variables are written as $z = z' + \mathrm{j}z''$ where $z' = \Re\{z\}$, $z'' = \Im\{z\}$ and $\mathrm{j} = \sqrt{-1}$. Conjugate is written $\bar{z}$, magnitude is denoted as $|z|$ and argument as $\angle z$. Exponential functions are denoted $\mathrm{e}^{\mathrm{j}\Phi}$. Vector quantities are represented with a tilde $\underset{\sim}{a}$, matrices with bold letters $\mathbf{X}$ and transposes with T as in $\mathbf{X}^{\mathrm{T}}$. An element of a matrix can be expressed as $(1,2) = X_{12}$ which refers to the first row and second column of $\mathbf{X}$ with a value X_{12}. A filtration of a stochastic process are written as $\mathcal{F}^n = \{\Phi_i : i = 1, \ldots, n\}$ and can be described by expectancy $E(\Phi)$, variance $V(\Phi)$, observed average $\langle\Phi\rangle$, observed smallest value $m(\Phi)$ and observed largest value $M(\Phi)$. Consider a number of independent observations $\mathbb{F}^m = \{\mathcal{F}_1, \ldots, \mathcal{F}_m\}$. This allows considerations largest of largest values $M(M(\mathbb{F}^m))$ and average of largest values $\langle M(\mathbb{F}^m)\rangle$. An uniformly distributed random variate between $\{-1, +1\}$ is denoted U.

Abbreviations

FEA	Finite element analysis
FRF	Frequency response function
iid	Independent and identically distributed
MC	Monte Carlo
SEA	Statistical energy analysis

Notation

Greek Upper-Case Letters.

Δ	Jump
Δ_e	Jump direction
Δ_M	Magnitude of largest jump
Δ_w	Jump weight
Ξ	Magnitude of uncertainty
Ω	Spectrum
Π	Power
Π^{diss}	Dissipated power
Π^{in}	Excitation power

Φ Extremal value
Ψ Expectancy function

Greek Lower-Case Letters.

α, β Beta distribution parameter
γ Smoothness parameter
ϵ Strain
ϵ Perturbation function
ζ Jump constrain
η Loss-factor
$\overleftrightsquigarrow{\eta}$ Coupling loss-factor
λ Wavelength
ξ Material or geometrical parameter
ρ Density
σ Tensile stress
ω Angular frequency

Latin Upper-Case Letters.

$\underset{\sim}{\mathrm{B}}$ Boundary values
E Young's modulus
F Longitudinal force
$\overleftrightsquigarrow{\mathrm{F}}$ Coupling force
F^{in} Excitation force
$\mathbb{H}$ Structural ensemble
$\mathcal{H}$ Structural system
L Complex Young's modulus
N Modal density
$\mathcal{O}$ Vibrational measure
S Cross-section surface
U Uniform random variete
$\mathcal{W}$ Subsystem
$\mathbf{X}$ Linear system matrix
Y Mobility
Z Characteristic impedance
$\overleftrightsquigarrow{\mathrm{Z}}$ Coupling impedance
$\overleftrightsquigarrow{\mathcal{Z}}$ Junction

Latin Lower-Case Letters.

$\underset{\sim}{\mathrm{a}}$ Wave amplitudes
d Displacement

f Frequency
f_0 Fundamental frequency
g General pointer
gg General pointer
h Cross-section height
i Pointer to subsystem partition
ii Pointer to subsystem
j Imaginary unit
k Wavenumber
l Length
n Number of segments
p Junction position
$\overleftrightsquigarrow{r}$ Damper
$\overleftrightsquigarrow{s}$ Spring
t Time
u Longitudinal speed
w Cross-section width
x Spatial coordinate

Script Upper-Case Letters.

$\mathbb{C}$ Complex domain
$\mathbb{R}$ Real domain

Contents

Part 1

A Priori

CHAPTER 1

Introduction

During the past 50 years has research around statistical energy analysis (SEA) or statistical prediction models focused on ensemble average response of complex structures. On the other hand has little concern been given to prediction of extremal response, needed in order to properly understand vibrational behavior of complex systems where uncertainty cause severe response differences or where similar parts share eigenspace. Furthermore; design engineers can be expected to be interested in how robust a structure is to uncertainty.

1. Background

Modern analysis of complex structures rely on numerical procedures which demand large and fast computational resources capable of solving detailed modeling of physical structures. In principle can numerical deterministic models, such as finite element analysis (FEA), be used to analyze high frequency vibration response of uncertain systems using Monte Carlo (MC) approaches. However; it is neither practical nor economically feasible as computational demand increase rapidly with geometric and material complexity, as well as frequency resolution. Further on requires such approaches knowledge of the unavoidable uncertainty of precise dynamic properties; for example damping distribution and boundary conditions. Deterministic models are often tuned against one realization from a statistical ensemble, causing deviation from other structures. In reality, nominally identical structures are observed to differ by large margins. [**1, 2**]

Analytical methods for vibration prediction, such as traveling wave or modal approach, is based on a deterministic view where structural properties are considered to be known. As uncertainty are pronounced for high frequencies, when the wavelength shortens and gets in the order of geometrical or material defects, can such models describe only low-frequency response. [**2**]

To increase robustness of high-frequency vibration prediction where statistical energy analysis (SEA) which depend only on a minimum description of a system, such as total subsystem energy, derived. One of the fundamental ideas are that the relative magnitude and phase of a frequency response at a given point of a subsystem are unpredictable; one should treat them as random quantities. In other words are no information of spatial distribution of response variables, or the

parameters them self, necessary. As long as radiation efficiency is weak can in-vacuo conditions be used to derive wave intensity distributions or energy density. Another assumption of energy-conservative couplings result in that SEA can be used as an estimate of worst-case structural response. [**2**]

The simplicity of SEA causes deviation when subsystems are similar or tonal excitation is considered. Even worse is system failure, or malfunction, due to excessive local response and not global response characteristics which SEA cannot predict. Another example where SEA is not applicable is highly damped structures which do not have uniformly distributed energy density. [**2**]

Contrary to SEA, which predicts ensemble average behavior, is the concern of this thesis extremal response of dynamic systems in the low- and midfrequency range. The aim was formulated as a hypothesis, which state: small-scale random imperfections of large-scale system properties explains the largest response of dynamic systems. This statement is the underlying premise of this work. Also, imperfection cause deviation between measurements and prediction models which neglect geometrical, material, and boundary uncertainty. In order to investigate extremal behavior was a traveling wave approach which accounts for small-scale random imperfections developed.

2. Aim

The primary aim of this thesis is to investigate a hypothesis 1; which state that small-scale uncertainty explains extremal response of systems. A secondary goal is to provide the reader with understanding of how uncertainty influence vibrational response of a dynamic system; however, the discussion is based around how different kind of uncertainty compare to each other rather then to develop an model for extremal response or precise dynamical properties of uncertain systems. Emphasize is on dynamic systems which consists of one freely suspended or two spring coupled self-similar (not identical) subsystems.

HYPOTHESIS 1. *Inherent uncertainty of small-scale properties of large-scale structures or structural parts explain extremal dynamic response.*

3. Delimitation

This master's thesis is concerned explicitly with linear time-invariant systems where one-dimensional quasilongitudinal motion occur. Subsystems are considered to be of finite dimensions, linear-elastic materials, rectangular cross-sections and disordered; where the word "disordered" indicate stochastic and spatial variant properties. A traveling wave approach is used to describe the motion in each subsystem which are coupled by impedance junctions. Subsystems are excited by

a point time-harmonic force. In-vacuo condition is assumed so no energy is radiated. Finally; junction, material and geometrical uncertainty are modeled by jump processes and uniform distributions.

4. Outline

The first part, A Priori, concerns classification, modeling and impact of structural uncertainty. It is followed by a second part, Modeling, which uses a traveling wave approach developed for the purpose of investigating power flow between and vibrational behavior of uncertain dynamic systems. A third part, Findings, presents different numerical cases which where investigated and analyzes obtained results. The final and fourth part, A Posteriori, discusses and concludes on the result and gives some ideas of future work.

CHAPTER 2

Structural uncertainty

Research on uncertainty has different purposes; which can be generalized into a few distinct groups. Those are strategies to classify uncertainty, cope with uncertainty, modeling of uncertainty and numerical or experimental validation. During design are strategies for reducing effect, economical or functional, of uncertainty important. Strategies rely on underlying assumptions of inherent structural properties, which phenomena should be considered or neglected. In order to achieve a strategy for structural analysis with confidence on the outcome has different parameter uncertainty to be classified. Attempt of modeling uncertainty can be carried out once the interesting phenomena has been selected. Once the model is setup are numerical or experimental validation necessary.

1. Classification

There are four distinct groups of uncertainty. Uncertainty from within a system is said to be endogenous. An example could be the fluctuation of Young's modulus or phase speed along a waveguide. The opposite are changes from the outside, exogenous. This could be effects from random loads, such as wind, or electromagnetic noise disturbing signal cables, which are unexplained or outside of the model. Uncertainty due to incomplete knowledge or ignorance of phenomena is called epistemic from Greek episteme which means knowledge. Uncertainty due to the inherent randomness of phenomena is called aleatory which comes from Latin alea which means throwing a dice. [**3**]

2. Strategies

Takewaki et al. proposed a design strategy for earthquake safe construction. For such models is uncertainty of structural parameters and uncertainty of ground motion necessary to take into account simultaneously. This can be done by info-gap robustness analysis. It is based on the assumption that an optimized functional performance of a building corresponds to minimized robustness in regards to uncertainty. Parameters should be considered by satisfying and not minimizing cost functions; which depend on dynamical properties by operating on transfer functions. Robustness can then be defined as the error between a nominal design transfer function and a model which incorporates uncertainty. An info-gap

model for uncertainty of dynamic behavior of a structure is the unbounded family of structural ensembles which satisfies all cost functions, given an amount of uncertainty. An interesting conclusion of this is that there is no worst-case structural response, only satisfying or non-satisfying models. [**4**]

Donders et al. studied how an envelope of an uncertain dynamic response can be modeled by the short transformation method. Deterministic FEM models are limited by the fact that most parameters are not known, which should be incorporated in the model by e.g. fuzzy logic. A numerical method based on the α-sublevel method was carried out to compute uncertain transfer functions. It was stated that uncertain parameters with global effect on response characteristics have monotonic dependency on frequency of resonances at best, while response levels does not depend on the input in similar fashion. Combinatorics where parameters are assigned either the minimal or maximal allowed value was used to construct the fuzzy FRF. Different fuzzy parameter membership functions where used, truncated Gaussian and triangle. The method was validated using Monte Carlo data for a FE model, and fuzzy representation of the FE models FRF. A response envelope with generally good compliance was demonstrated, although the model was computationally costly. [**5**]

3. Modeling

Structural uncertainty can be observed at large-scale and/or small-scale structural details. A parameter subjected to uncertainty can therefore be thought of in terms of global uncertainty, e.g. a distribution of expected behavior, and local uncertainty, e.g. small-scale variation of the expected behavior. Homogeneous models can be made uncertain by assigning parameters from statistical distributions, which incorporates global uncertainty. Heterogeneous models allow both large-scale differences of a parameter and small-scale spatial fluctuations, albeit being more mathematical and numerical cumbersome. It is not known if the uncertainty is aleatory or epistemic, both are treated as random quantities.

Endogenous parameters relate to material or geometrical properties while exogenous properties model boundaries and excitation. Structural uncertainty can be classified as global or local phenomena which effects endogenous or exogenous, excitation and surrounding, parameters. An example is given in figure 2.1.

Material uncertainty can be caused by random lattice imperfections in crystalline material, which cause small-scale variations of mechanical and acoustical properties. Measurement of Young's modulus for such a material usually gives only an ensemble average or distribution of spatial averages of elasticity [GPa], while suppressing information of fluctuation. In other words are measurement

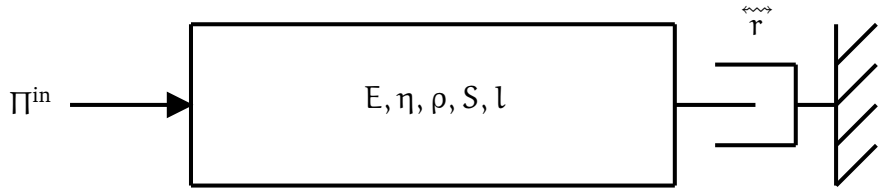

Figure 2.1: A dynamic system where endogenous and exogenous parameters are subject to uncertainty.

data for global uncertainty often quite easy to find, while local uncertainty should be modeled such that the spatial average coincides with measures. [**6**]

Náprstek studied longitudinal wave propagation in a one-dimensional semi-infinite stochastic bar where the density and elasticity where centered random Gaussian homogeneous processes along the propagation dimension. He found that when only the density is varied the apparent damping of the system is increased. In general was a drop of response mean with an increase of response variance observed. [**7**]

Sapoval et al. studied extreme geometrical disorder using fractal geometry. Using numerical investigations they found that a number of modes where confined at the boundary, and that the amplitude of inner resonances where small. The tendency to localization increases with geometrical irregularity. The effect of localization is to locally enhance the response magnitude at regions where the energy is dissipated. The level spacing decreases and becomes more regular. [**8**]

4. Validation

An example of observed phenomena due to uncertainty is given by Loyau and Weinachter; they found large differences of mobility response in an experimental study of apparent identical steel structures. They conducted experiments on coupled plates; where small changes of the coupling angle resulted in large differences. The measures where conducted under similar conditions, already at low frequencies differed the resonances several Hz and for magnitude levels by more then 30 dB. [**11**]

In automotive industry is computational structural-aucoustic models introducing uncertainties during the modeling process due to the complexity of the structure and internal acoustic cavities in terms of geometry, material and boundary conditions. A stochastic computational model based on Monte Carlo solver and convergence analysis of an entire car was demonstrated with good agreement in low frequency range; where mean value and confidence region was compared to

experimental measurements of narrowband FRF. Comparing individual measurements are large response level and frequency spread seen; which partly can be expected due to the customization possibilities of modern cars.[**9**]

A second example is a Monte Carlo stochastic finite element implementation of a satelite and corresponding rocket launcher by the European Space Agency; evaluating the robustness of the nominal design. The article focuses on two different models of uncertainty; parametric and non-parametric. For the parametric response is each parameter of interest defined in terms of a coefficient of variation and probability distribution. The non-parametric model is based on based on replacing the mean reduced matrices of the FE model with random matrices whos etrencies are constructed according to the principle of maximum entropy. The confidence region shows increasing sensitivty with frequency and more then 20 dB spread in a low-frequency band. The main advantage of a non-parametric approach is that it accounts for model uncertainties and not only data uncertainties. This allows different kinds of model robustness to be investigated. [**10**]

Part 2

Modeling

CHAPTER 3

Overview

To investigate effects of uncertainty in dynamic systems, was a numerical model based on a traveling wave ansatz developed. The model treats the problem in five separate stages. The first stage, the user interface, requires an explicit definition of a structural filtration of expected properties and present uncertainties as well as number of realizations and frequencies of interest for the problem at hand. After the first stage comes three iterative stages, one for each realization. The second stage, generation, creates hypothetical subsystems and junctions in accordance to the specification. Once all parameters are known are the third stage, solution, concerned with assembling linear equations into a matrix equation which allows unknown wave amplitudes to be solved using Gaussian elimination, this is repeated for each frequency of interest. Vibrational measures are then computed from the wave amplitudes during the fourth stage, processing. A final fifth stage, postprocessing, computes statistical measures from the vibrational ones, for example largest observed power flow.

The approach indicates that three separate mathematical problems has to be dealt with. On one hand is a deterministic model, a wave approach solution of an equation of motion, which results in knowledge of wave amplitudes needed. On the other hand is stochastic or statistical models needed to assign material, geometrical or boundary values which fits to the structure and uncertainty of interest needed. Finally, once the uncertain system can be generated and predicted is processing and data analyzing required. Combined together can the vibrational behavior of uncertain dynamic systems be investigated. A graphical summary of the ideas can be found in figure 3.1.

As with all deterministic models are the end result a mirror of the specification. If no suitable filtration can be setup, or uncertainty cannot be generated in an appeasing way can the model not be expected to give insight. Further on as the model utilize randomness should the result be treated in a statistical way, there is no certain vibrational behavior of an uncertain system.

1. Limitation

To simplify the mathematical model is this thesis limited to dynamic systems defined by filtrations on the form

$$\mathcal{H} = \{\overleftrightsquigarrow{\mathcal{Z}}_a, W_a, \overleftrightsquigarrow{\mathcal{Z}}_{ab}, W_b, \ldots\} \tag{3.1}$$

of chains, where W denote subsystems and $\overleftrightsquigarrow{\mathcal{Z}}$ impedance junctions. Define a subsystem W as

$$W = \{E, \eta, p, S, l\}. \tag{3.2}$$

A parameter is described by initial values and a generation function. For each realization of the system is the generation function outputting parameter values using the initial values. Typically, initial values are a tolerance, kind of uncertainty and an expected value. Coupling junctions are described by spring or dashpot impedance elements as given by

$$\overleftrightsquigarrow{\mathcal{Z}} = \{\frac{\overleftrightsquigarrow{s}}{j\omega}, \overleftrightsquigarrow{r}\}. \tag{3.3}$$

Equations describing the motion of such a filtration are written in a condensed format by use of pointers; a concept which is introduced here. In order to denote the ansatz are a subset of integers defined as the English alphabet $\overset{1}{a}, \ldots, \overset{26}{z}$ used to denote subsystems. Let ii be a pointer in the system $\mathcal{H}$ such that $ii = k$ means the k:th subsystem. Basic algebraic laws govern the behavior of pointers such as if $ii = c$ then $ii + a = d$. Each subsystem ii has a number $n_{ii} - 1$ of quasidiscontinuities, and hence n_{ii} partitions. Furthermore, let the pointer i in the sequence $1, \ldots, n_{ii}$ target a partition of ii. In other words are ii a pointer to a given subsystem and i to a partition of that particular subsystem.

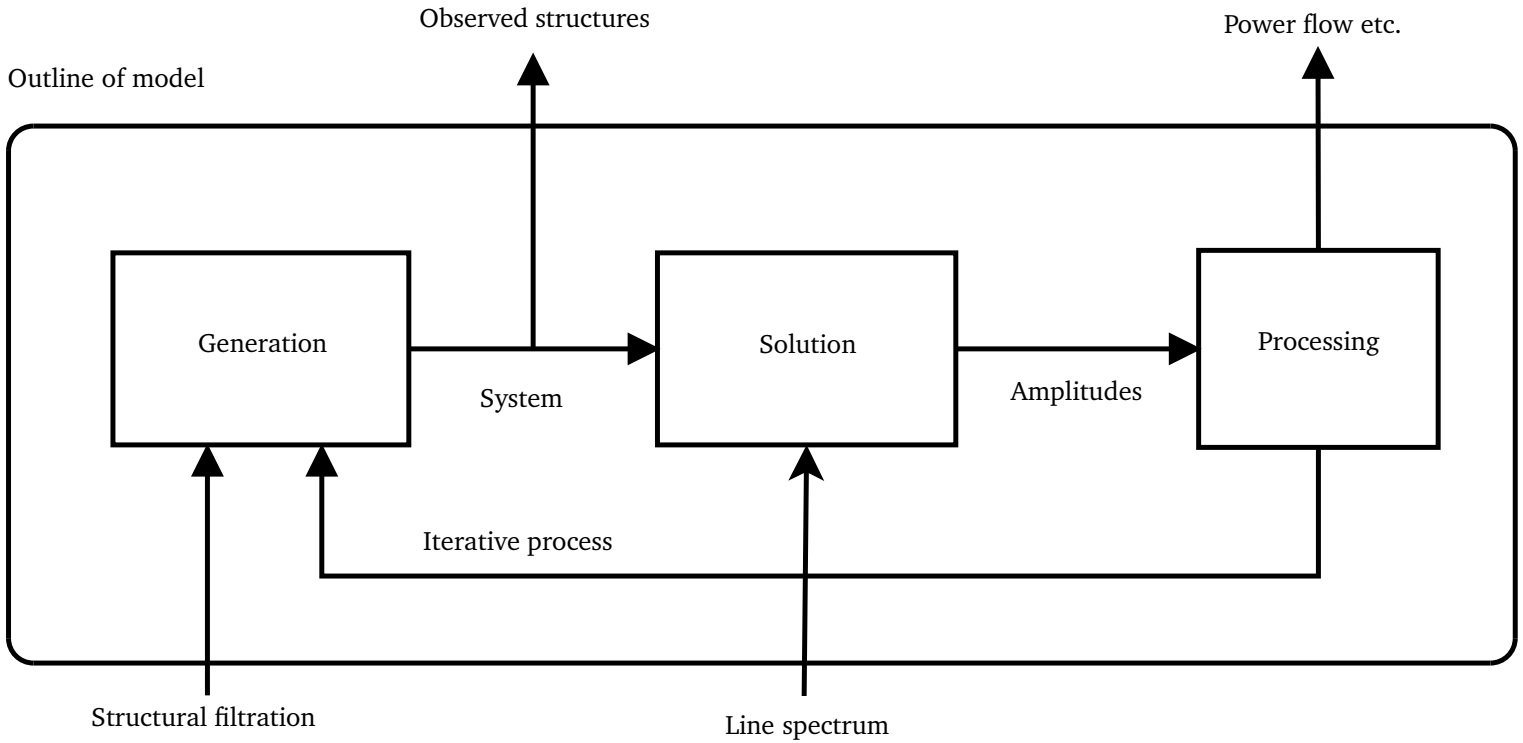

Figure 3.1: A summary of different components and usage of the numerical model. The user specifies a structural filtration and a spectrum of interest, the model outputs hypothetical structures and their vibrational behavior.

CHAPTER 4

Generation

Introducing structural uncertainty into a model requires artificial methods to render subsystems and junctions. Hence, this chapter is devoted to generation of an artificial parameter ξ which fluctuates along a spatial dimension of a subsystem, or which represents an impedance junction. Discrete changes can be used to approximate spatial fluctuations of a physical parameter by a sample and hold function, see figure 4.1. An important note is that some structural changes are inherently discrete, for example a saw cut in a wooden structure. Only if a sampling process of a physical parameter can be simulated by a stochastic process or a statistical distribution can a successful generation be carried out. [**12**]

Spatial fluctuation can be decomposed into an expectancy and a perturbation of the expected value. Perturbation ε can be thought of as the relative distance between the current value of a stochastic process and its expectancy in %-percentage. Assume that a parameter ξ has a spatial invariant expected value Ψ. E.g. a homogeneous beam is often assigned a certain value Young's modulus [GPa]. Local perturbations of expectancy can then be thought of in terms of a stochastic process or statistical distribution that distorts the value one. There are numerous mathematical functions that could model perturbation but a special class are named zero mean processes which has the properties required not to alter the expected value

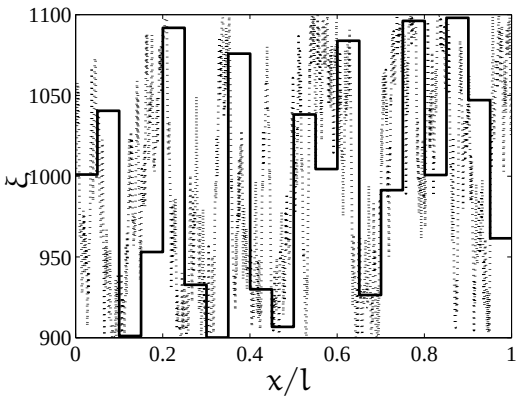

Figure 4.1: Sample and hold representation of ξ; a dotted physical signal and filled sampled signal is shown.

over an ensemble average. Due to manufacturing tolerances and physical limitations, the perturbation should be considered to be bounded between a minimal ξ_m and maximal ξ_M value. This idea could be written down as

$$\xi = \Psi\left(1+\epsilon\right), \xi_m \leq \xi \leq \xi_M, \tag{4.1}$$

and summarizes how generation of hypothetical subsystems can be performed. Global uncertainty phenomena can be modeled by allowing fluctuation of expectancy according to a statistical distribution. Local uncertainty phenomena can be modeled by stochastic processes or statistical distributions; albeit, a suitable mesh is pre-required. Furthermore; investigation of structural uncertainty can be done in fuzzy sets where the amount of uncertainty is increased from one computational set to another.

1. Membership functions and system uncertainty

A fundamental question in system modeling is the amount of uncertainty assumed to be present in different parameters, which can be modeled by several classes of mathematical functions. An alternative is to make use of fuzzy set theory, see [**5**] for in detail discussion of the topic. In short is a membership function used to compute a parameter state domain for each subsystem and junction. For each domain is a number of independent and identically distributed (iid) realizations computed.

A simple computational domain is a polygon generated by triangle membership functions. Imagine walking downwards on a pyramid (membership function) where each cross-section perpendicular to the height represents a level of uncertainty (domain), the pyramid represents an entirely deterministic problem at the top while effects of uncertainty gets pronounced the further down one get. A continuous domain contains an infinite amount of state possibilities, computational complexity motivate a finite amount of states drawn uniformly over the domain. An important benefit of the approach is an dramatic reduction of degrees of freedoms in the model, by knowledge of the distance from the top is the complete domain known. Further on is uncertainty mapped into a normalized space for the case when a height interval of $\Xi \in \{0, 1\}$ is used. [**5**]

In general for a parameter ξ is a core value, and an interval between an allowed minimum and maximum value defined for the largest amount of tolerated uncertainty. If there is no uncertainty present, $\Xi = 0$, is the parameter represented by its core value ξ_0. For the other extreme, when $\Xi = 1$, is the parameter distributed between the minimal ξ_m and maximal ξ_M values. See figure 4.2. [**5**]

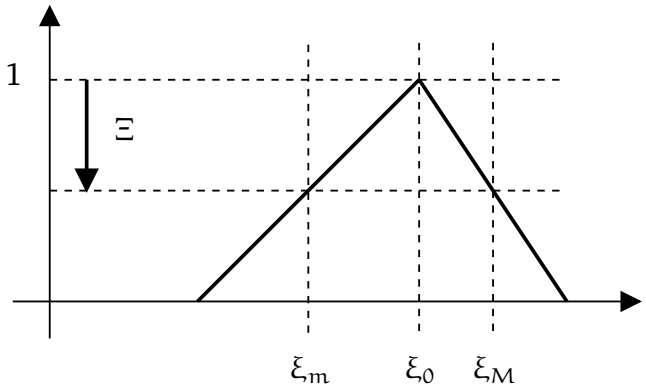

Figure 4.2: A triangle transformation which gives an interval $\{\xi_m, \xi_M\}$ with core ξ_0 given a number $\Xi \in \{0, 1\}$.

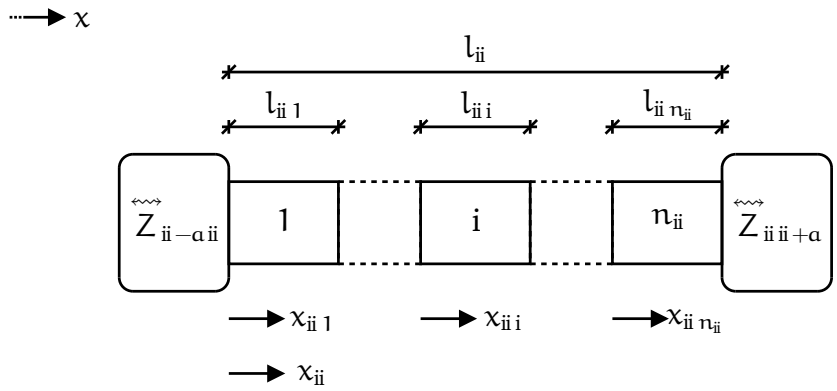

Figure 4.3: A discretized subsystem where local and global coordinate systems and lengths are shown.

2. Subsystem mesh

Discrete changes requires a suitable mesh of a structural continuum. While partitioning is a common topic in finite element analysis, it is unusual in traveling wave approaches. In fact, and as will be discussed later, is the wave field not discretized but continuous and only the material and geometrical properties of subsystems are discretized using an imaginative analog to digital converter, see figure 4.3.

Consider a specific subsystem ii and a partition i of that particular subsystem. A 1D mesh is defined by a number of segments, $i = 0, ..., n_{ii}-1$, which are confined between endpoint positions

$$p_{ii\,0}, p_{ii\,1}, p_{ii\,2}, \ldots, p_{ii\,n_{ii}-1} \tag{4.2}$$

generated in a monotonic fashion $p_{ii\,i-1} \leq p_{ii\,i}$. The first partition would be confined between the two first endpoints; per definition is $p_{ii\,0} = 0$ and $p_{ii\,n_{ii}-1} < l_{ii}$.

The amount of partitions are found, once the subsystem length is known, from the spatial sampling frequency f_x [1/m] using

$$n_{ii} = l_{ii} f_x, \tag{4.3}$$

which allow all positions to be found from

$$p_{ii\,i} = i\,\Delta l \tag{4.4}$$

where $\Delta l = \frac{1}{f_x}$. A segment can then be thought of as a constant phase continuum between a position $p_{ii\,i}$ and a segment length Δl. As will be discussed later can a local coordinate system be introduced as

$$x_{ii\,i} = x - \sum_{g=0}^{i-1} p_{ii\,g}, \tag{4.5}$$

constrained by $0 \leq x_{ii\,i} \leq \Delta l$.

A side effect of spatial sampling is that endogenous properties can be examined by a discrete Fourier transform. An interesting note is that as the segments are assumed to be constant can resampling to a high spatial frequency be made, allowing local uncertainty to be represented by spectrums.

3. Expectancy

A homogeneous beam can be modeled as globally uncertain by randomly assigning parameter values according to a statistical distribution. This will result in level and spacing differences of eigenfrequencies. An expectancy function represents the expected value of a spatial variant parameter for a realization.

3.1. Uniformly distributed. The most simple model for global uncertainty is to assign homogeneous parameter values for an ensemble of structures by an uniformly distributed expectancy. This can be written on the form

$$\Psi\,[ii] = \Psi_0\,(1 + \Psi_w\,U\,[ii])\,, \tag{4.6}$$

where Ψ_0 is the expected value, Ψ_w is a weight and $U\,[ii]$ is a uniform random number. A zero weight $\Psi_w = 0$ would result in an ensemble with a fixed expected parameter value.

4. Perturbation

Local uncertainty is generated by bounded discrete-step continuous-state zero-mean random processes. Perturbation functions represent spatial fluctuation of parameter expectancy and are thought to simulate sampling processes.

4.1. Jump process. A perturbation function in the form of a Markov jump process can be expressed as

$$\epsilon\left[\mathrm{i}\right] = \epsilon\left[\mathrm{i}-1\right] + \Delta\left[\mathrm{i}\right], \mathrm{i} \geq 2, \tag{4.7}$$

where $\epsilon\left[\mathrm{i}-1\right]$ is the state of the previous segment and $\Delta\left[\mathrm{i}\right]$ is a jump. An initial value $\epsilon\left[1\right]$ is drawn from a distribution. Properties of jump processes are governed by the step function $\Delta\left[\mathrm{i}\right]$, which can be seen if the equation is rewritten as

$$\epsilon\left[\mathrm{i}\right] = \epsilon\left[1\right] + \sum_{\mathrm{g}=2}^{\mathrm{i}} \Delta\left[\mathrm{g}\right]. \tag{4.8}$$

Depending on $\Delta\left[\mathrm{g}\right]$ is the process state bounded or unbounded, smooth or volatile, continuous or discrete. [**13, 14**]

4.2. Bounded jump process. In order to confine a Markov jump process is a first step to recognize that a step from one state to another can be described by a direction, a largest possible step size and a weight. This idea can be written down as

$$\Delta\left[\mathrm{g}\right] = \Delta_e\left[\mathrm{g}\right] \Delta_{\mathrm{M}}\left[\mathrm{g}\right] \Delta_w\left[\mathrm{g}\right]. \tag{4.9}$$

Where $\Delta_e\left[\mathrm{g}\right]$ is a unit vector in the direction of the jump, $\Delta_{\mathrm{M}}\left[\mathrm{g}\right]$ is the largest possible jump (the distance between the current state and the constrain in the direction of $\Delta_e\left[\mathrm{g}\right]$) and $\Delta_w\left[\mathrm{g}\right]$ is a weight which defines the jump size. Define the bounded process as symmetrically constrained between

$$-\zeta \leq \epsilon\left[\mathrm{i}\right] \leq \zeta. \tag{4.10}$$

Here, ζ is referred to as the tolerance of local uncertainty and represent the largest deviation from the expected value. The largest value of a jump can then be described by

$$\Delta_{\mathrm{M}}\left[\mathrm{g}\right] = \zeta - \Delta_e\, \epsilon\left[\mathrm{i}-1\right]. \tag{4.11}$$

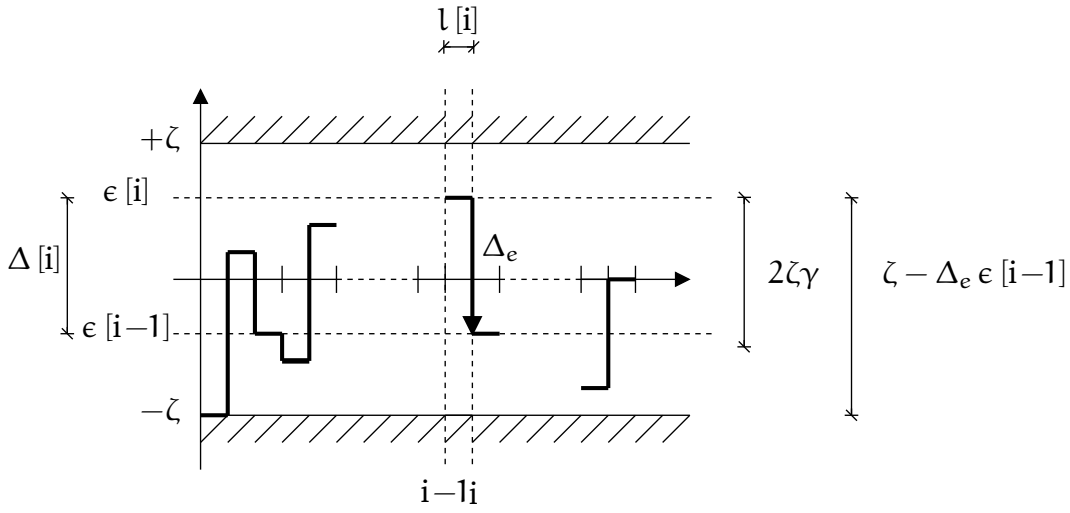

Figure 4.4: Illustration of jump generation for a bounded Markov jump process. First is the direction decided and distance to boundary computed, a jump $i-1$ to i is then decided by the weight distribution.

As can be seen must the direction be determined before the largest value can be computed. The most simple way of determining the direction is to consider a coin flip which gives "up" or "down" depending on outcome. The direction, increase $+1$ or decrease -1, can be determined by

$$\mathrm{P}\left(\Delta_e = +1 \mid \mathrm{U}\right) = \mathrm{P}\left(\mathrm{U} \geq 0.5\right) = 0.5. \tag{4.12}$$

Due to symmetric constraints are jumps $\Delta\,[i]$ bounded by a weight $0 \leq \Delta_w \leq 1$ of a maximum jump Δ_M. Such processes are always constrained and governed by the weight Δ_w, which determines if a jump is small or transient, if the process is smooth or volatile. An initial value is uniformly drawn in $\{-\zeta, +\zeta\}$.

4.2.1. *Smoothness.* Characteristics of a jump process is governed by the weight distribution Δ_w and the maximum allowed jump Δ_M. A jump process is either transient or smooth. Transient processes allow jumps between the limits within a few jumps, while a smooth process may not allow changes between the limits along a subsystem realization. A mathematical model for this is to include a smoothness parameter $\gamma \in \{0, 1\}$ which relates how large a jump can be in proportion to the maximal jump according to

$$\Delta_M\,[g] = m \begin{cases} 2\zeta\gamma, \\ \zeta - \Delta_e\,\epsilon\,[i-1]\,. \end{cases} \tag{4.13}$$

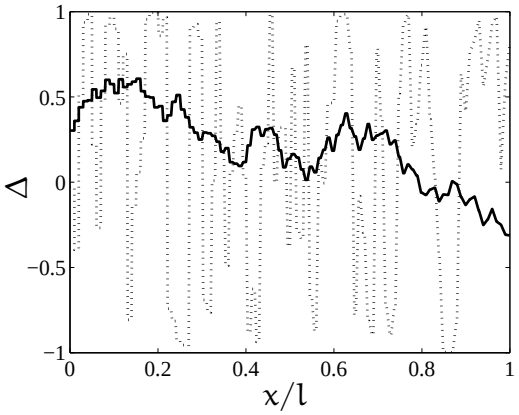

Figure 4.5: Examples of different smoothness for jump processes with uniformly distributed weight.

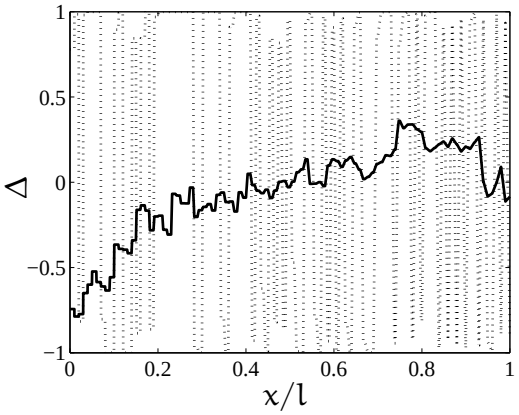

Figure 4.6: Examples of jump processes with different weight distribution parameter for the case when $\gamma \ll 1$.

A smooth process $\gamma \ll 1$ implies that the weight distribution is working against a strict (fixed) scale, which makes the process similar to an unbounded process. Transient behavior $\gamma \gg 0$ result in non-linear scaling of the weight distribution. Examples using different smoothness can be seen in figure 4.5.

4.2.2. *Weight distribution.* A weight distribution is limited by $\{0, 1\}$. It could be any statistical distribution that describes how likely a large or small jump occurs in relation to the maximum jump; i.e. volatility of the process. A skewed process which mainly gives small jumps could be used to represent a less volatile process. In the most simple form is a uniform random distribution used. A more general choice would be a Beta distribution; which allows a skewed distribution and a more controlled volatility. Beta distributions are governed by two parameters α, β. A uniform distribution represents the special case of $\alpha = \beta = 1.0$. Examples of Beta distributed jump processes can be seen in figure 4.6.

CHAPTER 5

Solution

Uncertain dynamic systems can be described by structural filtrations; which describe all possible outcomes of subsystem properties and structural junctions. A graphical overview of the filtration considered can be seen in figure 5.1. Subsystems are associated with material and geometrical properties; which may be deterministic or stochastic in their nature. Therefore, each material or geometrical parameter should be treated in terms of generation functions and initial values, as described in the previous chapter. The focus of this chapter is to describe a solution of the longitudinal motion using a traveling wave ansatz. The solution will take the form of a matrix equation

$$\mathbf{X}^{\mathrm{T}} \underset{\sim}{a} = \underset{\sim}{B}, \tag{5.1}$$

where $\mathbf{X}^{\mathrm{T}}$ is boundary conditions, $\underset{\sim}{a}$ wave amplitudes and $\underset{\sim}{B}$ boundary values. This equation has to be assembled and solved for each frequency of interest.

An important consequence of the traveling wave approach is the large, sparse and costly matrix equations that has to be solved for each frequency of interest for all realizations. Fortunately, numerical solution is straight forward and MATLAB use Gaussian elimination to compute the unknown wave amplitudes. The model requires memory proportional to the square of the total amount of endogenous junctions.

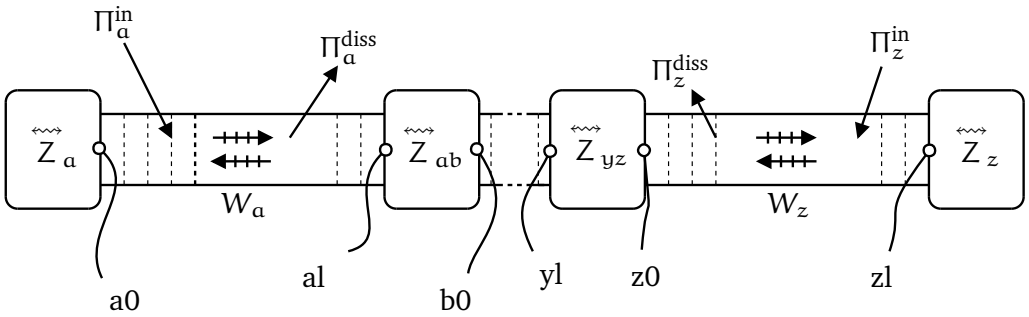

Figure 5.1: A stochastic system consisting of a number of chain connected subsystems. Impedance junctions, subsystem excitation and dissipation as well as pick-up points can be seen.

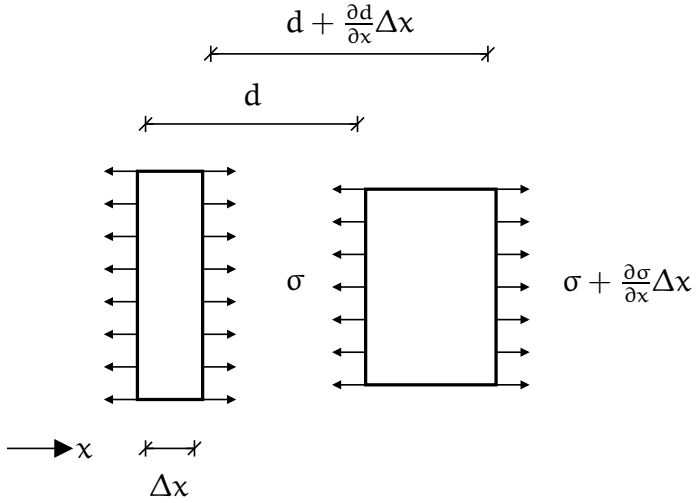

Figure 5.2: Positive direction of stresses σ, longitudinal displacement d and deformations of a small element of a subsystem.

1. Wave equation

Quasilongitudinal motion can be understood by the relative displacement of both sides of a small element of a waveguide. For a body at rest are those planes parallel to each other and perpendicular to the direction of propagation. During quasilongitudinal motion are those planes expanded, or compressed, due to cross-contraction while shifted apart, see figure 5.2. An interesting consequence of cross-contraction, which results in transverse motion, is that it enables sound radiation into surrounding mediums that cannot support shear stresses; for example air. [**15**]

A first step in deriving an equation of motion is to consider two planes of a small element. A plane, initially at x, is displaced a distance d and at the other side of the element a plane a distance Δx away is displaced $d + \frac{\partial d}{\partial x}\Delta x$. Thus, an element between x and $x + \Delta x$ experiences a strain $\epsilon = \frac{\partial d}{\partial x}$. For linear-elastic material is strain related to stress by Hooke's law $\sigma = L\epsilon$; where L is longitudinal stiffness.

During motion is a net unbalanced stress acting on the element, which corresponding equation of motion can be written as

$$\sigma + \frac{\partial \sigma}{\partial x}\Delta x - \sigma = \rho \Delta x \frac{\partial^2 d}{\partial t^2}. \tag{5.2}$$

By introduction of particle velocity $u = \frac{\partial d}{\partial t}$ and longitudinal force $F = -S\sigma$ can the relation above be written as two equations

$$\rho S\frac{\partial u}{\partial t}+\frac{\partial F}{\partial x}=0,\frac{\partial F}{\partial t}+LS\frac{\partial u}{\partial x}=0, \tag{5.3}$$

which couples the quasilongitudinal wave field. The sign convention of stresses imply that longitudinal force F is positive for compression. Alternatively, combination of the coupling equations 5.3 yield a second order partial differential equation on the form

$$L\frac{\partial^2}{\partial x^2}(u,F)-\rho\frac{\partial^2}{\partial t^2}(u,F)=0, L\in\mathbb{C},\rho\in\mathbb{R}. \tag{5.4}$$

Equation 5.4 is in the following called the wave equation. Linear steady-state solutions to the wave equation can be found by a wave ansatz or by a modal ansatz, a wave approach solution is considered in this thesis. An in detailed derivation of the wave equation can be found in [**15**].

2. Wave approach

One solution of the longitudinal wave equation is given by superposing traveling waves. In order to solve the wave equation for a structural filtration as discussed above are some definitions necessary as well as an explanation of the ansatz. Thereafter is a description of how the matrix equation should be assembled given for exogenous and endogenous junctions. A note may be that the derivation is based on geometrical considerations of simpler cases in combination with algebraic solutions to the encountered boundary conditions. By studying simple matrix solutions was a geometrical pattern of applied boundary conditions encountered; this is conceptually presented by so called pointers.

2.1. Definitions. An uncertain system $\mathcal{H}$ consist of a number of connected subsystems $a,\ldots,M$ where $M=M(ii)$, each subsystem a disordered quasilongitudinal waveguide. To each subsystem is an associated amount of partitions $n_a,n_b,\ldots,n_M$ belonging.

If the problem is considered without coupling is each independent system ii described by a matrix equation $\mathbf{X}_{ii}^{T}\underset{\sim}{a}_{ii}=\underline{B}_{ii}$ where $\mathbf{X}_{ii}^{T}$ is a $[2n_{ii},\ 2n_{ii}]$ matrix. Therefore must the combined system matrix have the dimension $[2\sum_{gg=1}^{M}n_{gg},2\sum_{gg=1}^{M}n_{gg}]$. The amount of non-zero elements are $4+8\left(\sum_{gg=a}^{M}(n_{gg}-1)\right)$ and the total number of elements are $\left(2\sum_{gg=1}^{M}n_{gg}\right)^2$. It turns out that matrix elements are positioned along the diagonal, and the matrix is sparse even for a moderate number of subsystems. Let us define the number sequence

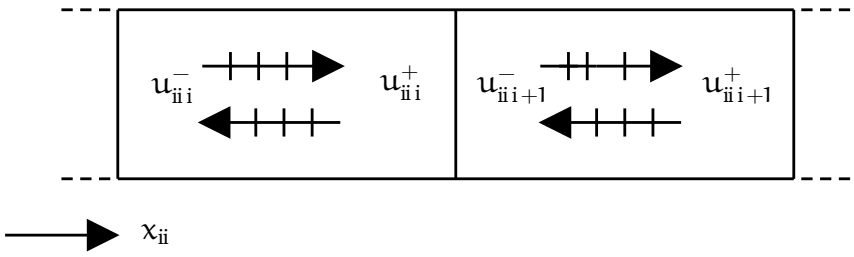

Figure 5.3: Forth and backward traveling waves in two adjacent partitions of a waveguide.

$$H_a, H_b \ldots, H_M = 0, n_a, \ldots, n_a + \ldots + n_{M-1} \tag{5.5}$$

given by

$$H_{ii} = \begin{cases} \sum_{gg=a}^{ii-a} n_{gg}, & b \leq ii \leq M + a \\ 0, & ii = a \end{cases} \tag{5.6}$$

where each number describes where in $\mathbf{X}^T$ a subsystem $ii-a$ ends; such that $(2H_{ii}+1, 2H_{ii}+1)$ is the first element in $\mathbf{X}^T$ corresponding to ii. Further on, define a sequence of unknown amplitudes

$$\underset{\sim}{a}^T = a^+_{a1}, a^-_{a1}, \ldots, a^-_{an_a}, a^+_{b1}, \ldots, a^-_{Mn_M}, \tag{5.7}$$

and boundary values

$$\underset{\sim}{B}^T = -\underline{F}^{in}_a, 0, \ldots, 0, -\underline{F}^{in}_M \ldots, 0, \tag{5.8}$$

where $\underline{F}^{in}_a$ correspond to the force amplitude of time-harmonic exogenous excitation $F^{in}_a = \underline{F}^{in}_a e^{+j\omega t}$; the position of occurrence is discussed below. An important note is that the definition of $\underset{\sim}{a}^T$ imply how junctions are applied in the matrix $\mathbf{X}^T$; row and column element indexes are only valid for this particular order.

2.2. Traveling waves. Considering particle velocity, a wave ansatz for longitudinal motion in a partition $ii\,i$ of $\mathcal{H}$ can be written as an forth, in the positive x direction, traveling wave

$$u^+_{ii\,i} = a^+_{ii\,i} e^{-j k_{ii\,i} x_{ii\,i} + j\omega t}, \tag{5.9}$$

and a back, in the negative x direction, traveling wave

$$u^{-}_{ii\,i} = a^{-}_{ii\,i}\, e^{+j\,k_{ii\,i}x_{ii\,i}+j\,\omega t}, \tag{5.10}$$

denoted with + and - respectively; where harmonic time dependency on the form $e^{+j\,\omega t}$ has been assumed. See figure 5.3. Waves are scattered at material discontinuities or structural junctions; incident waves are both reflected and transmitted. Material, geometry and subsystem couplings determine the unknown wave amplitudes $a^{+}_{ii\,i}$ and $a^{-}_{ii\,i}$. Using the principle of superposition the longitudinal wave field in a partition can be found; particle velocity according to

$$u_{ii\,i} = u^{+}_{ii\,i} + u^{-}_{ii\,i}, \tag{5.11}$$

and longitudinal force from

$$F_{ii\,i} = Z_{ii\,i}\,(u^{+}_{ii\,i} - u^{-}_{ii\,i})\,. \tag{5.12}$$

In principle can wave amplitudes be superposed from any amplitude defining a physical variable; for example displacement or stress. The choice of superposing particle velocity amplitudes are due to simplicity when impedance junctions are considered. In order to solve the wave equation is first and second time and spatial derivatives of longitudinal velocity and force needed. By insertion into mentioned coupling equations 5.3, it is found that field quantities in each partition $ii\,i$ are related by characteristic impedance $Z_{ii\,i} = S_{ii\,i}\sqrt{L_{ii\,i}\rho_{ii\,i}}$ and traveling with a constant phase speed $c_{ii\,i} = \sqrt{\frac{L_{ii\,i}}{\rho_{ii\,i}}}$; where longitudinal stiffness $L_{ii\,i}$ relate to a loss-factor $\eta_{ii\,i}$ and Young's modulus $E_{ii\,i}$ as $L_{ii\,i} = E_{ii\,i}(1 + j\eta_{ii\,i})$. In addition is each partition associated with a length $l_{ii\,i}$ and local coordinate system $0 \leq x_{ii\,i} \leq l_{ii\,i}$ which depend on the applied mesh. [**16, 15**]

Damping is introduced, as discussed above, by inclusion of a loss-factor which allow different damping mechanisms, including non-material and material phenomena, to be modeled. A loss-factor results in a complex modulus which results in a complex phase speed and complex characteristic impedance. That damping has been introduced can be seen in the phase of the ansatz, equation 5.11 and 5.12, where a complex wavenumber approximately results in waves on the form

$$u^{+}_{ii\,i} = a^{+}_{ii\,i}\, e^{-j\,\omega\sqrt{\frac{\rho_{ii\,i}}{E_{ii\,i}}}x_{ii\,i} - \omega\frac{\eta}{2}\sqrt{\frac{\rho_{ii\,i}}{E_{ii\,i}}}x_{ii\,i}+j\,\omega t}. \tag{5.13}$$

In other words are the propagating waves dying out exponentially; the first part carries phase information while the second represent damping. [**17, 15**]

2.3. Exogenous junctions. Predicted vibrational behavior of dynamic systems can be expected to depend strongly on the assumption of junctions; the interaction between waveguides governs the overall response. An incident wave at a junction is reflected back and transmitted; in addition parts of the energy is absorbed. In the following derivation is impedance couplings between neighboring subsystems ii and $ii+a$ discussed; it is assumed that transmission and reflection impedances govern a coupling. Assuming that couplings are reciprocal in regard to energy, the four different impedances are related according to

$$\overleftrightarrow{Z}_{ii\,n_{ii}\,ii\,n_{ii}} = \overleftrightarrow{Z}_{ii+a1\,ii+a1} = -\overleftrightarrow{Z}_{ii\,n_{ii}\,ii+a1} = -\overleftrightarrow{Z}_{ii+a1\,ii\,n_{ii}}, \tag{5.14}$$

which is denoted $\overleftrightarrow{Z}_{ii\,ii+a}$. The notation of the four impedances above should be read as $\overleftrightarrow{Z}_{in\,out}$, the incident subsystem and partition are given first and followed by the subsystem and partition of the transfered energy. As mentioned only longitudinal motion is considered; therefore, it is assumed that no energy is transfered to other wave modes.

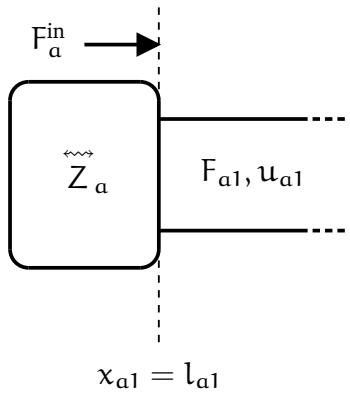

Figure 5.4: Exogenous boundary conditions shown for the left hand side of the first subsystem.

2.3.1. *Left end of first subsystem.* Force equilibrium at an impedance junction at $x_{a1} = 0$ for subsystem a gives the following boundary condition

$$F_{a1}\Big|_{x_{a1}=0} + \overleftrightarrow{Z}_{a1a1} u_{a1}\Big|_{x_{a1}=0} + F_a^{in} = 0, \tag{5.15}$$

see figure 5.4. Inserting the ansatz, equation 5.11 and 5.12, results in

$$(\mathbf{X}^T : 1,1) = +Z_{a1} + \overleftrightarrow{Z}_{a1a1}, \tag{5.16}$$

$$= +Z_{a1} + \overleftrightarrow{Z}_{a}, \tag{5.17}$$

$$(\mathbf{X}^T : 1,2) = -Z_{a1} + \overleftrightarrow{Z}_{a1a1}, \tag{5.18}$$

$$= -Z_{a1} + \overleftrightarrow{Z}_{a}. \tag{5.19}$$

External excitation correspond to $B^T(1) = -\underline{F}_a^{in}$.

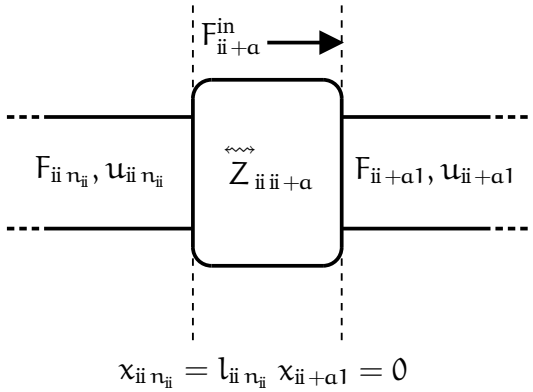

Figure 5.5: Exogenous boundary conditions shown an impedance junction between two subsystems.

2.3.2. *Junction between subsystems.* Between neighboring subsystems ii and ii+a a coupling impedance $\overleftrightarrow{Z}_{ii\,ii+a}$ is acting, see figure 5.5. A coupling impedance is modeled by a mechanical circuit and may show mass, dashpot or spring characteristics. In the following the pointer ii is valid between a to $M-1$ for a system with M subsystems, given that $M \geq 2$. In addition it can be seen in the coupling equations that for the case when $\overleftrightarrow{Z}_{ii\,ii+a} = 0$ the subsystems are independent of each other.

At the right end of subsystem ii force equilibrium can be expressed as

$$F_{ii\,n_{ii}}\Big|_{x_{ii\,n_{ii}}=l_{ii\,n_{ii}}} = \overleftrightarrow{Z}_{ii\,n_{ii}\,ii\,n_{ii}} u_{ii\,n_{ii}}\Big|_{x_{ii\,n_{ii}}=l_{ii\,n_{ii}}} + \overleftrightarrow{Z}_{ii+a1\,ii\,n_{ii}} u_{ii+a1}\Big|_{x_{ii+a1}=0}, \tag{5.20}$$

which correspond to

$$(\mathbf{X}^{\mathrm{T}} : 2H_{ii+a}, 2H_{ii+a} - 1) = \left(+Z_{ii\,n_{ii}} - \overleftrightsquigarrow{Z}_{ii\,n_{ii}\,ii\,n_{ii}}\right) e^{-j\,k_{ii\,n_{ii}}\,l_{ii\,n_{ii}}}, \tag{5.21}$$

$$= \left(+Z_{ii\,n_{ii}} - \overleftrightsquigarrow{Z}_{ii\,ii+a}\right) e^{-j\,k_{ii\,n_{ii}}\,l_{ii\,n_{ii}}}, \tag{5.22}$$

$$(\mathbf{X}^{\mathrm{T}} : 2H_{ii+a}, 2H_{ii+a}\quad) = \left(-Z_{ii\,n_{ii}} - \overleftrightsquigarrow{Z}_{ii\,n_{ii}\,ii\,n_{ii}}\right) e^{+j\,k_{ii,n_{ii}}\,l_{ii,n_{ii}}}, \tag{5.23}$$

$$= \left(-Z_{ii\,n_{ii}} - \overleftrightsquigarrow{Z}_{ii\,ii+a}\right) e^{+j\,k_{ii,n_{ii}}\,l_{ii,n_{ii}}}, \tag{5.24}$$

$$(\mathbf{X}^{\mathrm{T}} : 2H_{ii+a}, 2H_{ii+a} + 1) = -\overleftrightsquigarrow{Z}_{ii+a1\,ii\,n_{ii}}, \tag{5.25}$$

$$= +\overleftrightsquigarrow{Z}_{ii\,ii+a}, \tag{5.26}$$

$$(\mathbf{X}^{\mathrm{T}} : 2H_{ii+a}, 2H_{ii+a} + 2) = -\overleftrightsquigarrow{Z}_{ii+a1\,ii\,n_{ii}}, \tag{5.27}$$

$$= +\overleftrightsquigarrow{Z}_{ii\,ii+a}. \tag{5.28}$$

At the left end of subsystem $ii+a$ is equilibrium expressed as

$$F_{ii+a1}\Big|_{x_{ii+a1}=0} + \overleftrightsquigarrow{Z}_{ii+a1\,ii+a1} u_{ii+a1}\Big|_{x_{ii+a1}=0} + \overleftrightsquigarrow{Z}_{ii\,n_{ii}\,ii+a1} u_{ii\,n_{ii}}\Big|_{x_{ii\,n_{ii}}=l_{ii\,n_{ii}}} + F^{\mathrm{in}}_{ii+a} = 0, \tag{5.29}$$

which give

$$(\mathbf{X}^{\mathrm{T}} : 2H_{ii+a} + 1, 2H_{ii+a} - 1) = +\overleftrightsquigarrow{Z}_{ii\,n_{ii}\,ii+a1}\, e^{-j\,k_{ii\,n_{ii}}\,l_{ii\,n_{ii}}} \tag{5.30}$$

$$= -\overleftrightsquigarrow{Z}_{ii\,ii+a}\, e^{-j\,k_{ii\,n_{ii}}\,l_{ii\,n_{ii}}}, \tag{5.31}$$

$$(\mathbf{X}^{\mathrm{T}} : 2H_{ii+a} + 1, 2H_{ii+a}\quad) = +\overleftrightsquigarrow{Z}_{ii\,n_{ii}\,ii+a1}\, e^{-j\,k_{ii\,n_{ii}}\,l_{ii\,n_{ii}}} \tag{5.32}$$

$$= -\overleftrightsquigarrow{Z}_{ii\,ii+a}\, e^{+j\,k_{ii\,n_{ii}}\,l_{ii\,n_{ii}}}, \tag{5.33}$$

$$(\mathbf{X}^{\mathrm{T}} : 2H_{ii+a} + 1, 2H_{ii+a} + 1) = +Z_{ii+a1} + \overleftrightsquigarrow{Z}_{ii+a1\,ii+a1} \tag{5.34}$$

$$= +Z_{ii+a1} + \overleftrightsquigarrow{Z}_{ii\,ii+a}, \tag{5.35}$$

$$(\mathbf{X}^{\mathrm{T}} : 2H_{ii+a} + 1, 2H_{ii+a} + 2) = -Z_{ii+a1} + \overleftrightsquigarrow{Z}_{ii+a1\,ii+a1} \tag{5.36}$$

$$= -Z_{ii+a1} + \overleftrightsquigarrow{Z}_{ii\,ii+a}. \tag{5.37}$$

At each left end of a subsystem an external time-harmonic force is acting. Alternatively, excitation can occur wherever the waveguide has an endogenous junction. I.e. each position $(2H_{ii+a}+1, 2H_{ii+a}+1)$ in X^{T} corresponds to a subsystem excited by an external force F^{in}_{ii+a} at $x_{ii+a1} = 0$, which gives $B^{\mathrm{T}}(2H_{ii+a}+1) = -\underline{F}^{\mathrm{in}}_{ii+a}$.

2.3.3. *Right end of last subsystem.* At the right end of the last subsystem M an additional impedance junction is acting. It is constrained by

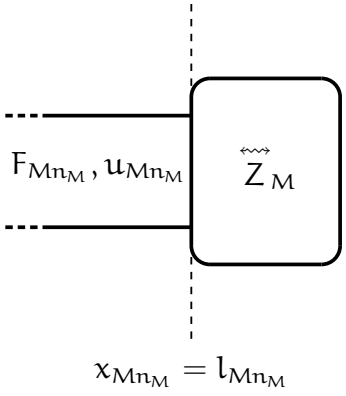

Figure 5.6: Exogenous boundary conditions shown for the right hand side of the last subsystem.

$$F_{Mn_M}\Big|_{x_{Mn_M}=l_{Mn_M}} = \overleftrightarrow{Z}_{Mn_M Mn_M} u_{Mn_M}\Big|_{x_{Mn_M}=l_{Mn_M}}, \tag{5.38}$$

which gives

$$(\mathbf{X}^T : 2H_{M+a}, 2H_{M+a}-1) = \left(+Z_{Mn_M} - \overleftrightarrow{Z}_{Mn_M Mn_M}\right) e^{-j k_{Mn_M} l_{Mn_M}}, \tag{5.39}$$

$$= \left(+Z_{Mn_M} - \overleftrightarrow{Z}_{M}\right) e^{-j k_{Mn_M} l_{Mn_M}}, \tag{5.40}$$

$$(\mathbf{X}^T : 2H_{M+a}, 2H_{M+a}\quad) = \left(-Z_{Mn_M} - \overleftrightarrow{Z}_{Mn_M Mn_M}\right) e^{+j k_{Mn_M} l_{Mn_M}}, \tag{5.41}$$

$$= \left(-Z_{Mn_M} - \overleftrightarrow{Z}_{M}\right) e^{+j k_{Mn_M} l_{Mn_M}}. \tag{5.42}$$

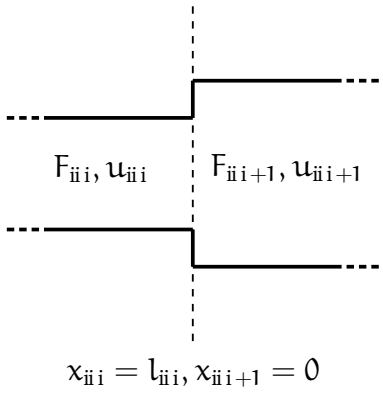

Figure 5.7: Endogenous boundary conditions shown for a junction between two partitions of a subsystem.

2.4. Endogenous junctions. An important step towards a wave approach solution for a disordered subsystem is the study of field-conservative junctions. Such

junctions govern the vibrational field behavior from changes inside a solid, see figure 5.7. Such a change may be a locally increased density or a change of elasticity. In the most simple form field-conservative junctions state that on each side of a change the field quantities, velocity $\mathfrak{u}$ and force F, must not be altered.

A well-known example from noise control in HVAC equipment is that air-borne sound on each side of a ventilation duct, where the cross-section has been changed, must the dynamic pressure and air flow be conserved. Field-conservation in air-borne applications is only working well for small-changes, or not arbitrarily high changes, of the cross-section and below the cut on frequency of cross-sectional modes [**15**]. A solution in air-borne applications is to use correction impedance factors as discussed by for example [**18**].

In structure-borne sound does such junctions occur whenever the cross-section, damping property or any other parameter changes inside of a structure. A number of small-scale changes such as lattice defects on a large-scale, yet small, region of a beam is enough to change density, elasticity and other properties by small margins. The region boundaries will be governed by field-conservative junctions. A general discussion of discontinuities in quasilongitudinal waveguides can be found in [**15**].

As been stated before, endogenous junctions are quasidiscontinous; while the material and geometry is discretized are the wave motion continuous. Hence, the boundary conditions are given by conservation of the field.

2.4.1. *Particle velocity.* Conservation of velocity through a discontinuity between two adjacent partitions is described by

$$\mathfrak{u}_{\mathrm{ii\,i}}\Big|_{x_{\mathrm{ii\,i}}=l_{\mathrm{ii\,i}}} = \mathfrak{u}_{\mathrm{ii\,i+1}}\Big|_{x_{\mathrm{ii\,i+1}}=0}, \tag{5.43}$$

which can be written as

$$(\mathbf{X}^{\mathrm{T}} : 2H_{\mathrm{ii}} + 2\,\mathrm{i}, 2H_{\mathrm{ii}} + 2\,\mathrm{i} - 1) = + e^{-\mathrm{j}\,k_{\mathrm{ii\,i}}\,l_{\mathrm{ii\,i}}}, \tag{5.44}$$

$$(\mathbf{X}^{\mathrm{T}} : 2H_{\mathrm{ii}} + 2\,\mathrm{i}, 2H_{\mathrm{ii}} + 2\,\mathrm{i}\quad) = + e^{+\mathrm{j}\,k_{\mathrm{ii\,i}}\,l_{\mathrm{ii\,i}}}, \tag{5.45}$$

$$(\mathbf{X}^{\mathrm{T}} : 2H_{\mathrm{ii}} + 2\,\mathrm{i}, 2H_{\mathrm{ii}} + 2\,\mathrm{i} + 1) = -1, \tag{5.46}$$

$$(\mathbf{X}^{\mathrm{T}} : 2H_{\mathrm{ii}} + 2\,\mathrm{i}, 2H_{\mathrm{ii}} + 2\,\mathrm{i} + 2) = -1. \tag{5.47}$$

2.4.2. *Longitudinal force.* Conservation of force on both sides of a discontinuity can be expressed as

$$F_{ii\,i}\Big|_{x_{ii\,i}=l_{ii\,i}} = F_{ii\,i+1}\Big|_{x_{ii\,i+1}=0}, \tag{5.48}$$

which yield

$$(\mathbf{X}^{\mathrm{T}} : 2H_{ii} + 2\,i+1, 2H_{ii} + 2\,i-1) = +Z_{ii\,i}\,e^{-j\,k_{ii\,i}\,l_{ii\,i}}, \tag{5.49}$$

$$(\mathbf{X}^{\mathrm{T}} : 2H_{ii} + 2\,i+1, 2H_{ii} + 2\,i\quad) = -Z_{ii\,i}\,e^{+j\,k_{ii\,i}\,l_{ii\,i}}, \tag{5.50}$$

$$(\mathbf{X}^{\mathrm{T}} : 2H_{ii} + 2\,i+1, 2H_{ii} + 2\,i+1) = -Z_{ii\,i+1}, \tag{5.51}$$

$$(\mathbf{X}^{\mathrm{T}} : 2H_{ii} + 2\,i+1, 2H_{ii} + 2\,i+2) = +Z_{ii\,i+1}. \tag{5.52}$$

3. Limitation

The model cannot be expected to give physical results above the cut on frequency for cross-sectional modes, a phenomenon which is neglected. Cut on frequency for cross-section resonances given a rectangular surface is given by

$$f^{\mathrm{cross}}_{ii\,i} = \frac{1}{2\,m\,(w,h)}\sqrt{\frac{E_{ii\,i}}{\rho_{ii\,i}}}. \tag{5.53}$$

An interesting upper frequency limit is when localization or resonances occur in partitions of a subsystem. As a uniform distribution of partitions length is considered a resonance is observed when a (half-) wavelength get in the order of the partitions length. Phenomenon of localization is not taken into account and it is therefore of importance to use a fine mesh, to push the upper limit away from the observed spectrum. Partition localization cut on is defined by

$$f^{\mathrm{partition}}_{ii\,i} = \frac{n_{ii}}{2l_{ii}}\sqrt{\frac{E_{ii\,i}}{\rho_{ii\,i}}}. \tag{5.54}$$

As the elasticity and density fluctuates should the lowest cut on frequency be considered. Partition resonances imply that each partition is acting as a beam in itself, rather then a small part of a subsystem. In other words subsystems are then acting like a long chain of field-conservative coupled deterministic subsystems rather than one uncertain subsystem.

CHAPTER 6

Processing

Estimation of vibrational measures and response characterization from wave amplitudes represent the last stage of the model. Overall system response can be estimated once the properties of individual realizations has been determined, an overview can be seen in 6.1.

1. Vibrational measures

Wave propagation can be described by several measures. Apart from the derived wave amplitudes are the field quantities the most brute way to describe system response. However; while fully describing the motion of a system is the measures not practical, a change of excitation or boundaries requires a new measure. Hence, normalized transfer functions are usually preferred. Driving-point mobilities Y relates excitation point force F^{in} to particle velocity u at an arbitrary measurable pick-up point of the structure. Transfer functions of this kind can be computed by

$$Y = \frac{u}{F^{in}}. \tag{6.1}$$

Driving-point mobilities represent an normalized system response; in this thesis are transfer mobilities from source excitation point to subsystem end points considered. Resonances occur as an phenomenon of wavetrain closure; the response

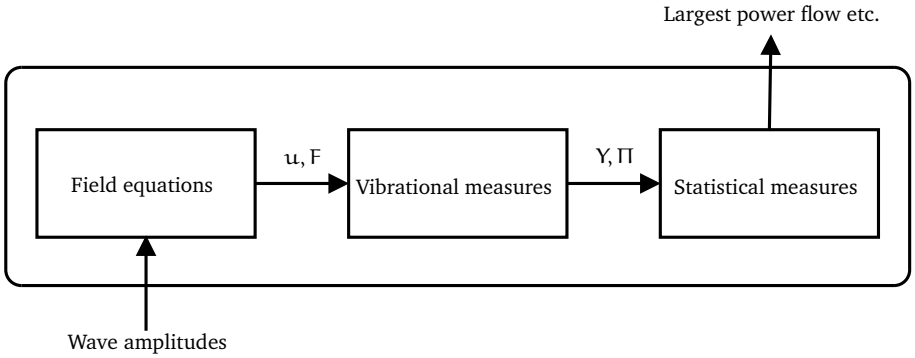

Figure 6.1: Overall system response characterization using wave amplitudes of realizations requires several steps of processing.

levels and frequencies depend on the assumption of junctions, geometry and material. Eigenfrequencies can be detected as local maximas in driving-point mobilities; for example by a peak detection algorithm used on narrowband data. In this thesis is an modified version of an off the shelf algorithm used [**19**]. [**15**]

Traveling waves are associated with net energy transport; the speed of energy transport is the group speed which for longitudinal motion are identical to the phase speed, in other words is the medium non-dispersive. Power flow can be found from the well-known relation $\Pi = 0.5\Re\{F\bar{u}\}$; inserting equation 5.11 and 5.12 is it found that power flow is given from

$$\Pi_{ii\,i} = 0.5\Re\{Z_{ii\,i}u^{+}_{ii\,i}\bar{u}^{+}_{ii\,i} - Z_{ii\,i}u^{-}_{ii\,i}\bar{u}^{-}_{ii\,i}\}. \tag{6.2}$$

Positive power flow is defined to be in the positive x-direction. As can be seen is power flow defined by the time-averaged behavior of wave propagation. [**20, 15**]

Narrowband data can be smoothened by averaging into octavebands. Using to low bandwidth designator results in that the differences introduced by structural uncertainty is averaged away. Using narrowband data means that a large amount of data has to be acquired and processed. Hence, one solution is to use an moderate one-third designator and present line spectrums where appropriate. [**21**]

2. Response characterization

Uncertain systems can on one hand be characterized by overall behavior and on the other by robustness to uncertainty. An possibillistic indication of the overall behavior is given by the envelope between the system smallest and largest response in one-third octaveband data, robustness to uncertainty is then indicated by the response level spread. Ensemble extremal response is computed by looking at the set largest and smallest response level for each octaveband of interest taken independent of each other; rather then to compute the overall largest level and choose the corresponding realization as extreme. The ensemble extreme value Φ [dB] of an octaveband, or line, in a spectrum Ω of an vibrational measure $\mathcal{O}$ (for example mobility) is defined by

$$\Phi(\Omega) = \begin{cases} \mathrm{M}(\mathcal{O}), \\ \mathrm{m}(\mathcal{O}). \end{cases} \tag{6.3}$$

The result is an response level envelope, which is computed for each amount of uncertainty and set of observations. For an ensemble with m sets of realizations

$$\mathbb{H}_m(\Omega) = \{\Phi_1, \ldots, \Phi_m\}, \tag{6.4}$$

are m different observations of the extremal value done; the largest and smallest values are treated separately. The extremal response is estimated by an average of extremes defined by

$$\langle \mathbb{H}_m \rangle = 20 \lg \left(\frac{1}{m} \sum_{i=1}^{m} 10^{\frac{\Phi_i}{20}} \right). \tag{6.5}$$

Alternatively, extremal response can be estimated by the extreme of extremes according to

$$M(\mathbb{H}_m), m(\mathbb{H}_m). \tag{6.6}$$

The procedure is illustrated in figure 6.2, which shows how an observed ensemble of realizations are transformed into a visualization of the extremes. In 6.2d, the filled spectrum is dark grey between the two averages of extremes, light grey between the smallest of smallest and largest of largest observed values and the observed domain is marked by a black line.

Eigenfrequencies are characterized by the largest observed domain, illustrated in figure 6.3. Acquired scatter data of a resonance is processed using Delaunay triangulation and the convex hull is computed for each amount of uncertainty. Finally, the domain is visualized using linear interpolation. Of interest is the response level spread ΔL and frequency spread Δf; as well as the shape of the observed domain.

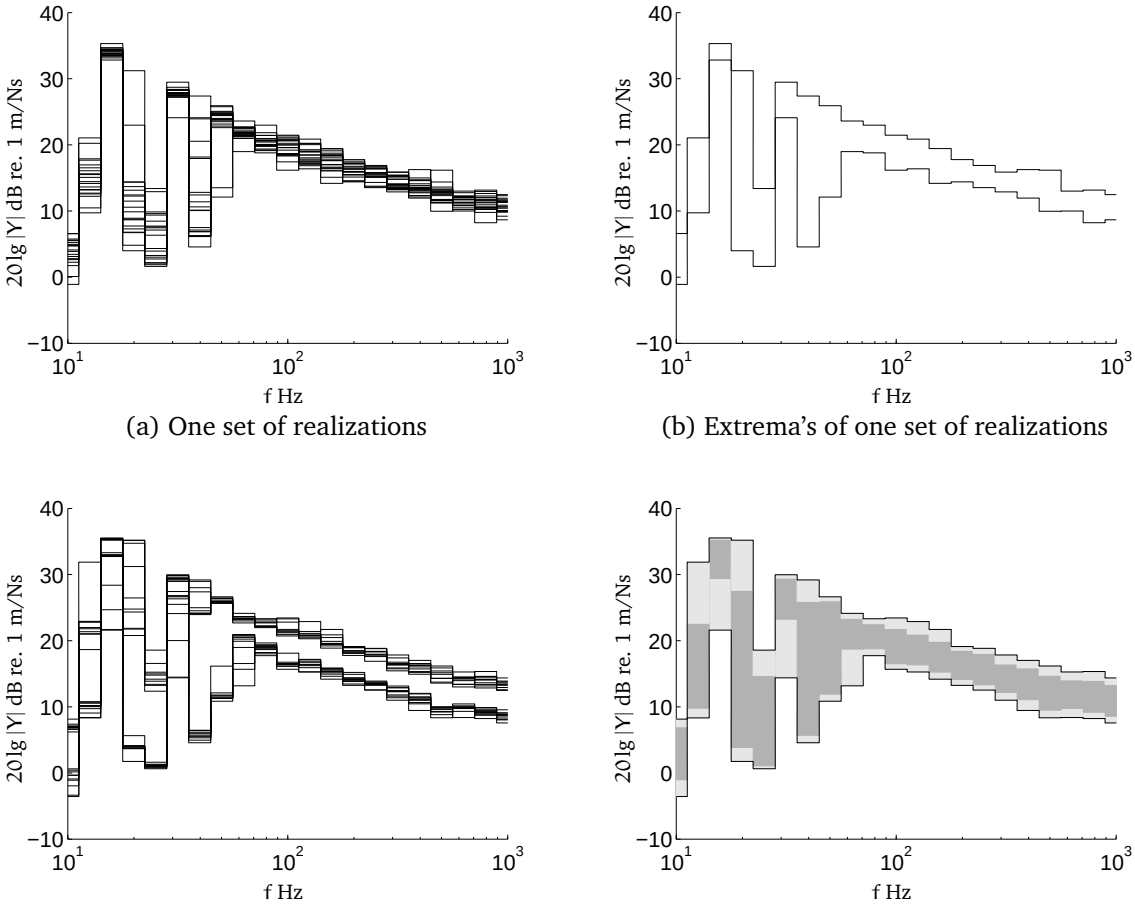

(a) One set of realizations

(b) Extrema's of one set of realizations

(c) Extrema's of each set

(d) Estimation of extremal response

Figure 6.2: Illustration of different computational steps involved in order to visualize extremal response. The filled envelope is a possibillistic approach to the response of uncertain dynamic systems.

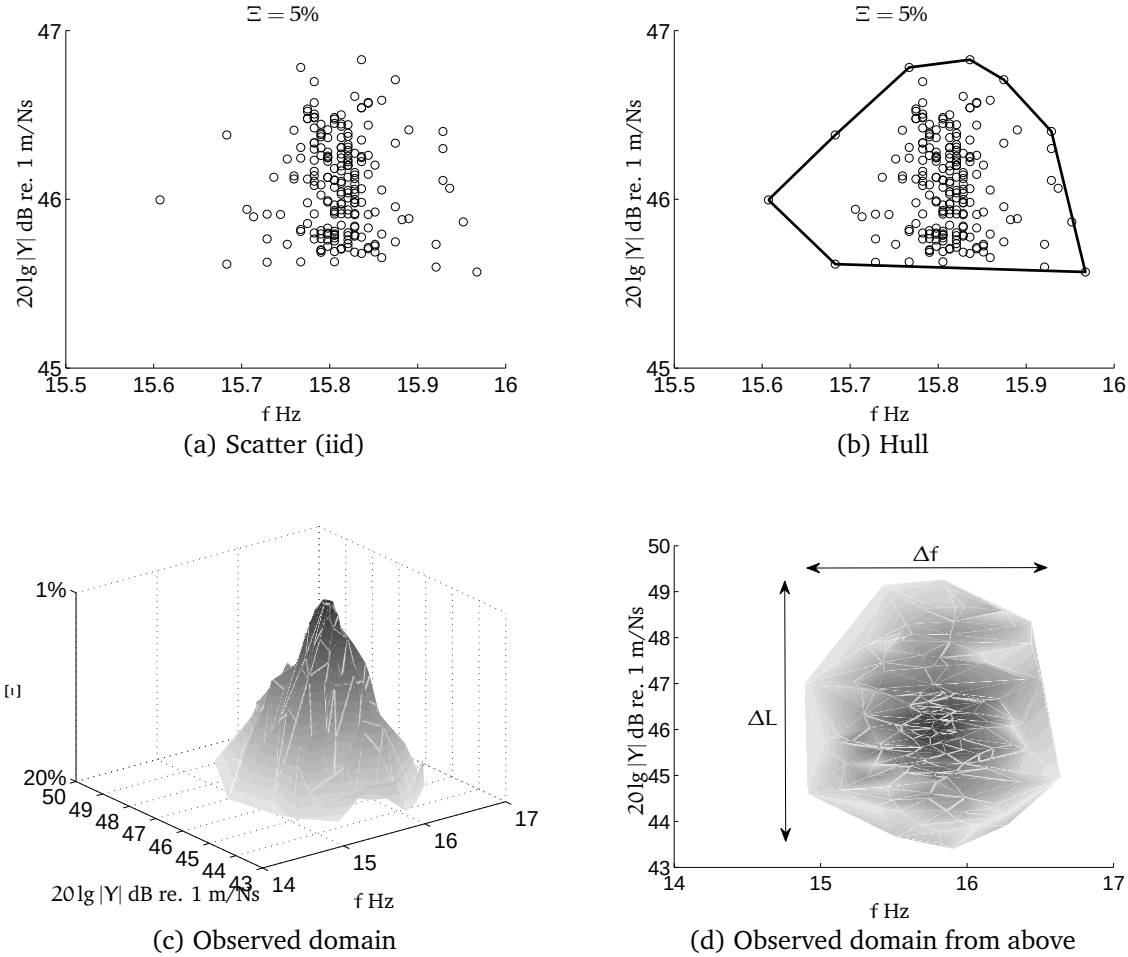

(a) Scatter (iid)

(b) Hull

(c) Observed domain

(d) Observed domain from above

Figure 6.3: Eigenfrequencies as detected by a peak detection algorithm represents a three dimensional domain which can be visualized by Delaunay triangulation. Observations "density" is lost in the process, only the shape of the domain is presented.

Part 3

Findings

CHAPTER 7

Nominal systems

Different numerical experiments of parameter uncertainty in dynamic systems of one or two self-similar coupled subsystems were conducted. A specific homogeneous subsystem was formulated and investigated by changing one parameter at a time to be uncertain. Phenomena related to different scales of uncertainty, local or global, and amount of uncertainty was investigated. In total was 20 levels of uncertainty ranging from $\pm 1\%$ to $\pm 20\%$ used, which in theory allow investigation of modest 2% to extreme 50% tolerated uncertainty. The experiments was divided into material uncertainty, geometrical uncertainty and coupling uncertainty. Ensemble vibrational measures is presented from 1 Hz to 1 kHz in one-third octave band averaged spectrums while nominal and extremal response is presented in line spectrums. For each case was 10 sets of 20 realizations computed. For each set was the largest and smallest measures used to compute the average extremal response. Alternatively; all 200 realizations where used to visualize resonances.

1. Reference waveguide

Most dynamic systems considered are assembled using one specific subsystem. The use of a reference subsystem was done in order to simplify comparison between different kind of uncertainty. Material parameters was chosen as Young's modulus 1 MPa, loss-factor 0.01 [-] and density 1000 kg/m^3. Each subsystem has a length 1 m and a cross-section surface of 0.01×0.001 m^2. A uniform mesh of one thousand partitions was used; in other words are partition resonances occurring from 15 kHz. A source system consists of a freely suspended beam while a source and receiver system are assembled from two beams coupled by a spring with stiffness 1000 kg/s^2. Excitation is considered to be a time-harmonic point force of 1 N acting at the left end of the source structure. Only longitudinal wave motion is considered in the reference subsystem.

The reference system can be made uncertain by modifying one or several parameters. Global uncertainty is modeled by a uniform distribution; centered around the expected value given above. Local uncertainty is generated using jump processes where the weight distribution is a Beta distribution. For each parameter generation is the weight distribution parameters α, β drawn uniformly between $[0.1, 10]$ while smoothness γ is drawn uniformly between $[0.001, 1]$. Hence, the

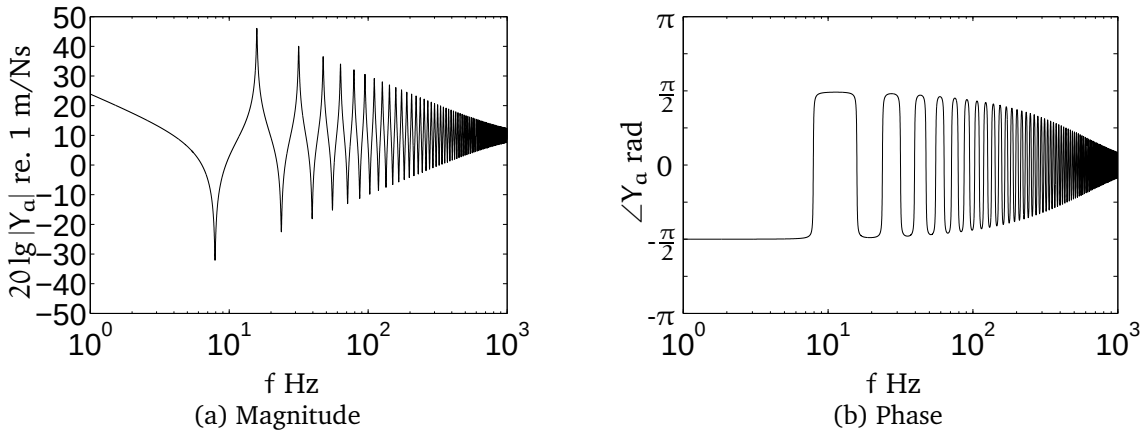

Figure 7.1: Magnitude and phase of driving-point mobility at the left end of the source waveguide.

fluctuation characteristics of two different realizations can differ by a large margin.

2. Source system

The source system is the most simple dynamic system which can be subjected to uncertainty in the model. It consists of a freely suspended beam excited at the left end by a point harmonic force. For the deterministic case, it is found that the first resonances occurs at 15.8, 31.6, 47.4, 63.3 and 79.0 Hz. The response level observed in the driving-point mobility is respectively 46.1, 40.1, 36.5, 34.0 and 32.1 dB re. 1 m/Ns. The response level of resonances at the right end compared to the left end is only minor different and neglected. Magnitude and phase of the left end can be seen in figure 7.1. The nominal system agrees with the result obtained for a homogeneous beam in appendix B.

3. Source and receiver system

In addition to the freely suspended beam is a coupled source and receiver system examined. The system consist of two self-similar subsystems coupled via a spring. The spring is deterministic and has a constant value for most of the cases. Self-similar indicates that both waveguides are uncertain, being different realizations of the same filtration.

For the deterministic case, it is found that the source and receiver subsystem has a resonance at 7.8, 15.8, 23.6, 31.6, 39.3 and 47.4 Hz, see figure 7.2. The subsystem coupling cause the system motion to act as a rigid beam at low frequencies;

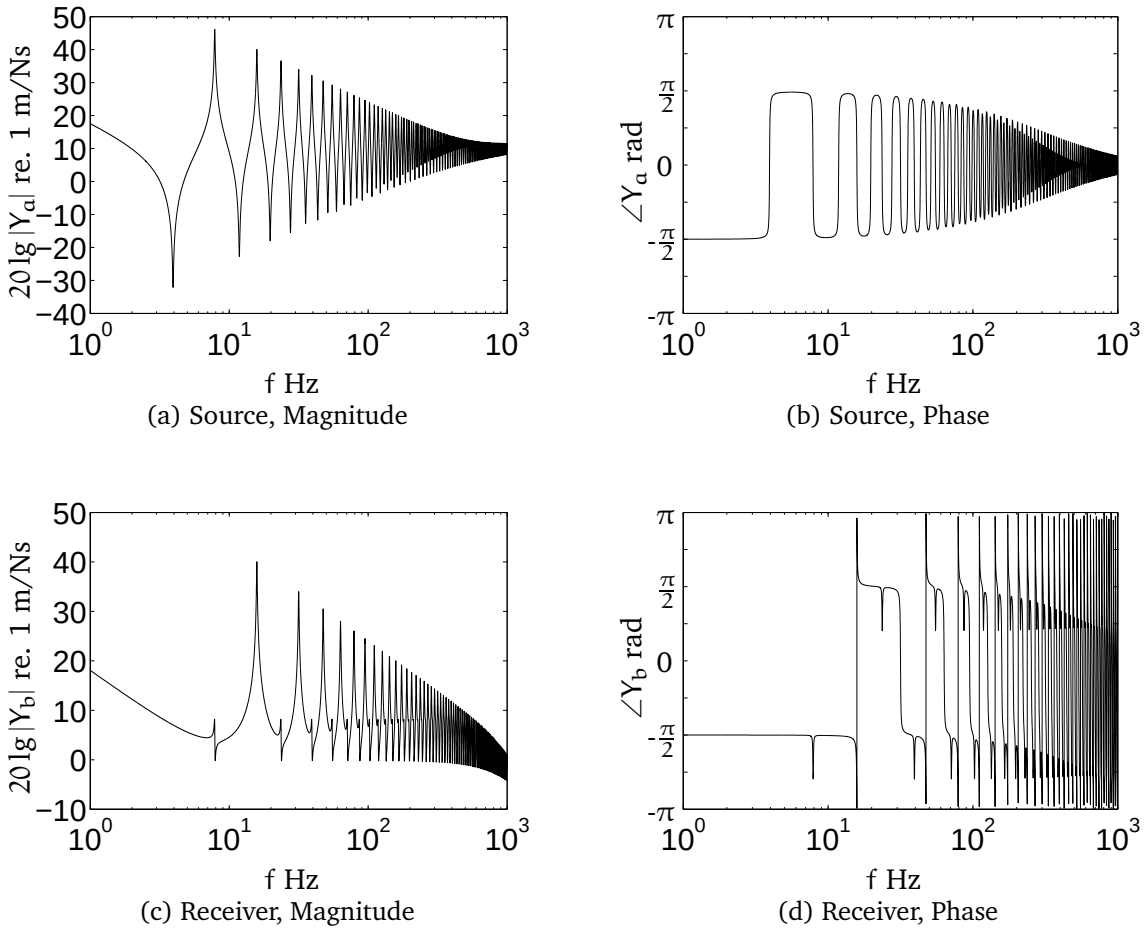

(a) Source, Magnitude (b) Source, Phase

(c) Receiver, Magnitude (d) Receiver, Phase

Figure 7.2: Magnitude and phase of driving-point mobility at the left end of the source and receiver waveguides. Resonances can be clearly seen as phase jumps, the coupling occurring as small dips, or as local maxima in the magnitude plots.

a softer spring would decouple the subsystems while a stiffer spring would couple them more strongly. At high frequencies acts the spring as a vibration isolation.

The effect of the soft spring is clearly seen on driving-point mobility data at the left end of the receiver subsystem. A jump in magnitude and phase can be seen at the first resonance. If the pickup-point was moved to the middle of a virtual spring rather then to the right end would the mobility data agree with the case of stiffer coupling; see figure 7.3.

The system can be compared to a beam with length 2 m and otherwise identical parameters, see figure 7.4. As can be expected is resonance frequencies unaltered. However; it can be seen that the first resonance in the rigid beam has an antiresonance that is not present in the coupled system. Modes that correspond to

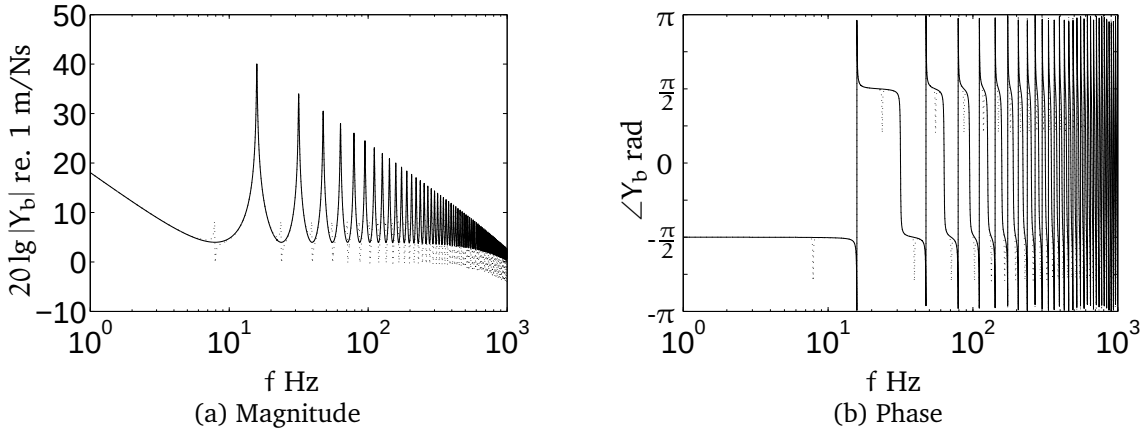

(a) Magnitude (b) Phase

Figure 7.3: Driving-point mobility at the left end of the receiver for the case of stiff spring coupling; the nominal case is dotted.

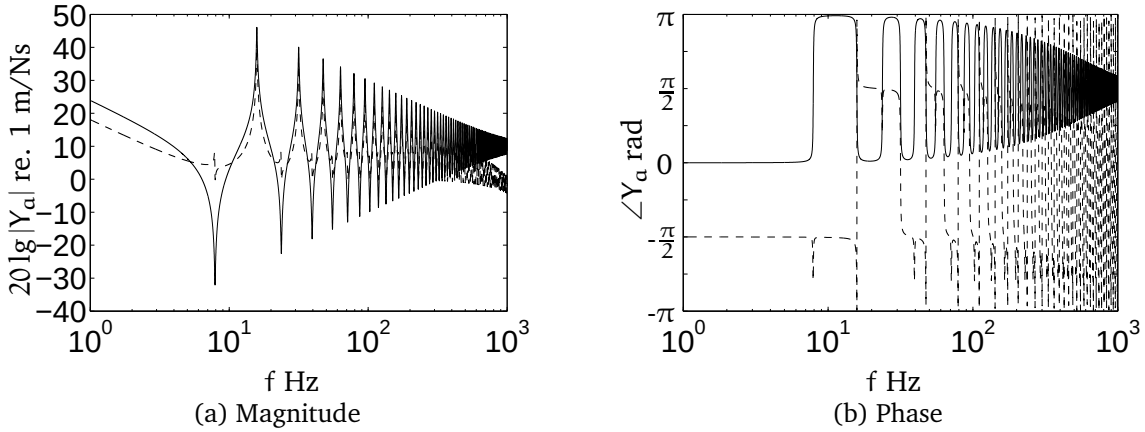

(a) Magnitude (b) Phase

Figure 7.4: Driving-point mobility at the middle of a source system where the length is 2 m; the nominal case is dashed.

subsystem modes in the source and receiver system agrees well with the 2nd and 4th mode in the source system although the response level is lower. At the peak around 15.8 Hz is there a -6.0 dB level difference. This difference is enlarged with frequency as the spring will act like vibration isolation.

A measure of power transport from the source to the receiver is given by relating the observed power input to each other; see figure 7.5. In the plot is three regions seen. Below the first resonance are a spring stiffness controlled region seen. The input force is pushing the source beam against the spring with no significant power transport to the receiver system. The second region is a plateau at

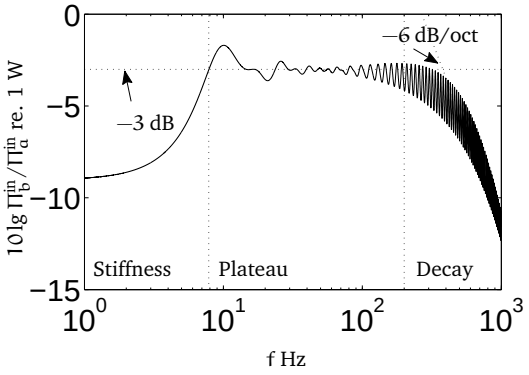

Figure 7.5: Power input difference between source and receiver subsystem.

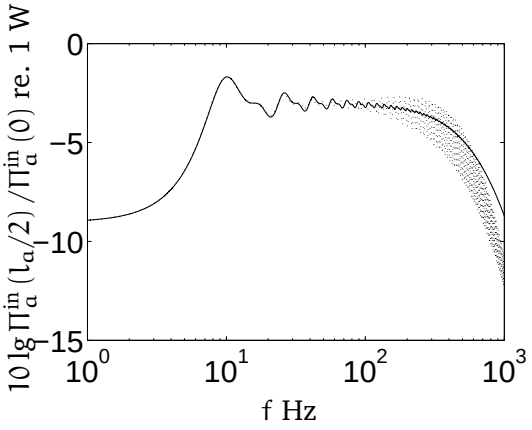

Figure 7.6: Power difference between input power and power flow in the middle of a 2 m long homogeneous beam compared to the nominal case (dotted).

-3.0 dB; the region is characterized by good transmission and half of the power is transported into the receiver system. The transmission is even higher at resonances. As the number of modes increases are the plateau more and more flat. The third region is characterized by the soft spring and the transmission is dropping at a rate of -6.0 dB/oct. Compared to power flow in a coupling with a stiff spring or inside of a rigid beam is the decay faster. The decay can be due to distance attenuation, internal damping in the source subsystem. However; this is not likely as the power flow in the middle of a 2 m long beam is attenuating at a slower rate, see figure 7.6. Hence; the decay is primarily due to that the soft spring acts like a vibration isolation. The transition from a system that acts like a homogeneous beam into a system where the source is isolated from the receiver is clearly seen and starts at around 100 Hz.

Power difference over the coupling is 0 dB due to the energy-conservative coupling. Power difference over the receiver subsystem is not meaningful as the free end demand the longitudinal force to be zero.

CHAPTER 8

Source system

The source system is a single freely suspended beam subjected to partial uncertainty; fluctuation occurs in one and only one parameter for each case. Phenomenon related to different amount of local, global or local and global uncertainty is examined for driving-point mobilities. In the discussion of eigenfrequencies are outliers (up to about 10 of 4000) sorted out. The main reason for their existence is the sensitivity of the peak detection algorithm; sometimes it skips or rather detects more peaks then it should. Realizations showing extreme behavior is presented in line spectrums.

1. Material uncertainty

Local and global effects of material uncertainty should be related to the fact that an increase of density correspond to a decrease of phase speed and increase of characteristic impedance, while an increase of elasticity increase both phase speed and characteristic impedance. In fact, opposite behavior is observed in the behavior of the fundamental resonance; see figures 8.2 and 8.5. For global density uncertainty is it clear that a high resonance frequency correspond to a high response level, while for the elasticity a high frequency gives a low response level. This agrees with the behavior of a mass-spring system; see appendix A. The reason behind is that the eigenfrequency depends on the phase speed while the response level depends on the characteristic impedance. Observations of an resonance in a system subject to local uncertainty creates a domain. However; if the level spread or frequency spread is plotted as a function of the magnitude of uncertainty is an almost linear (triangle) relationship seen, see figure 8.3. For the case of octaveband data is the behavior described above seen for low frequencies where one or few resonances determines the overall level, see 8.1 and 8.4. The resonance frequency shifting results in that the case of elasticity has a higher response level before the resonance cut on and lower above compared to the case of density uncertainty. As the modal density increase, the two kinds of material uncertainty gets more similar to each other. This effect is expected as the shifting of an individual resonance is less important.

For material uncertainty is it seen in the octaveband data that local uncertainty result in large spread at high frequencies while global uncertainty give a large

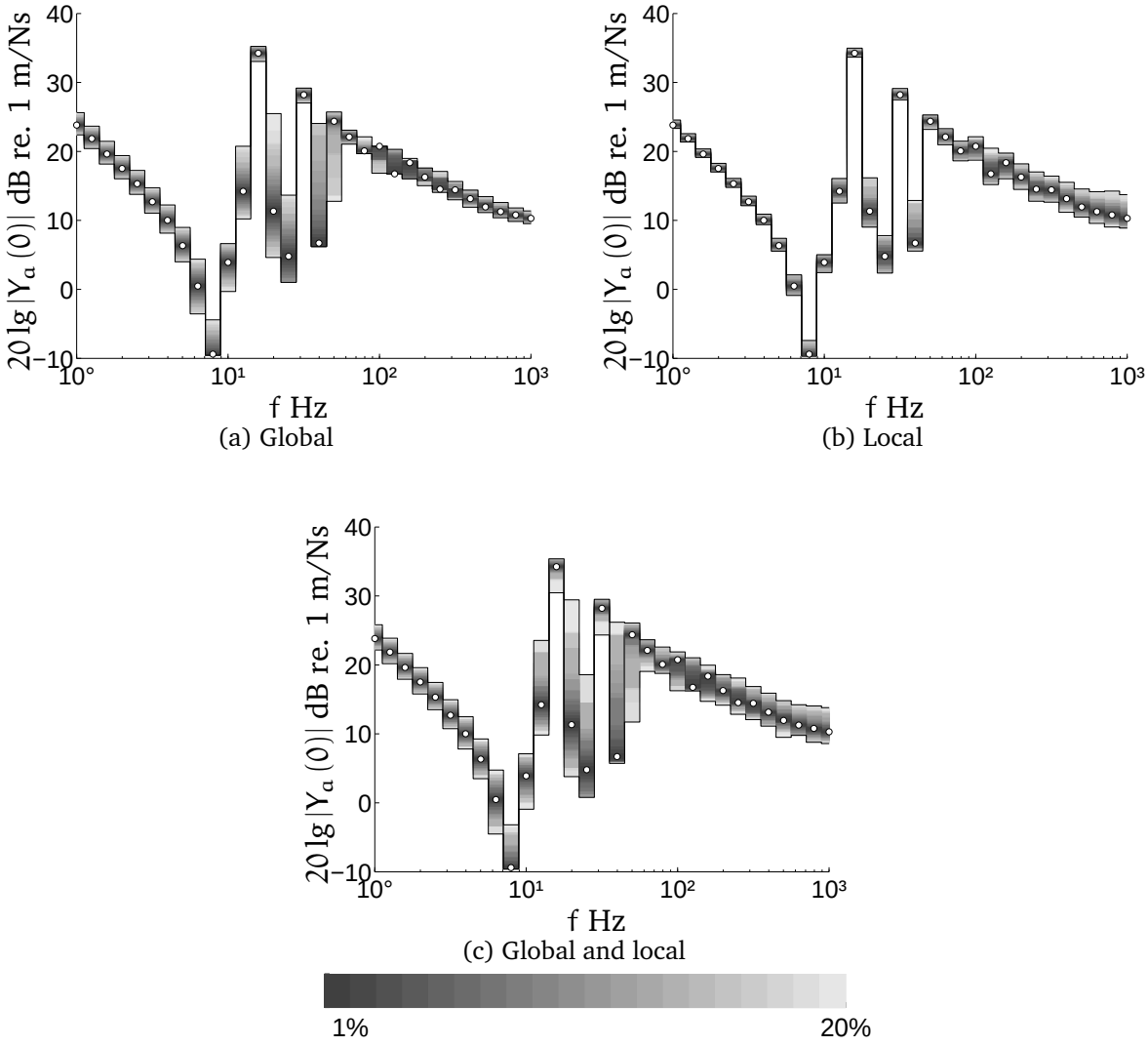

Figure 8.1: Driving-point mobilities dB for a beam subjected to density uncertainty presented in octaveband data. The case of global, local or global and local uncertainty is shown.

spread at low frequencies. As the wavelength shorten should effects of waveguide imperfections be pronounced; however, the cut on for partition resonances is above 15 kHz and clear effects of local uncertainty compared to global is seen from 50 Hz. It can be seen that the response level at high frequencies are exceeding the nominal response; especially, for the case of a large amount of uncertainty.

Realizations with local and global uncertainty has an overall big spread in low and high frequencies; almost as if it was superposed from the separate observations. As expected is the spread between realizations increasing with the amount of uncertainty; from 5% is the spread in a few dB.

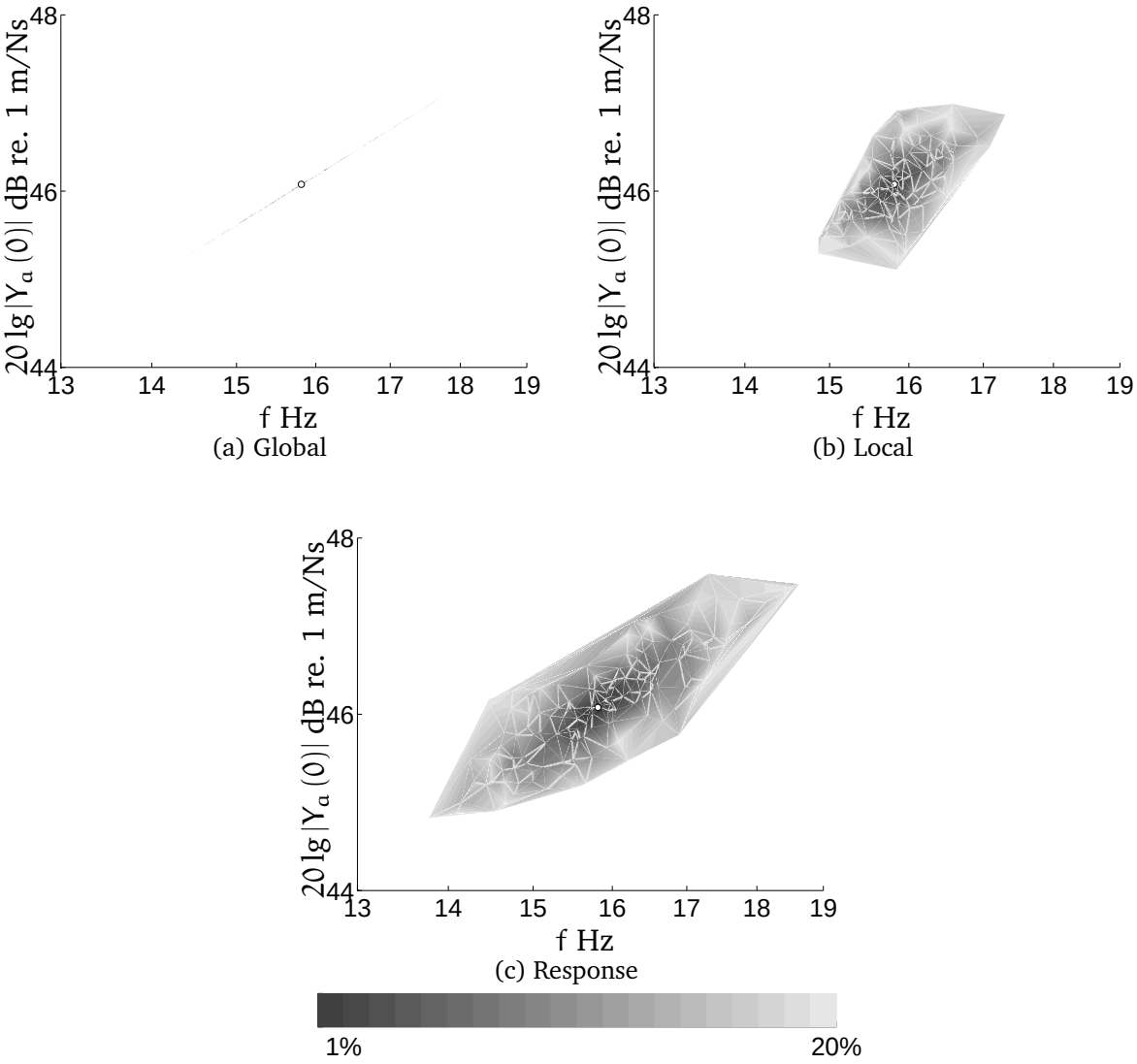

(a) Global

(b) Local

(c) Response

Figure 8.2: Mobility response for the fundamental resonance for a beam subjected to density uncertainty as detected by a peak detection algorithm.

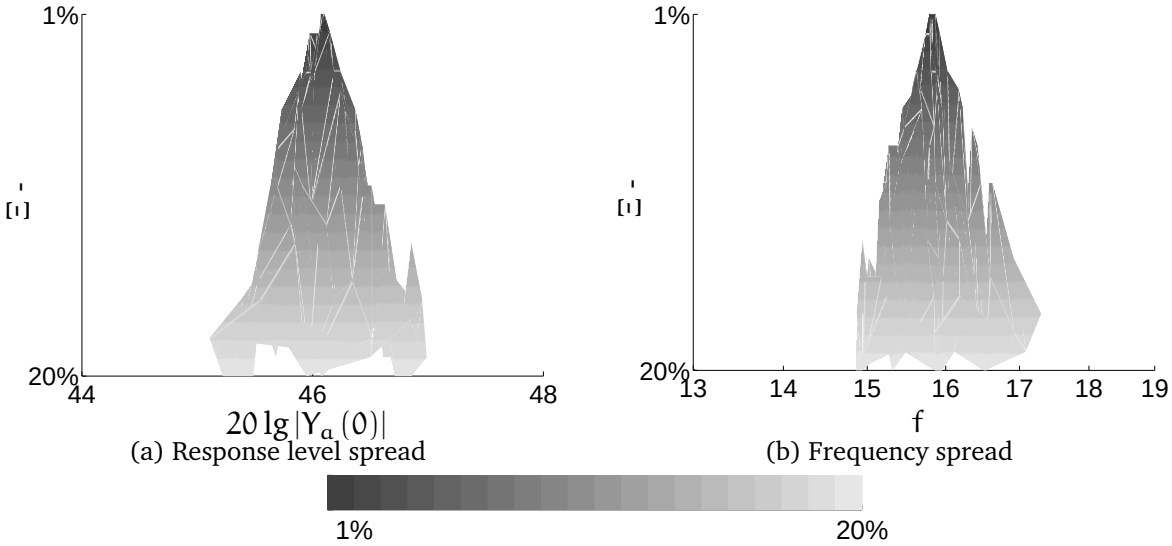

(a) Response level spread (b) Frequency spread

Figure 8.3: Response variation as a function of magnitude of uncertainty illustrated for the case of local density fluctuation in a beam. An almost symmetric and linear relationship has been observed for all examined eigenfrequencies; however the response as a function of level-frequency varies a lot.

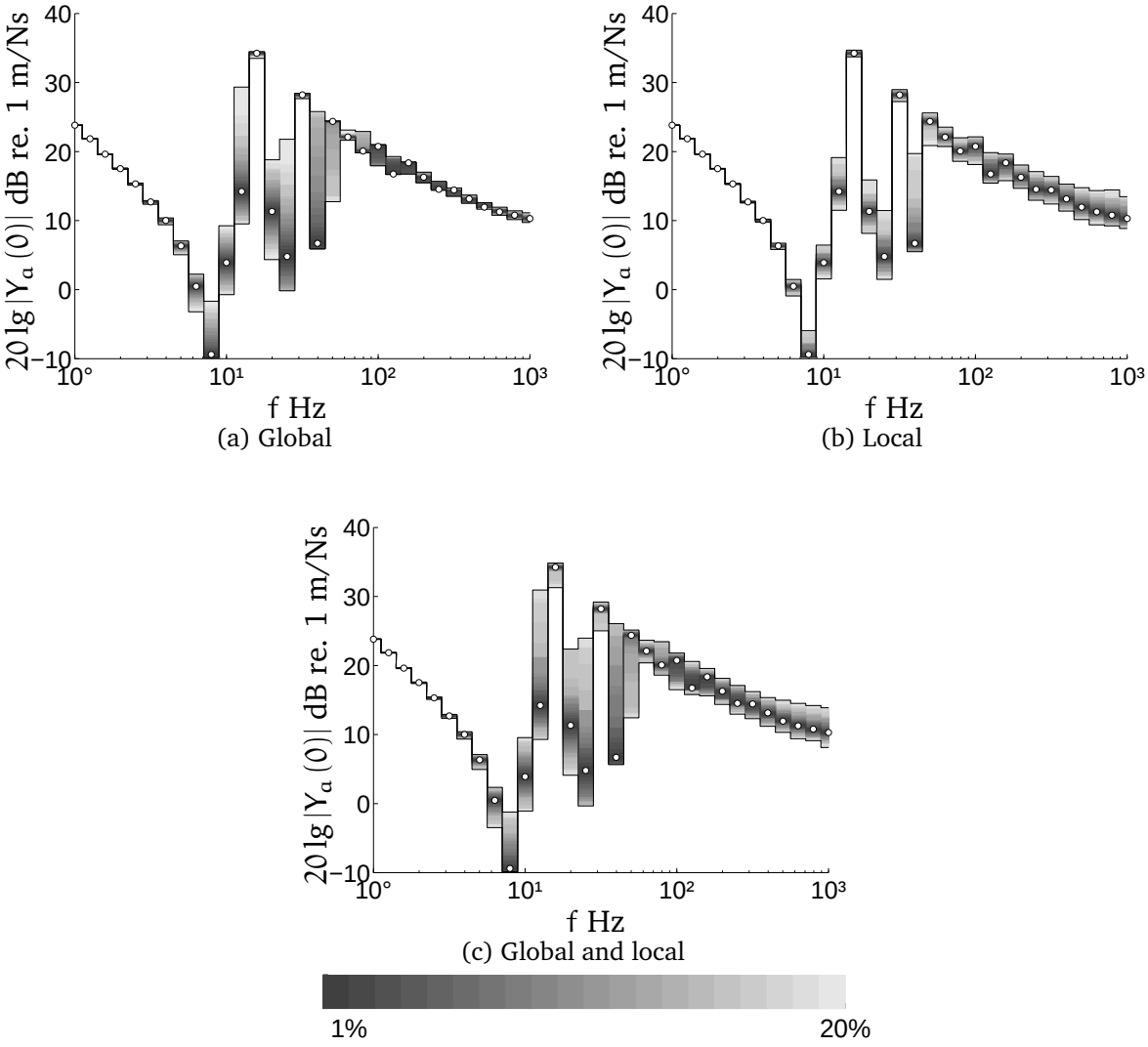

(a) Global

(b) Local

(c) Global and local

Figure 8.4: Driving-point mobilities dB for a beam subjected to elasticity uncertainty presented in octaveband data. The case of global, local or global and local uncertainty is shown.

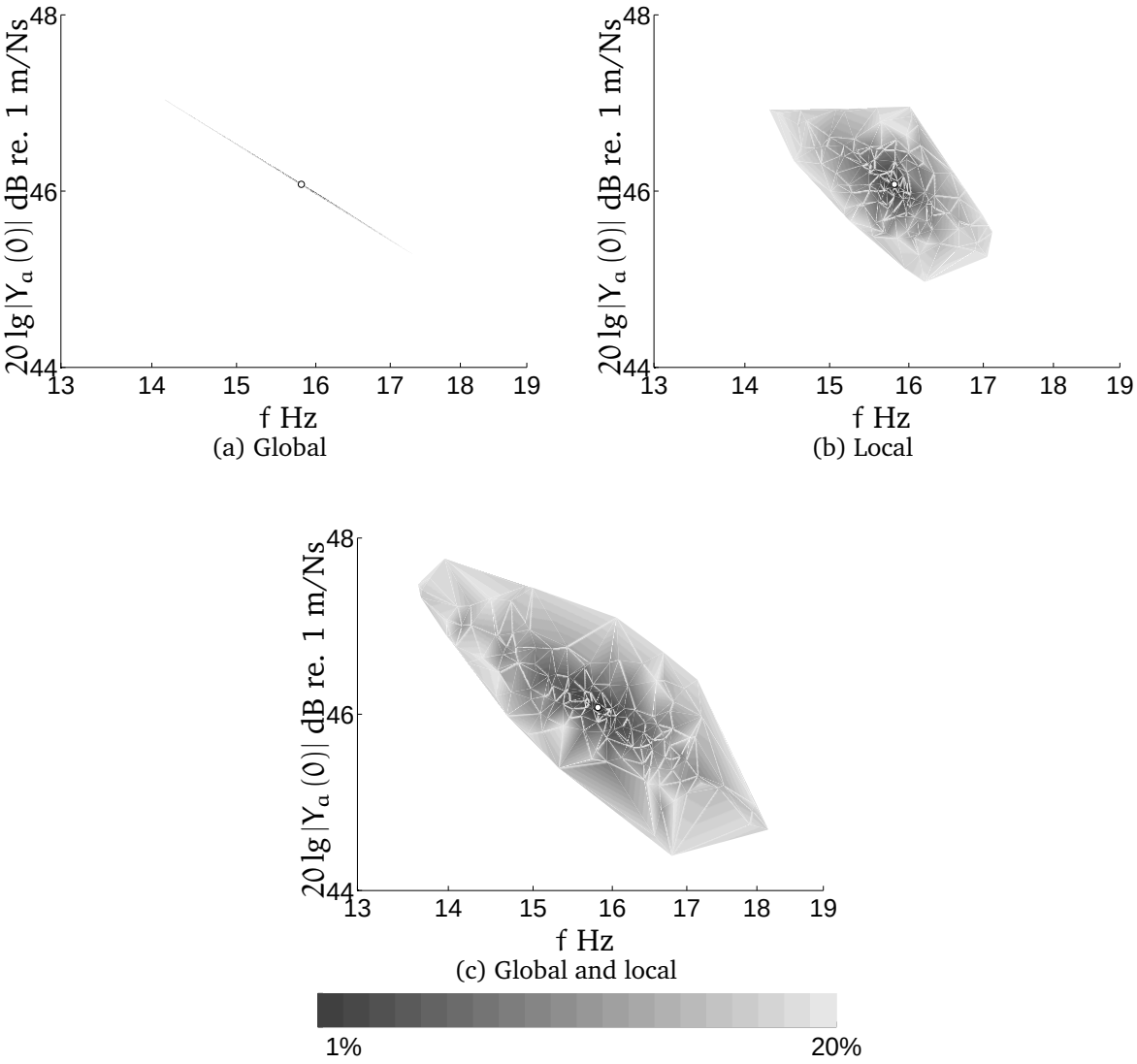

(a) Global

(b) Local

(c) Global and local

Figure 8.5: Mobility response for the fundamental resonance for a beam subjected to elasticity uncertainty as detected by a peak detection algorithm. The case of global, local or global and local uncertainty is shown. Outliers has been removed.

2. Damping uncertainty

The behavior of the fundamental resonance when the system is subject to loss-factor fluctuation agrees with the behavior of a mass-spring system. No shifting of frequency occurs while the response level is changed. An increase of loss-factor correspond to an increase of spatial attenuation. The outcome is therefore a straight line rather then an area. Global fluctuation has bigger effects on the response level compared to local fluctuation. As the modal density increase is the level spread decreasing. Furthermore; the response level has a symmetric linear relationship (triangle) to the amount of uncertainty present.

Examining observed mobilities, see 8.6, reveal that response level differences are much less pronounced then for other cases. This can be interpreted as that it is the variance of resonance frequencies of the eigenfrequencies rather then the resonance response levels that result in wideband spread of response levels. It is clear that the loss-factor only effects the response when there is modes in the octaveband.

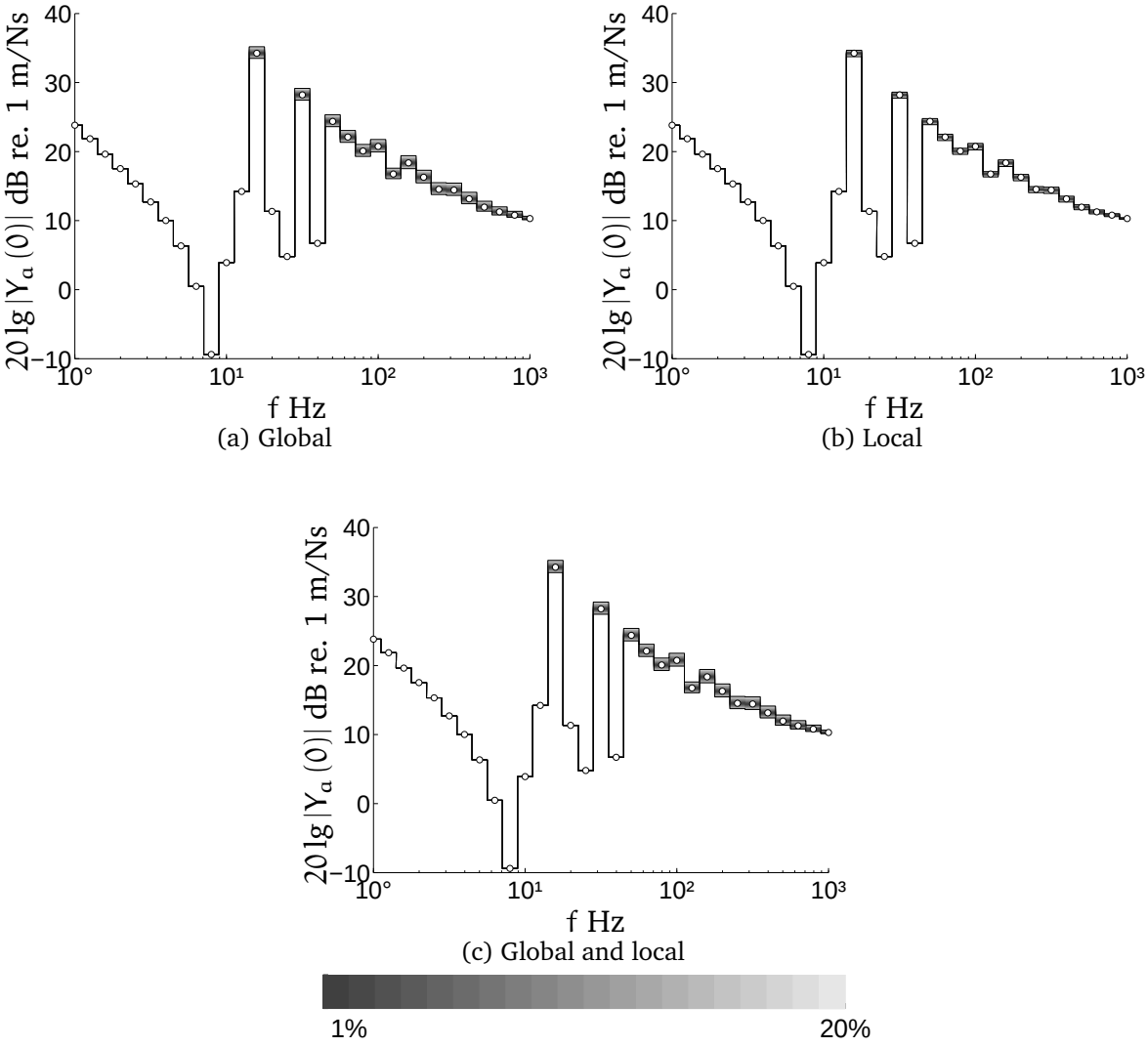

Figure 8.6: Driving-point mobilities dB for a beam subjected to loss-factor uncertainty presented in octaveband data. The case of global, local or global and local uncertainty is shown.

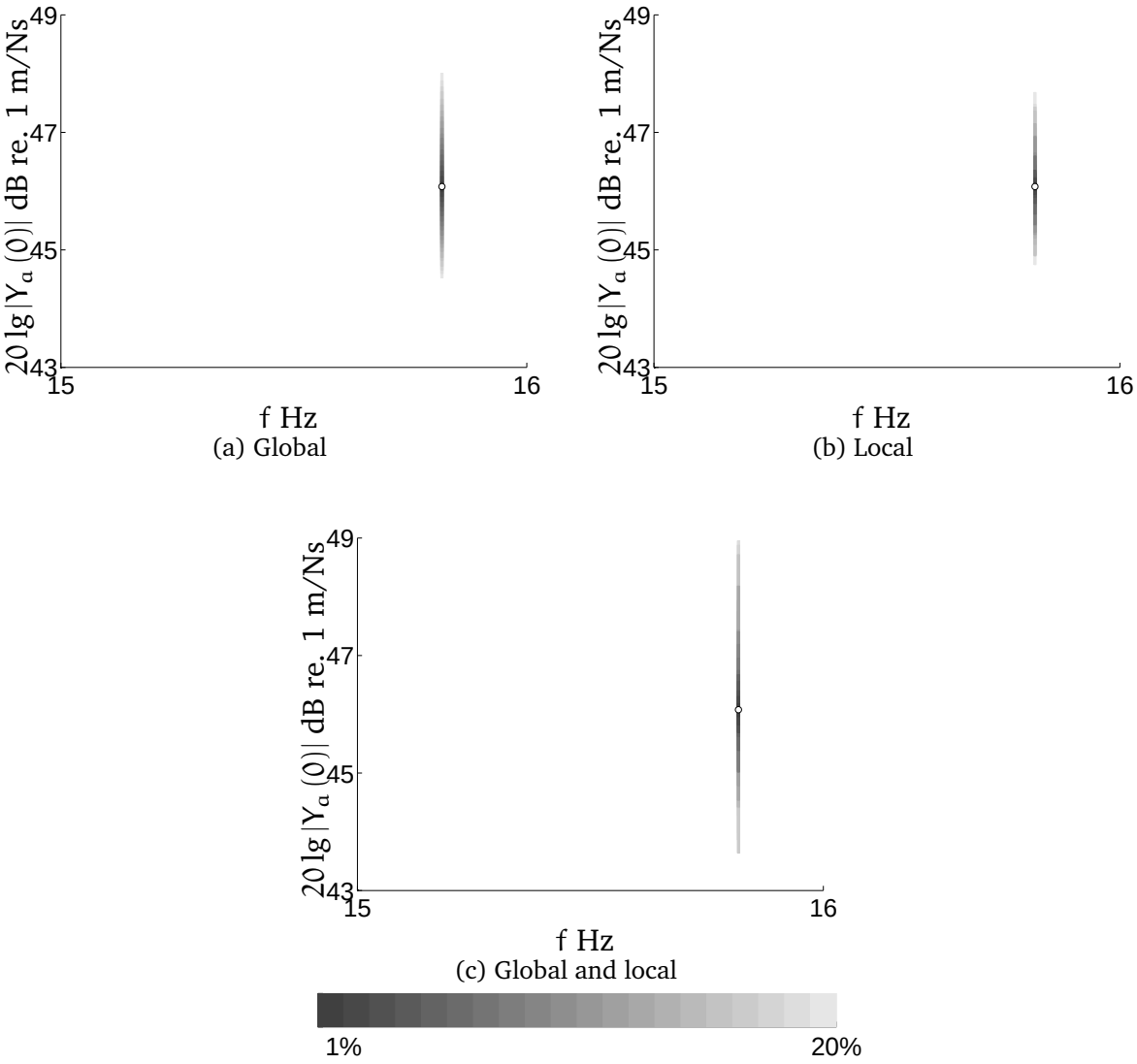

(a) Global

(b) Local

(c) Global and local

Figure 8.7: Mobility response for the fundamental resonance for a beam subjected to loss-factor uncertainty as detected by a peak detection algorithm. The case of global, local or global and local uncertainty is shown. Outliers has been removed.

3. Geometrical uncertainty

Fluctuation of cross-section surface has a higher impact on the response compared to damping and material cases. It can be expected as the characteristic impedance has a linear dependency on cross-section surface. On the other hand is the phase speed independent of cross-section surface. Hence; effects of impedance mismatch between partitions are seen.

Global uncertainty result in a frequency invariant scaling of driving-point mobility data, see 8.8. As the characteristic impedance is in the denominator is an increase of cross-section area corresponding to a decrease of response level; a result which agrees with a longitudinal rod in appendix A. As expected is the spread symmetric around the nominal behavior. Local uncertainty is different and large discrepancies compared to the nominal behavior is observed, especially for higher frequencies. The spread of response level is in the order of several dB even for moderate amount of uncertainty ($< 5\%$). Ensemble largest high frequency response is more flat in level decay compared to the other cases of uncertainty.

The fundamental resonance, see 8.9, is constant for the case of global uncertainty, only the response level fluctuates; which agrees with a mass-spring system in appendix A. The fluctuation of resonance response level is similar for the case of local uncertainty when examined from how it react to the amount of uncertainty. Local uncertainty result in a large domain for a given amount of uncertainty. That resonance frequency shift occurs for the local case can be explained by a change of mode shape. The combined case of local and global uncertainty is more “oval” in the shape compared to the “rectangular” local shape. The spread is also slightly bigger.

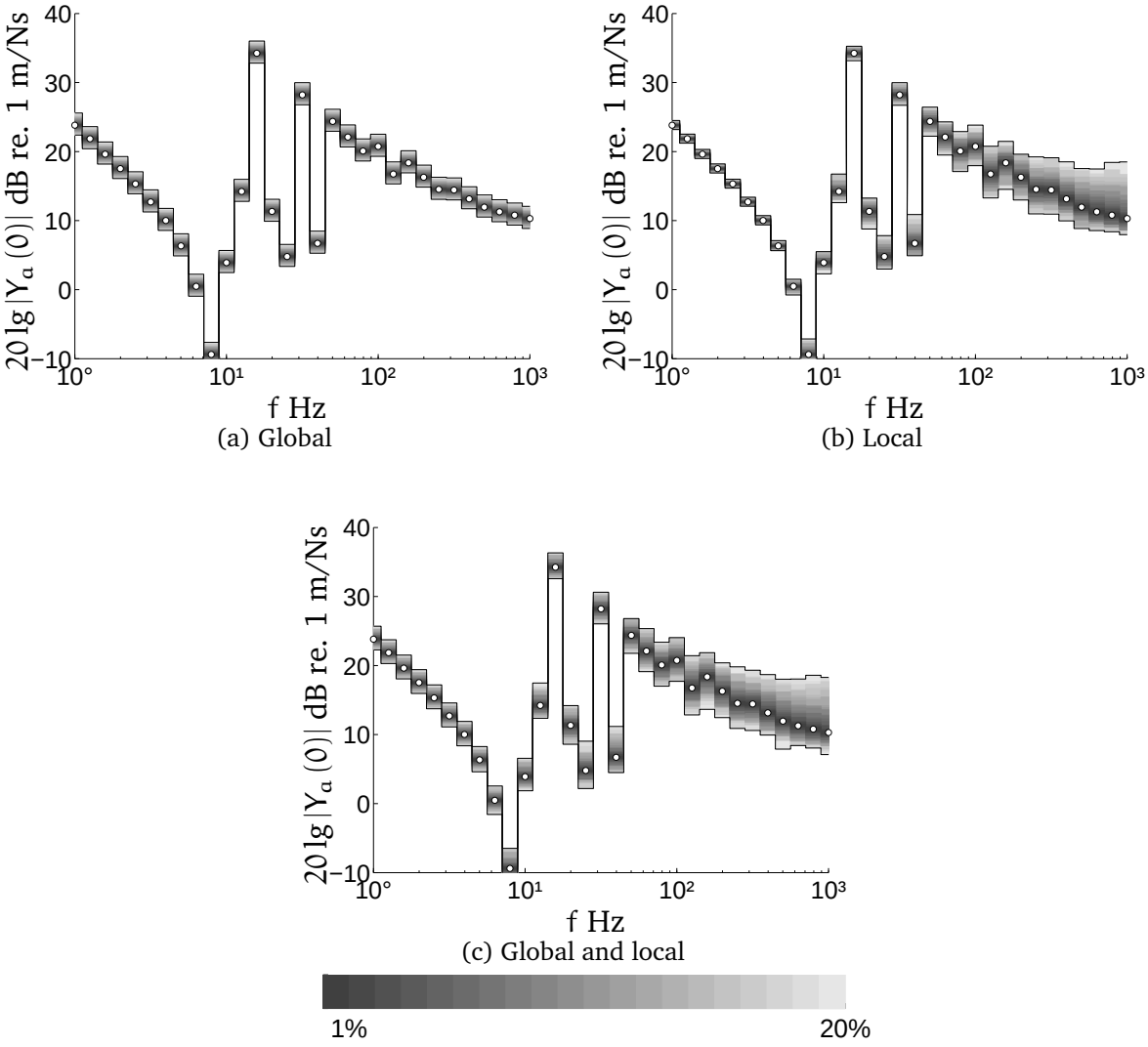

(a) Global

(b) Local

(c) Global and local

Figure 8.8: Driving-point mobilities dB for a beam subjected to cross-section surface uncertainty presented in octaveband data. The case of global, local or global and local uncertainty is shown.

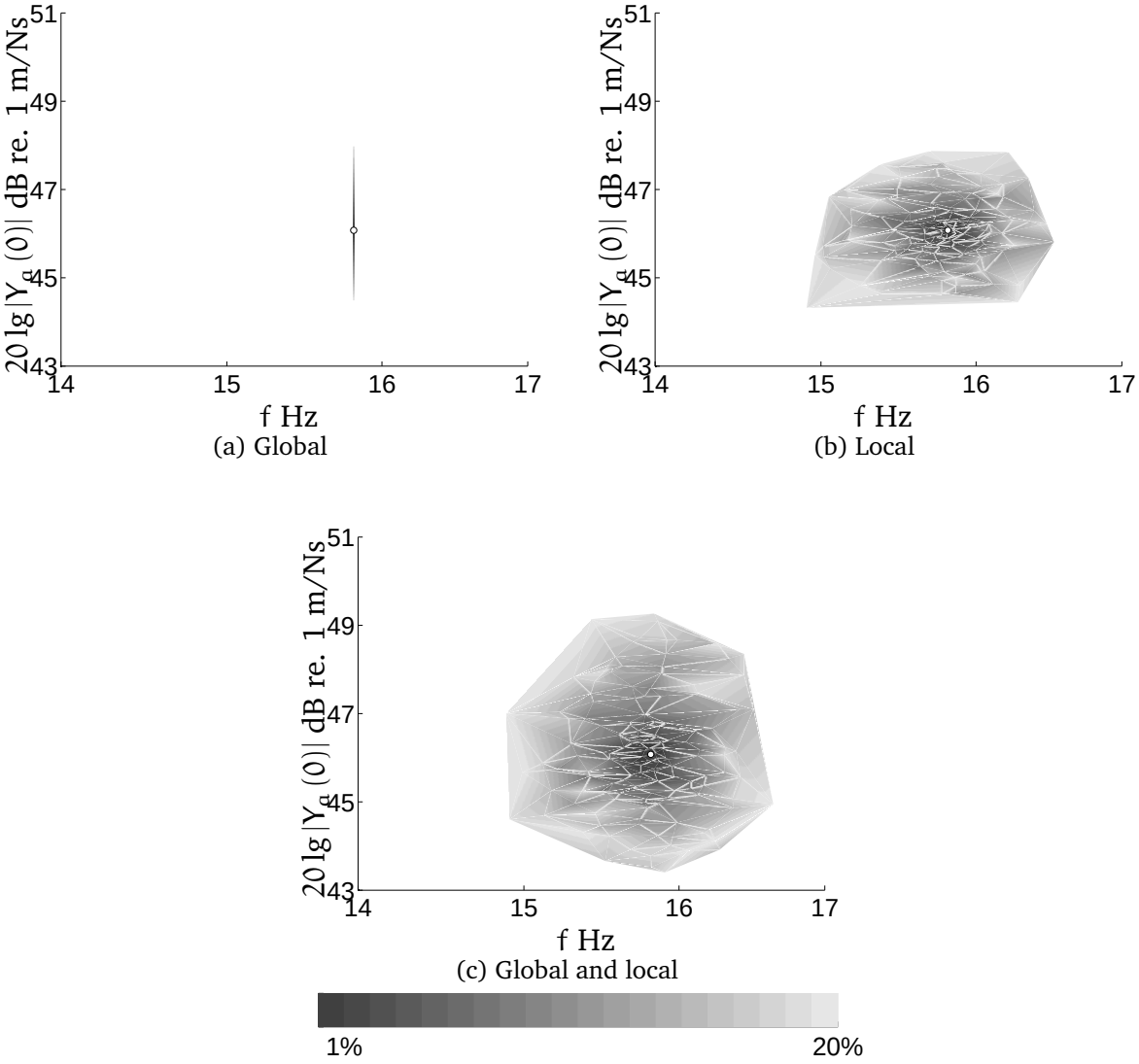

(a) Global

(b) Local

(c) Global and local

Figure 8.9: Mobility response for the fundamental resonance for a beam subjected to cross-section surface uncertainty as detected by a peak detection algorithm. The case of global, local or global and local uncertainty is shown. Outliers has been removed.

		Δf Hz	ΔL dB	
ρ	Global	3.2	1.8	Sym. line, level inc. with freq.
	Local	2.5	1.9	Small domain
	Both	4.9	2.8	Large domain
E	Global	3.2	1.8	Sym. line, level dec. with freq.
	Local	2.8	2.0	Small domain
	Both	4.5	3.4	Large domain
η	Global	0.0	3.5	Ver. line
	Local	0.0	2.9	Ver. line
	Both	0.0	5.3	Ver. line
S	Global	0.0	3.5	Ver. line
	Local	1.6	3.6	Large rectangular domain
	Both	1.8	5.1	Large oval domain

Table 8.1: A brief summary of spread on the fundamental resonance due to different kind of uncertainty. The spread between the largest of largest and smallest of smallest observed response level and resonance frequency is given for the case of $\pm$20% of uncertainty.

4. Summary

Geometrical, damping and material uncertainty has different characteristic. The global behavior agrees with a mass-spring system when resonances are examined. Local behavior is increasingly important with frequency. A brief summary of response spread for resonances can be found in table 8.1 and for driving-point mobility data in table 8.2. Observed phenomenon include frequency shifting which explain the large discrepancies at low frequencies, response scaling which is most clearly seen for cross-section surface, modal density explain why high frequency bands are less sensitive to shifting, internal attenuation which makes the precise loss-factor less important at high frequencies. Large response level exceedence compared to the nominal system has been demonstrated.

		$f < f_0^{nom}$ 1 - 10 Hz	$f \sim f_0^{nom}$ 12.5 - 20 Hz	$f > f_0^{nom}$ 25 - 80 Hz	$f \gg f_0^{nom}$ 100 - 1000 Hz	
ρ	Global	Scaling, 3.2-6.3	Shifting, 2.1-20.8	Shifting, 2-17.6	1.8-3.9	Shifting of few modes
	Local	0.9-1.9	2.7-4.6	1.4-7.3	3.4-5.2	Imp. mismatch inc. with freq.
	Both	3.5-6.3	4.9-25.5	3.8-20.5	4.3-5.3	
E	Global	0.0-8.5	Shifting, 1.0-19.8	Shifting, 0.8-21.7	1.0-3.0	Insignificant at low freq.
	Local	0.0-4.4	0.9-6.9	2.7-13.9	3.3-5.1	Insignificant at low freq., exceeds nom.
	Both	0.0-8.6	2.9-21.5	3.2-23.8	3.6-5.3	
η	Global	None, 0.0	No shifting, 0.0-1.7	0.0-1.7	0.5-1.8	Insignificant, only at resonances
	Local	0.0	0.0-0.9	0.0-0.9	0.2-0.9	Spread decrease with freq.
	Both	0.0	0.0-1.7	0.0-1.7	0.5-1.9	
S	Global	Scaling, 3.2	3.2	3.2	3.2	Freq. invariant
	Local	1.0-2.9	1.9-3.6	2.9-5.6	5.6-10.4	Imp. mismatch, exceeds nom.
	Both	3.4-4.3	3.7-5.1	4.3-6.2	5.6-10.7	

Table 8.2: A brief summary of spread on octaveband driving-point mobility data due to different kind of uncertainty. Smallest and largest spread between averages are given in dB for the case of $\pm 20\%$ of uncertainty.

CHAPTER 9

Source and receiver system

The source and receiver system consist of two spring coupled beams. The source subsystem is excited by an unit force at the left end and coupled at the right end; one of the main interesting things is to study how power flow to the receiver subsystem is effected by uncertainty. Phenomenon related to different amount of local, global or local and global uncertainty is examined.

1. Material uncertainty

Power transmission between the subsystems are at a first glance similar for the case of elasticity or density uncertainty, see figures 9.2 and 9.3. However; global elasticity fluctuation tend to have a bigger spread at low-frequencies (around 2.1 dB) compared than is observed for global density (up to 1.7 dB) uncertainty. On the other hand is the response level spread bigger at high-frequencies for density fluctuation. For the case of local uncertainty is only minor differences (< 0.1 dB) observed between density and elasticity fluctuation; likely due to that the relative effect on the characteristic impedance is the same. As expected is the spread increased as the wavelength shortens.

As the source and receiver where chosen to be identical, is the nominal case expected to correspond to the largest possible power transmission. As expected is the power transmission observed already at low magnitude of uncertainty (1%) to be far lower; but, only at the frequency region adjacent to the fundamental resonance. Examining the power input to the individual subsystems, a slightly higher power input to the receiver subsystem and slightly lower power input to the source subsystem is observed, see figure 9.1. The discrepancy can be seen in that the nominal value (represented by a dot) is not centered in the darker grey region. Better transmission than for the nominal system can be seen at frequencies further away from the fundamental resonance.

Driving-point mobilites are examined at the left end of the source subsystem and at the left end of the receiver subsystem, see figures 9.4 and 9.5. Global density fluctuation has large impact in octavebands adjacent to low-frequency resonance frequencies; the response can exceed the nominal subsystem with up to 17.8 dB for density and 14.2 dB for elasticity uncertainty. The same effect can be seen for global elasticity fluctuation. However; compared to the case of global

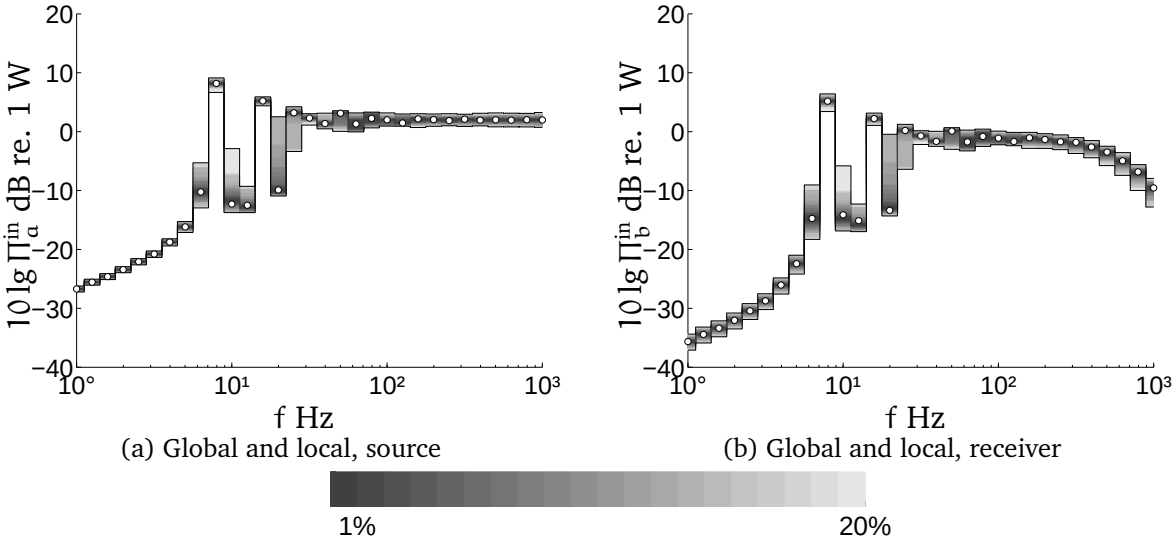

(a) Global and local, source

(b) Global and local, receiver

Figure 9.1: Input power to source and receiver in dB re. 1 W when density is fluctuating (local and global).

elasticity is the spread below or far above the fundamental resonance larger for density fluctuation. Inbetween is an area where a few modes determine the system response and where the spread is larger for elasticity fluctuation. The case of global and local uncertainty shows a spread at low and high frequencies due to the respective kind of uncertainty. Finally; as the magnitude of uncertainty increase tend the response level to increase at the source and decrease at the receiver subsystem; likely a result of increased impedance mismatch between the subsystems.

While the frequency and level spread in absolute numbers are almost identical, can major differences between elasticity and density uncertainty be seen when individual resonances are examined; see figure 9.7 and 9.8. The response is measured at the left end of the source and at the right end of the receiver due to that resonances are expected to have a maxima at the boundaries. If the left end of the receiver is used as pickup is the first resonance near to a region of low response; a nodal point in a rigid beam, which result in large sensitivity to the uncertainty, see figure 9.6. The difference is that density uncertainty result in a higher response level when the resonance is shifted upwards in frequency; while the opposite behavior is seen for elasticity uncertainty. Hence; the result agrees with the behavior seen for a longitudinal beam in the previous chapter and a mass-spring system. The frequency spread is as expected identical between the two subsystems; while the response level spread is about twice as large for the source subsystem.

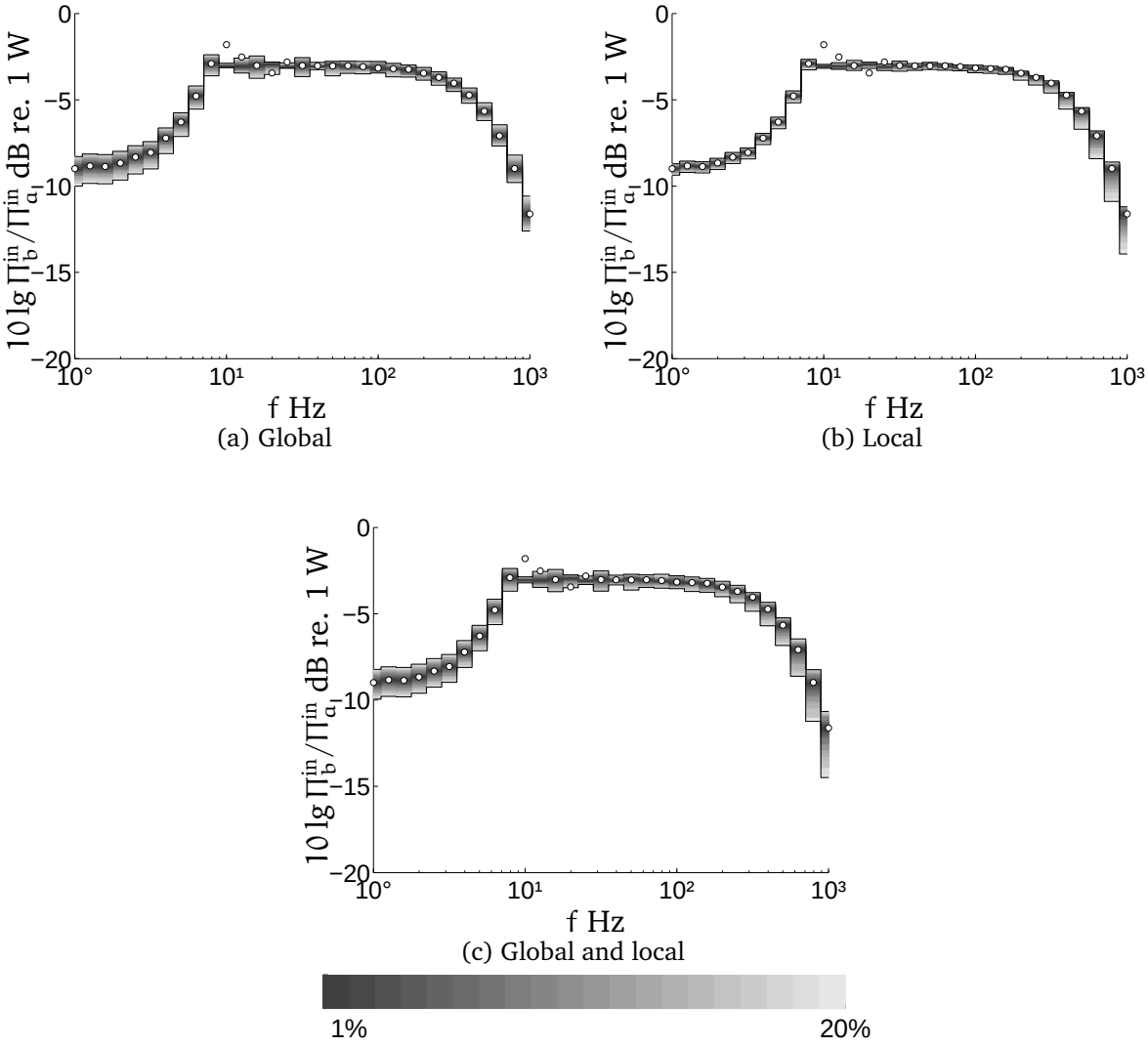

(a) Global

(b) Local

(c) Global and local

Figure 9.2: Input power difference between source and receiver in dB re. 1 W when density is uncertain. The case of global, local or global and local uncertainty is shown.

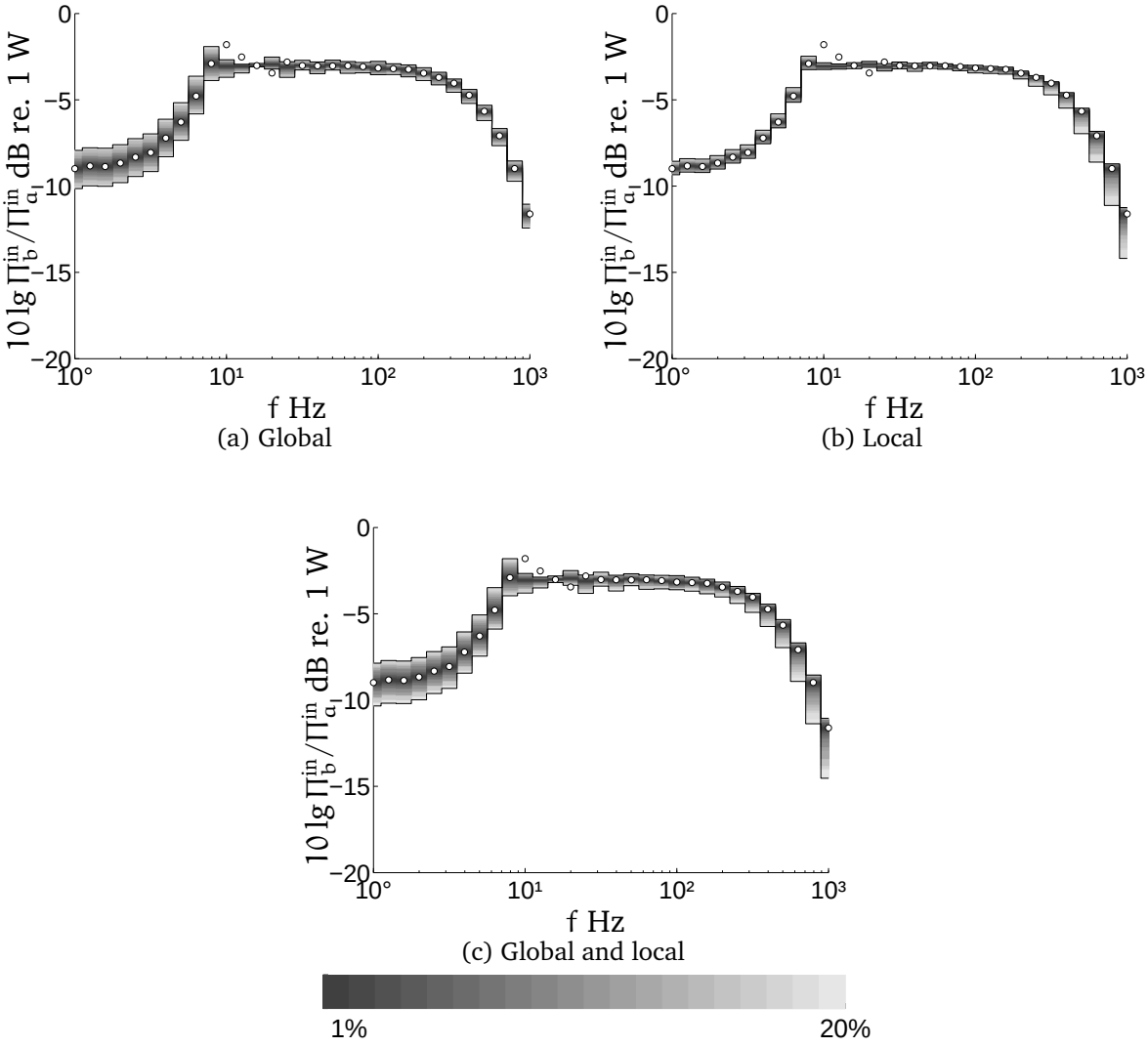

Figure 9.3: Input power difference between source and receiver in dB re. 1 W when elasticity is uncertain. The case of global, local or global and local uncertainty is shown.

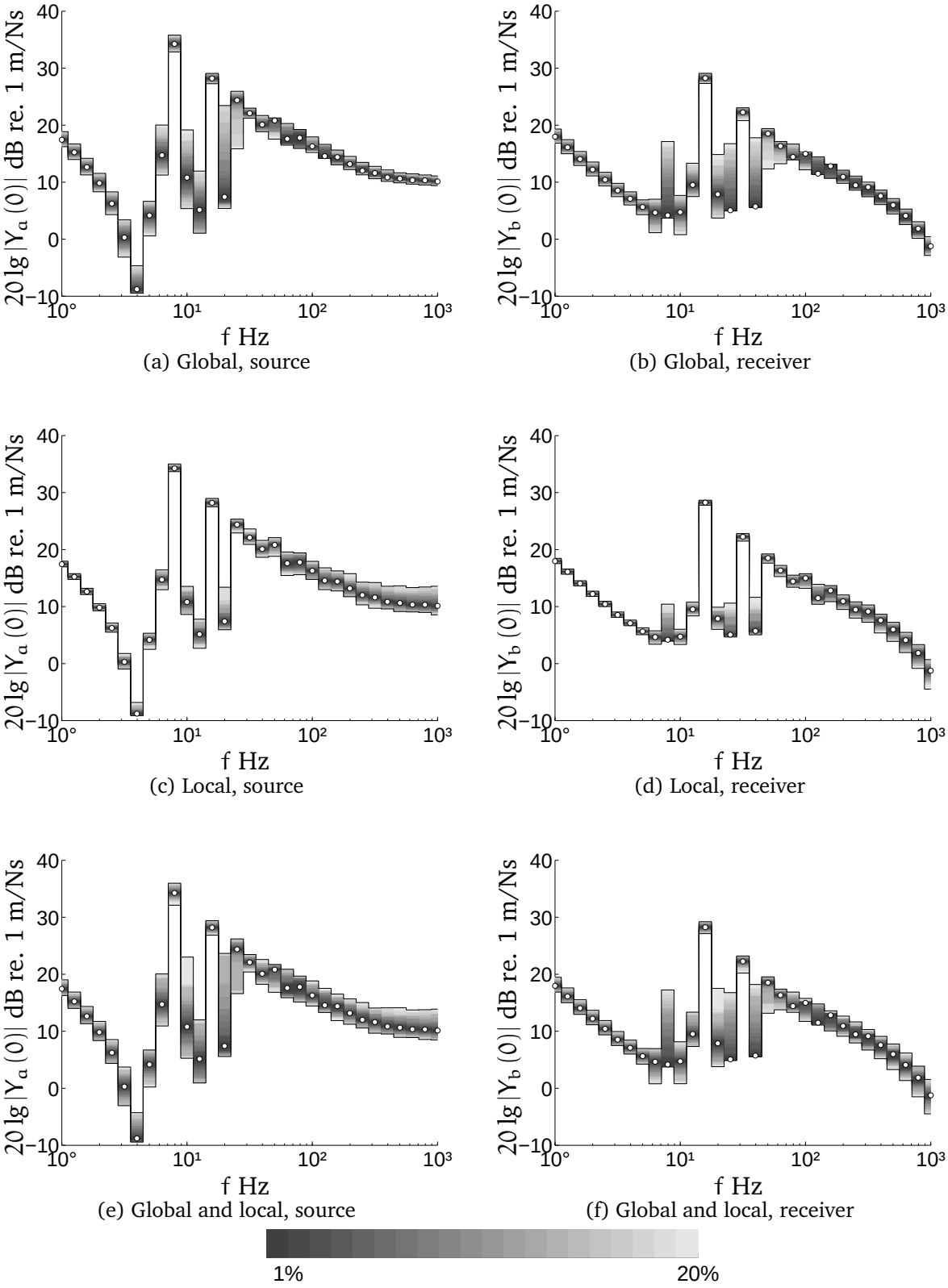

(a) Global, source
(b) Global, receiver
(c) Local, source
(d) Local, receiver
(e) Global and local, source
(f) Global and local, receiver

Figure 9.4: Averages of observed largest and smallest values of driving-point mobilities dB re. 1 for a source and receiver system for the case of density fluctuation. The case of global, local or global and local uncertainty is shown.

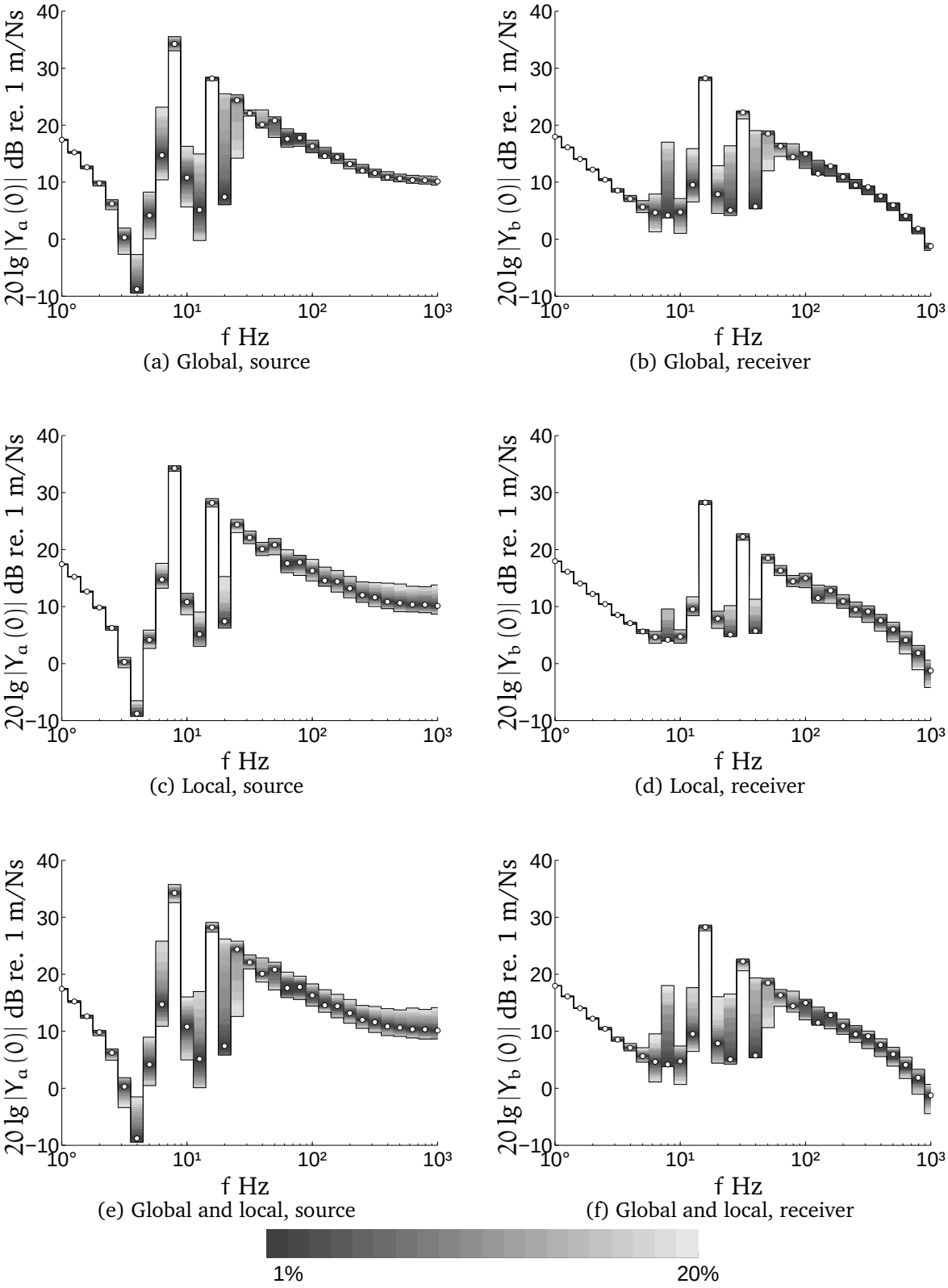

(a) Global, source
(b) Global, receiver
(c) Local, source
(d) Local, receiver
(e) Global and local, source
(f) Global and local, receiver

Figure 9.5: Averages of observed largest and smallest values of driving-point mobilities dB re. 1 for a source and receiver system for the case of elasticity fluctuation. The case of global, local or global and local uncertainty is shown.

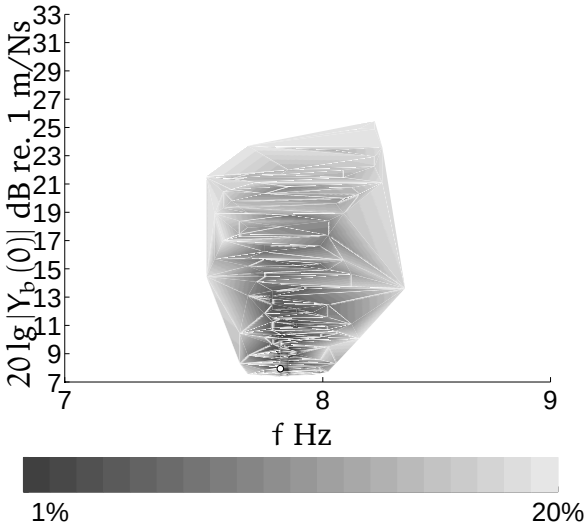

Figure 9.6: Observed spread of the first harmonic for the receiver system when density is fluctuating (local and global), the result is sensitive to uncertainty as the pickup point is near a region of low response.

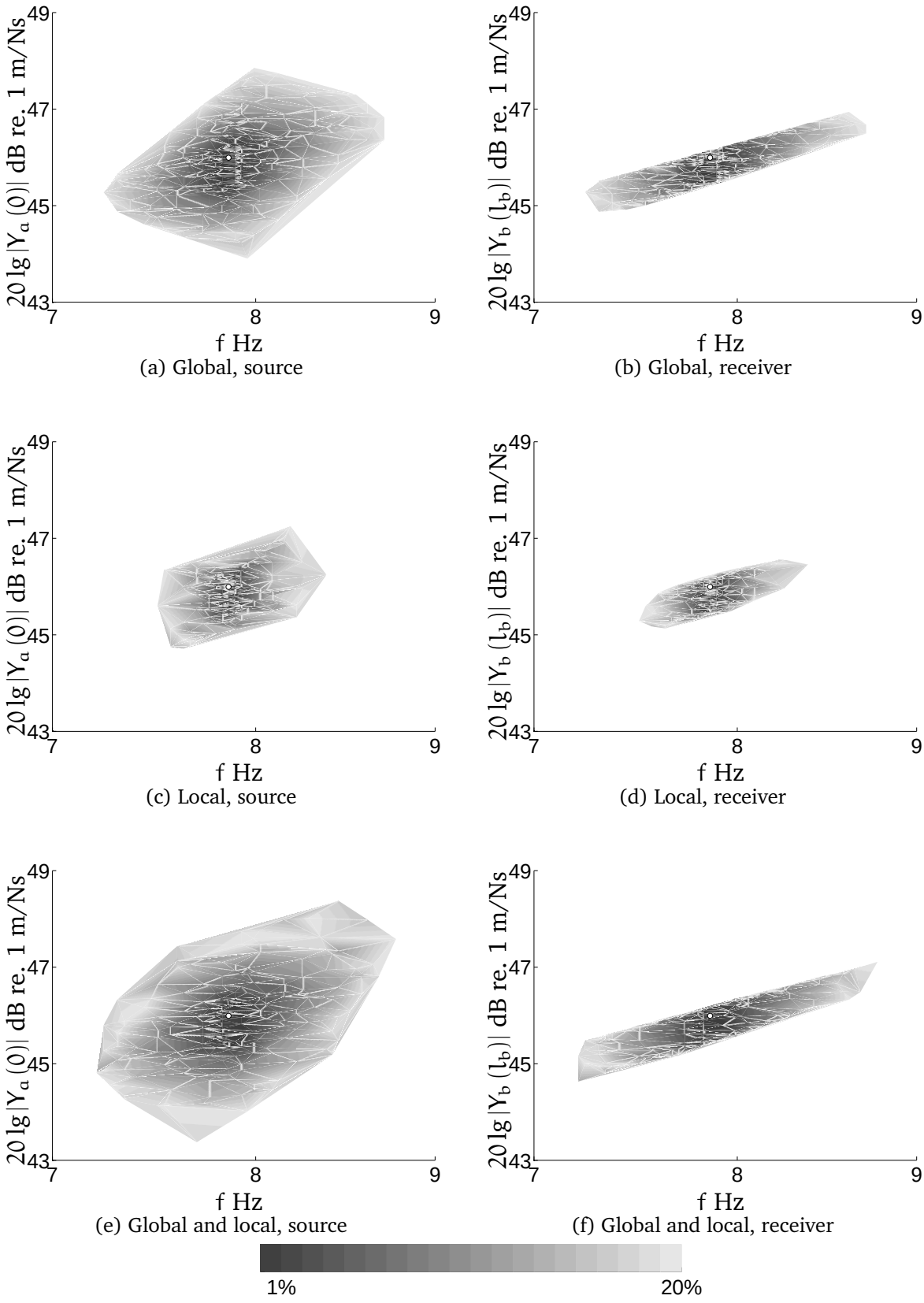

(a) Global, source
(b) Global, receiver
(c) Local, source
(d) Local, receiver
(e) Global and local, source
(f) Global and local, receiver

Figure 9.7: Observed spread of the first harmonic for a source and receiver system where density is fluctuating. The case of global, local or global and local uncertainty is shown.

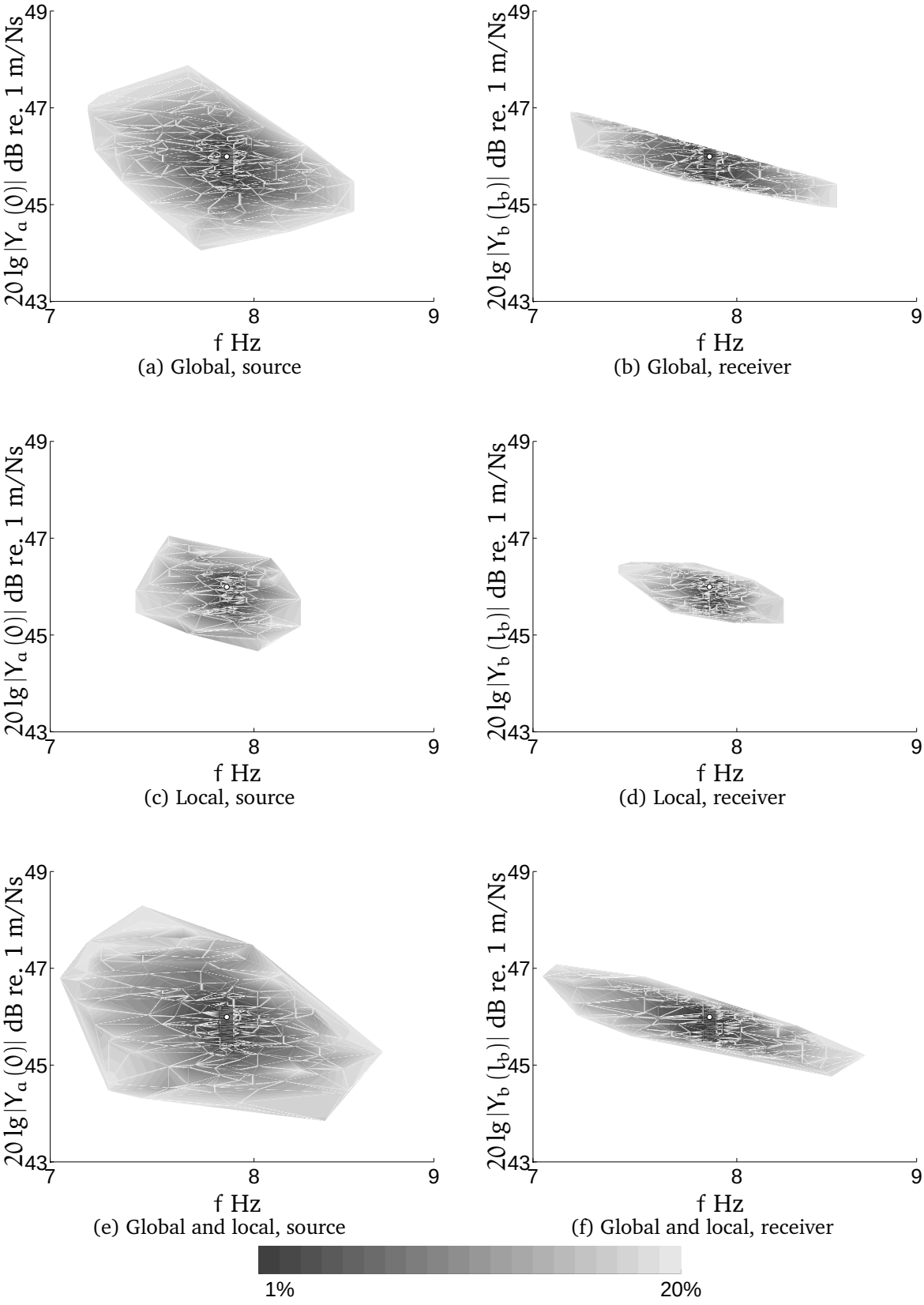

(a) Global, source
(b) Global, receiver
(c) Local, source
(d) Local, receiver
(e) Global and local, source
(f) Global and local, receiver

Figure 9.8: Observed spread of the first harmonic for a source and receiver system where elasticity is fluctuating. The case of global, local or global and local uncertainty is shown.

2. Damping uncertainty

Global fluctuation of loss-factor has a clear impact on the net power transport between the subsystems, see figure 9.9. The spread is symmetric around the nominal behavior. The spread is around 1.5 dB for the plateau region and increases below (up to 2.1 dB) and above (up to 3.2 dB) the region. The effect should be related to the difference in spatial attenuation in the source subsystem. Effects due to local fluctuation of loss-factor is negligible (less than 0.8 dB); the mean loss-factor is roughly constant. Global and local uncertainty is similar to the case of global uncertainty.

Minor effects due to damping uncertainty is seen in the mobility response, see figure 9.10. As the loss-factor only influence the damping of modes, no frequency shifting occur, are most low-frequency octavebands observed to be invariant. For higher frequencies are the spread decreasing with frequency for the source subsystem and increasing for the receiver subsystem. The largest spread is observed to be around 3 dB for the case of 20% of global and local uncertainty at the receiver pickup; which is very little compared to material or geometrical uncertainty.

Examining the fundamental resonance is quite interesting. Loss-factor fluctuation is the only source of uncertainty that was observed to influence the source and receiver pickup in exact the same way, see figure 9.12. No shifting occur for the fundamental resonance, only the response level is changed. However; an neglectable frequency shift (< 0.03 Hz) was observed for both local and global uncertainty at the receiver left end, see figure 9.11. The response level spread is notable bigger when global uncertainty is present (up to 3 dB); this can be expected as the mean loss-factor can be expected to fluctuate less for the case of local uncertainty.

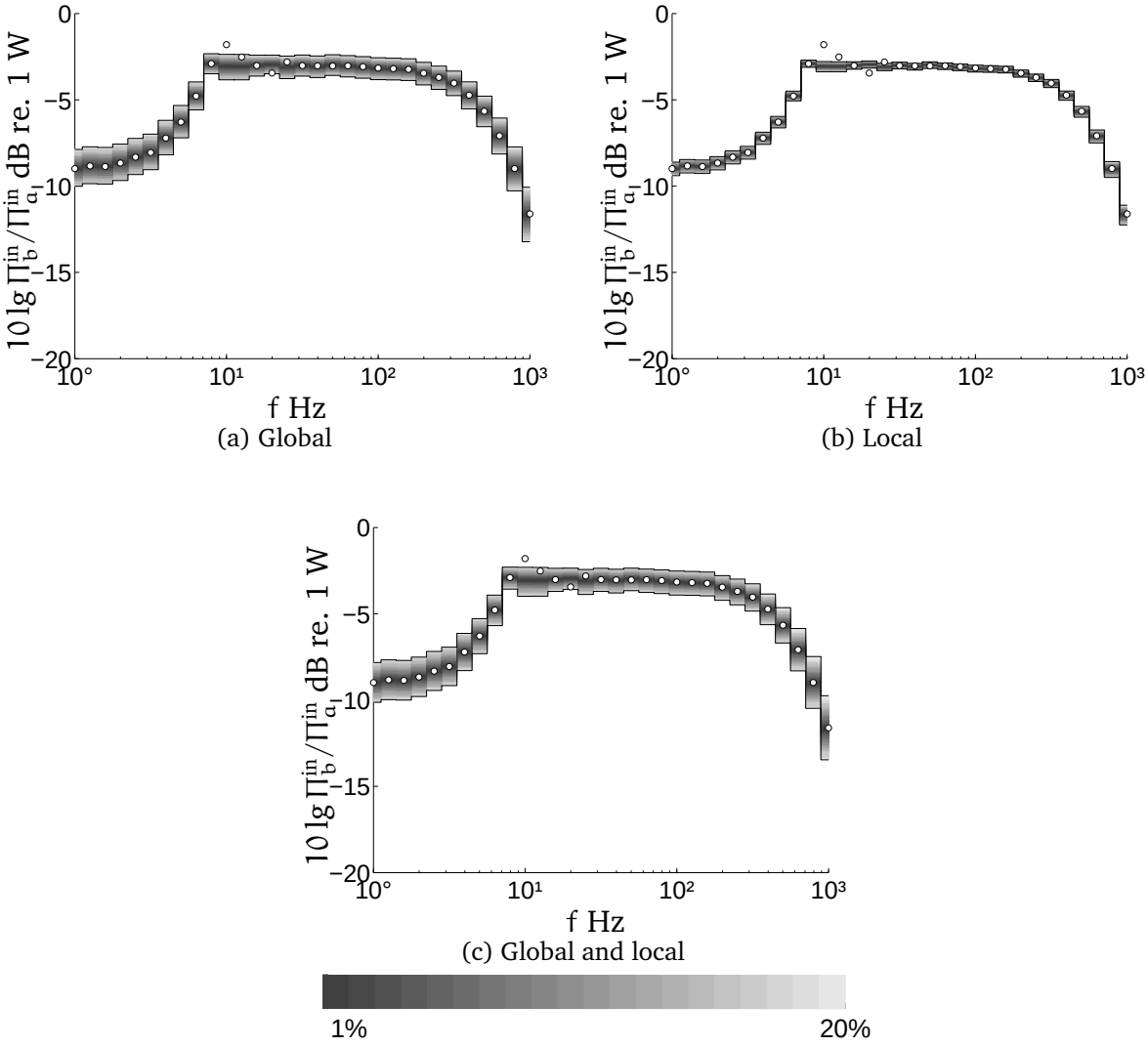

(a) Global

(b) Local

(c) Global and local

Figure 9.9: Estimation of extremal averages of power difference between source and receiver in dB re. 1 W when loss-factor is uncertain. The case of global, local or global and local uncertainty is shown.

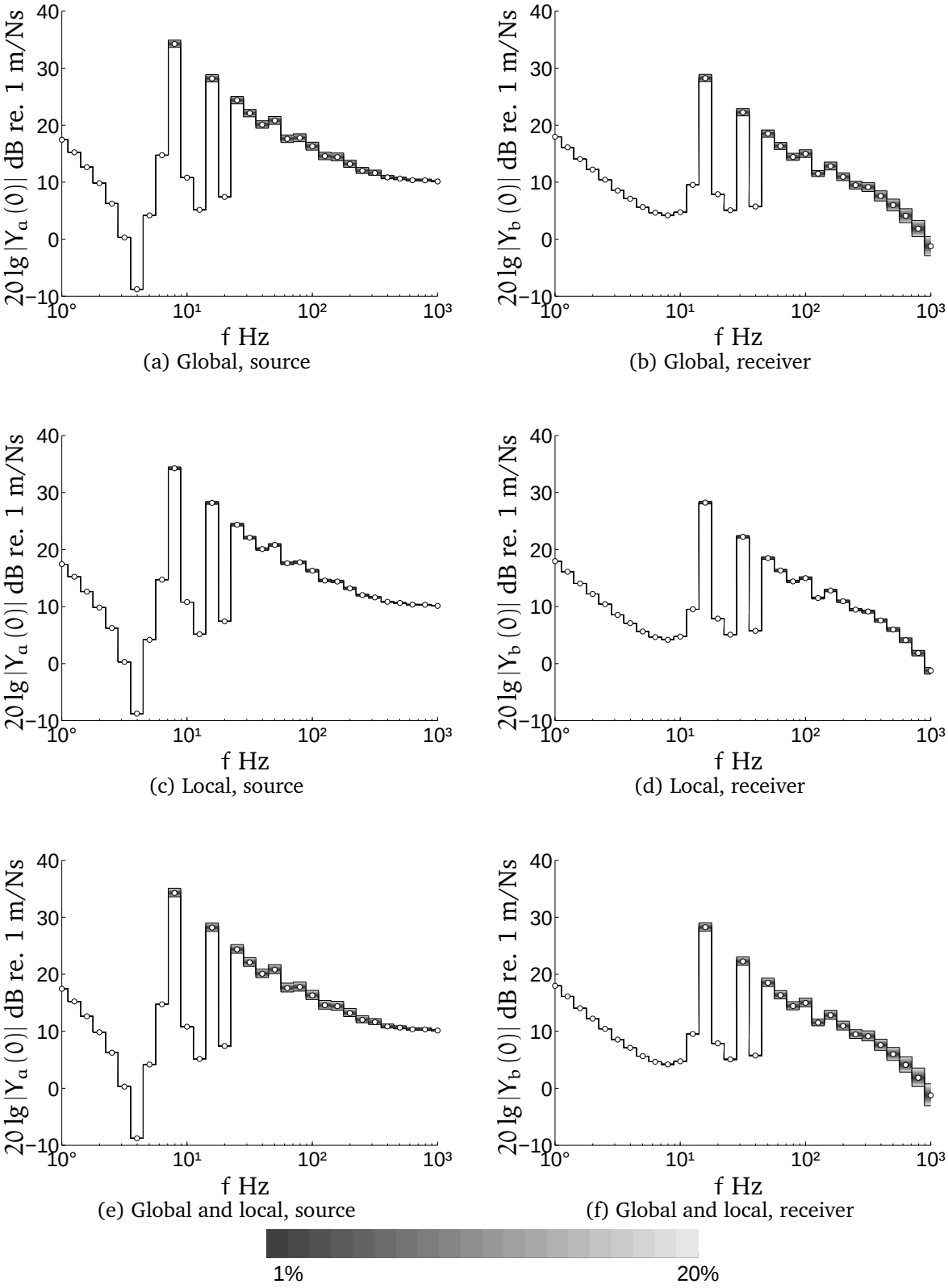

(a) Global, source
(b) Global, receiver
(c) Local, source
(d) Local, receiver
(e) Global and local, source
(f) Global and local, receiver

Figure 9.10: Averages of observed largest and smallest values of driving-point mobilities dB re. 1 for a source and receiver system for the case of loss-factor fluctuation. The case of global, local or global and local uncertainty is shown.

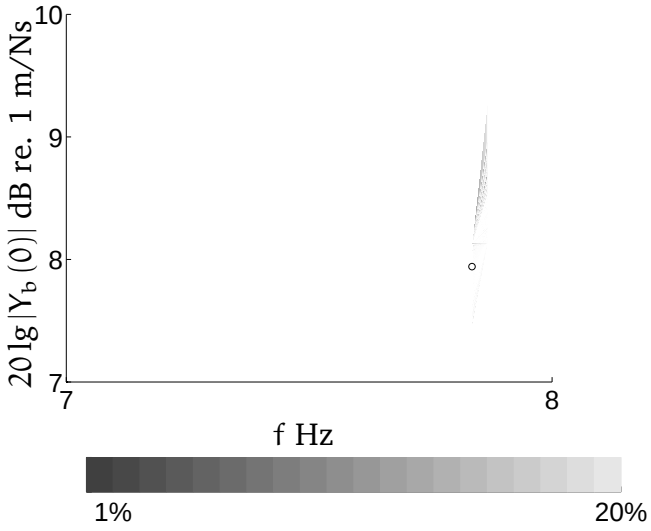

Figure 9.11: Observed spread of the first harmonic for the left end of the receiver system when the loss-factor is fluctuating.

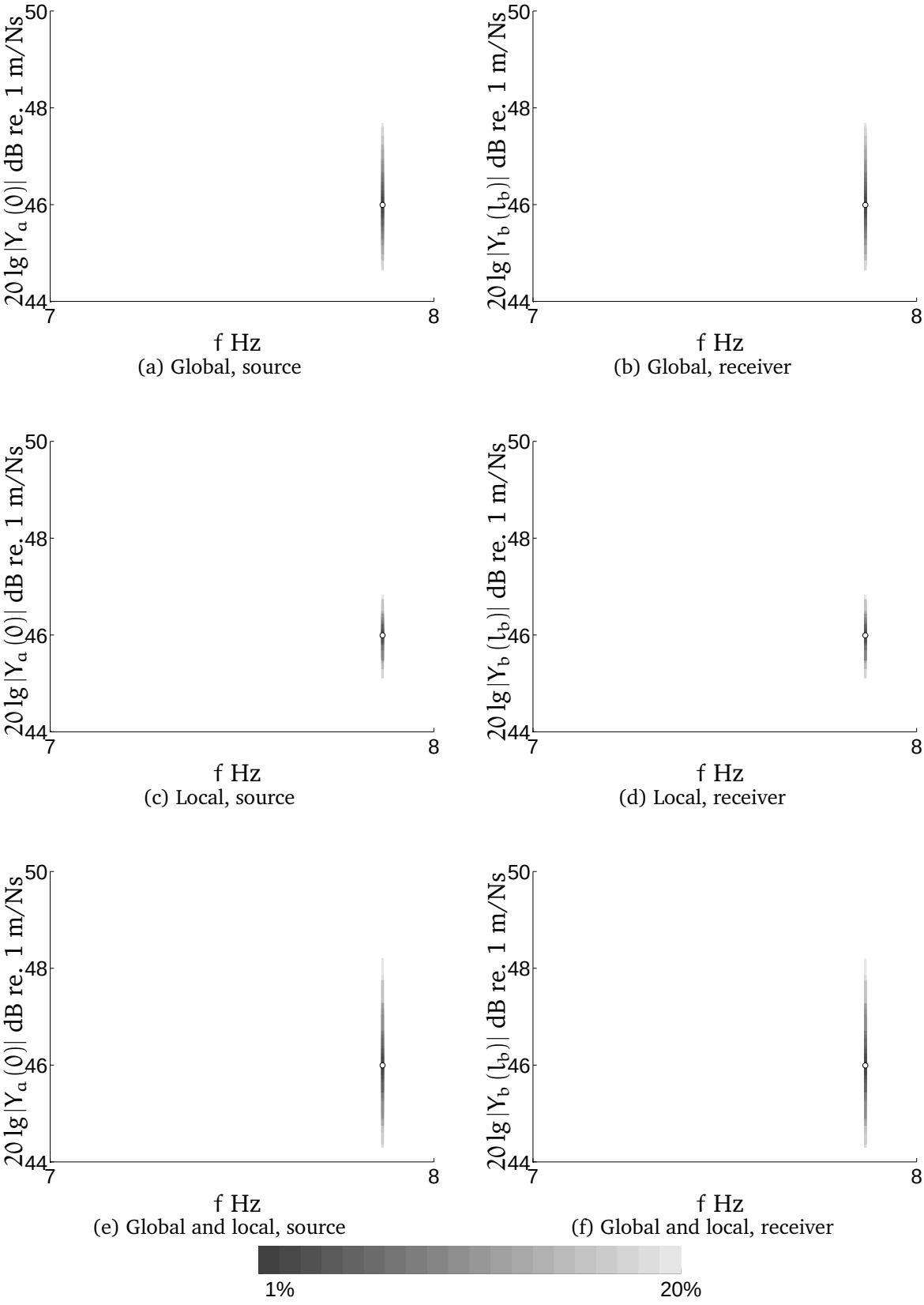

(a) Global, source
(b) Global, receiver
(c) Local, source
(d) Local, receiver
(e) Global and local, source
(f) Global and local, receiver

Figure 9.12: Observed spread of the first harmonic for a source and receiver system where loss-factor is fluctuating. The case of global, local or global and local uncertainty is shown.

3. Geometrical uncertainty

Power transmission between the source and receiver is almost invariant (less than 1.3 dB at 20% magnitude of uncertainty) to global cross-section surface fluctuation, see figure 9.13. In the plateau is the spread as low as 0.1 dB for most octavebands. On the other hand is the spread large for local fluctuation at high frequencies (up to 7.6 dB) and otherwise between 0.4-1.8 dB. The nominal case is observed as the extreme; with negligible exceedence. The power transport tend to decrease with the amount of uncertainty for local fluctuation; the smallest response is 10 dB below the nominal for high frequencies and large amount of fluctuation. This indicates that impedance mismatch between partitions are increasing the energy localization or damping; as the loss-factor is invariant.

The system response, mobility measures at the source and receiver subsystems, show large sensitivity to local cross-section fluctuation at high frequencies, see figure 9.14. The spread is observed to be up to 9.9 dB for the source subsystem, mainly exceeding the nominal response, and 6.7 dB for the receiver, mainly falling below the nominal behavior. Global fluctuation gives an frequency invariant and symmetric response spread (2.7 dB) for the receiver subsystem. The spread is between 0.2 and 7.5 dB for the source subsystem; the spread is due to that cross-section surface scales the magnitudes $Y \sim \frac{1}{S}$ and does not shift the resonance frequency.

No frequency shifting of the fundamental resonance occur for global cross-section uncertainty, see figure 9.15. The response level spread is larger at the source pickup (6.4 dB) than for the receiver pickup (2.7 dB). On the other hand is frequency shifting observed for local fluctuation (up to 0.7 Hz) with lightly lower response level spread (4.9 respectively 2.1 dB). This spread is larger than observed for material or damping uncertainty and due to that the characteristic impedance is linear to cross-section area and not square root of. The shifting of resonance frequency is thought to be due to a change of mode shape. The reason behind this is that as the phase speed and the length of the waveguide is invariant must the change of resonance frequency be due to a non-sinusoidal wave-train closure; considering that the system acts like a rigid beam at low frequencies.

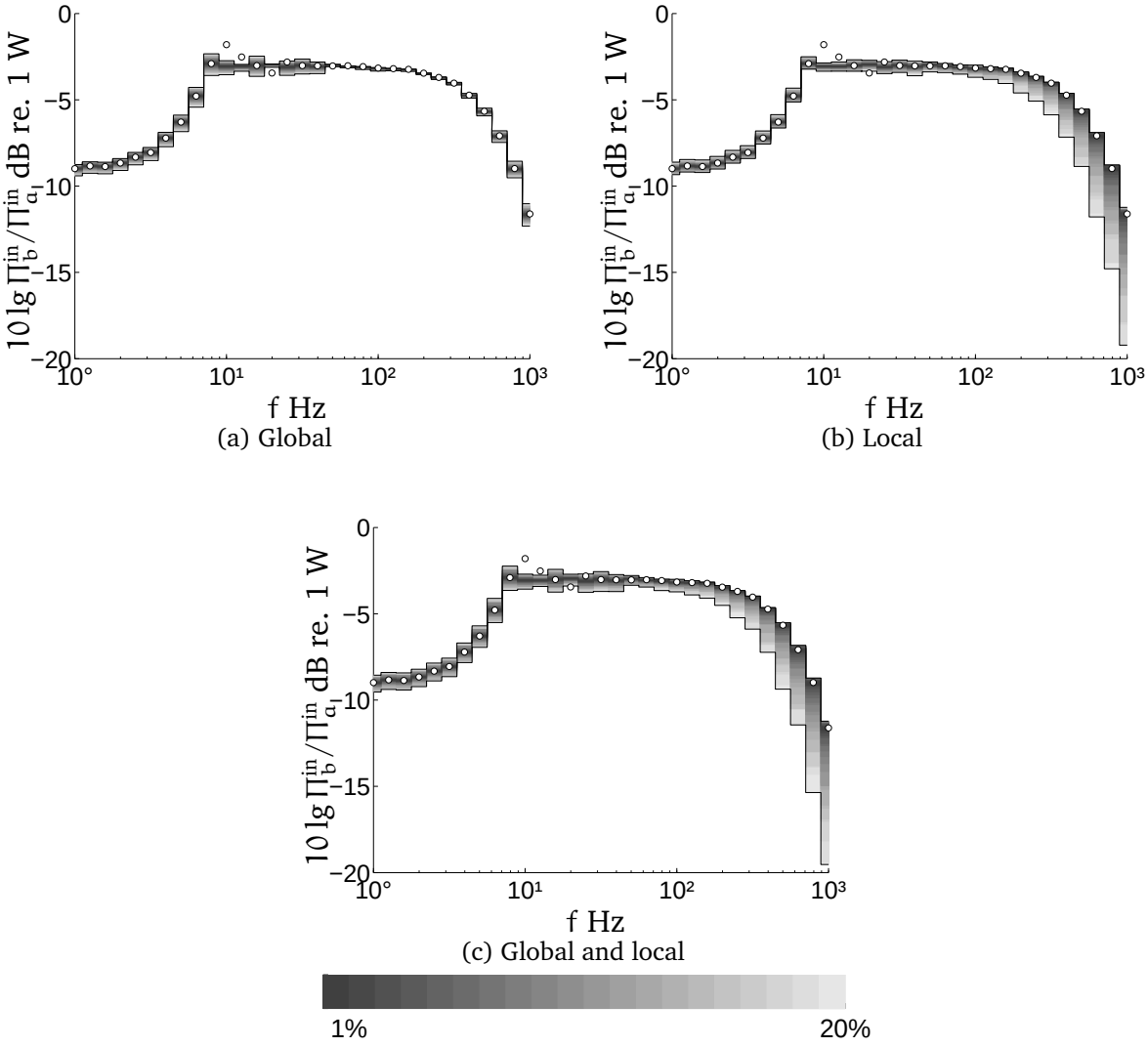

Figure 9.13: Estimation of extremal averages of power difference between source and receiver in dB re. 1 W when cross-section surface is uncertain. The case of global, local or global and local uncertainty is shown.

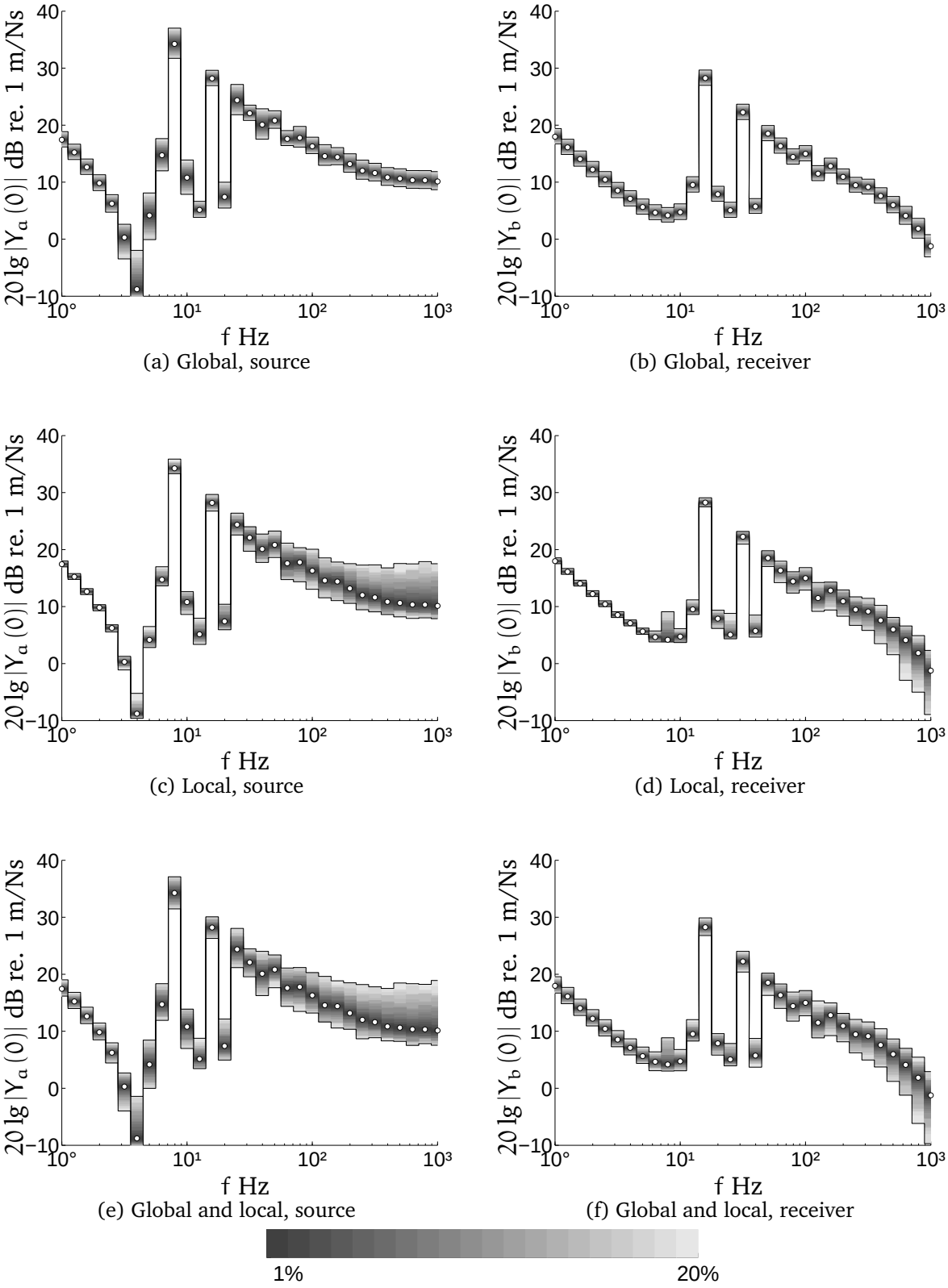

(a) Global, source
(b) Global, receiver
(c) Local, source
(d) Local, receiver
(e) Global and local, source
(f) Global and local, receiver

Figure 9.14: Averages of observed largest and smallest values of driving-point mobilities dB re. 1 for a source and receiver system for the case of cross-section surface fluctuation. The case of global, local or global and local uncertainty is shown.

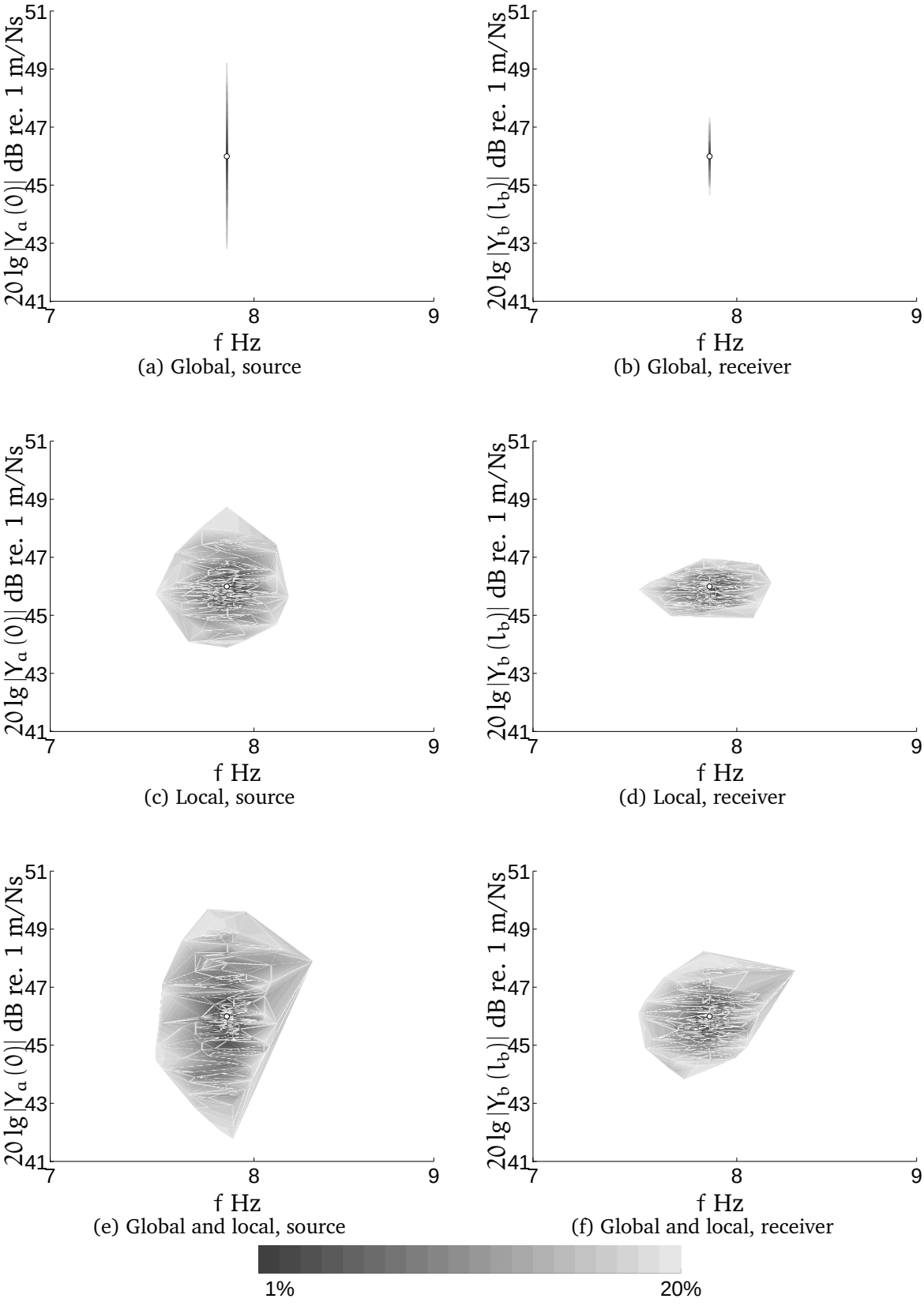

(a) Global, source
(b) Global, receiver
(c) Local, source
(d) Local, receiver
(e) Global and local, source
(f) Global and local, receiver

Figure 9.15: Observed spread of the first harmonic for a source and receiver system where cross-section surface is fluctuating. The case of global, local or global and local uncertainty is shown.

4. Summary

Examining the fundamental resonance of the source and receiver subsystem, it was found that it tend to agree with a mass-spring system; as concluded in the last chapter. The frequency shift is equal for both subsystems (up to 2 Hz, around 25%); while the response level spread is higher for the source subsystem (up to 8 dB). Damping fluctuation is different in that no frequency shifting occur and the response spread is identical both subsystems, see table 9.2. For driving-point mobility data is the response level of the source increased with uncertainty, while the response level of the receiver is decreased; see table 9.1. The largest response level discrepancies compared to the nominal system is observed at low frequencies when the modes are pushed into adjacent one-third octavebands (up to 20 dB). The reason should be an increased impedance mismatch at the coupling causing more wave energy to be reflected back into the source subsystem. This can be seen when the power input difference between the two subsystems are examined, see 9.3. The nominal system is the worst-case with good transmission between the subsystems, which results in that increased uncertainty lowers the transmission.

			$f < f_0^{nom}$	$f \sim f_0^{nom}$	$f > f_0^{nom}$	$f \gg f_0^{nom}$
			1 - 5 Hz	6.3 - 10 Hz	12.5 - 50 Hz	63 - 1000 Hz
ρ	Global	Src.	2.6-6.0	3.0-13.8	1.7-17.9	3.8-1.7, dec. with fre.
		Rec.	2.3-2.6	5.9-13.4	1.8-11.7	2.2-3.9
	Local	Src.	1.0-2.8	1.2-4.7, high adjacent to f_0^{nom}	1.4-6.4	3.0-5.0
		Rec.	0.9-1.2	2.4-6.5, high around f_0^{nom}	0.9-6.3	1.9-3.9
	Both	Src.	0.7-6.4	3.9-17.8	2.3-18.0	4.0-5.4
		Rec.	2.4-2.7	5.5-13.1	2.1-13.6	2.2-4.8
E	Global	Src.	0.2-8.1	2.5-11.9	0.6-19.4	1.4-2.9
		Rec.	0.1-2.1	6.0-13.1	0.6-13.0	1.1-2.8
	Local	Src.	0.0-2.7	0.9-3.8	1.4-9.0	3.0-5.0
		Rec.	0.0-0.7	2.0-5.0	0.7-5.7	1.7-3.8
	Both	Src.	0.2-8.0	2.7-14.2	1.4-20.3	3.7-5.4
		Rec.	0.1-2.5	6.7-14.1	0.9-13.7	1.7-3.9
η	Global	Src.	0.0, no spread	0.0-1.3, high around f_0^{nom}	0.0-1.4	0.2-1.4, spread dec. with freq.
		Rec.	0.0, no spread	0.0-0.2	0.0-1.3	1.0-2.9, spread inc. with freq.
	Local	Src.	0.0, no spread	0.0-0.5, high around f_0^{nom}	0.0-0.5	0.4-0.1, spread dec. with freq.
		Rec.	0.0, no spread	0.0-0.1	0.0-0.5	0.4-1.2, spread inc. with freq.
	Both	Src.	0.0, no spread	0.0-1.5	0.0-1.5	1.6-0.3, spread dec. with freq.
		Rec.	0.0, no spread	0.0-0.2	0.0-1.5	1.2-3.2, no freq. dep.
S	Global	Src.	0.2-7.5	5.0-5.7	2.7-5.0	2.6-3.6
		Rec.	2.7	2.5-2.7	2.6-2.7	2.7-3.5 (only at 800 Hz)
	Local	Src.	0.1-4.1	2.5-4.0	2.3-4.9	5.5-9.9
		Rec.	1.0-1.1	1.6-4.8	1.5-3.9	0.5 (only at 800 Hz) - 6.8
	Both	Src.	1.1-8.3	5.4-6.8	3.5-7.2	6.5-11.4
		Rec.	2.8-2.9	2.8-3.6	3.2-4.0	0.4 (only at 630) - 13.3

Table 9.1: A brief summary of spread on octavebands driving-point mobility data due to different kind of uncertainty. Smallest and largest spread between averages are given in dB for the case of $\pm 20\%$ of uncertainty.

		Δf Hz		ΔL dB	
		Src.	Rec.	Src.	Rec.
ρ	Global	1.5	1.5	4.0	2.1
	Local	0.9	0.9	2.5	1.4
	Both	1.6	1.6	5.0	2.5
E	Global	1.4	1.4	3.8	2.0
	Local	0.9	0.9	2.4	1.3
	Both	1.7	1.7	4.5	2.3
η	Global	0.0	0.0	3.0	3.0
	Local	0.0	0.0	1.7	1.7
	Both	0.0	0.0	3.9	3.9
S	Global	0.0	0.0	6.4	2.7
	Local	0.7	0.7	4.9	2.1
	Both	0.8	0.8	7.9	4.4

Table 9.2: A brief summary of spread on the fundamental resonance due to different kind of uncertainty for a source and receiver system. The spread between the largest of largest and smallest of smallest observed response level and resonance frequency is given for the case of $\pm 20\%$ of uncertainty.

		Mass	Plateau	Decay	
ρ	Global	1.2-1.7, freq. inc. spread dec.	0.3-1.2	0.9-2.0	Sym.
	Local	0.6-0.7	0.2-0.7	1.0-2.7	Sym., nom. worst case
	Both	1.6-1.4	0.3-1.3	1.3-3.8, freq. inc. spread inc.	
E	Global	2.1, const.	0.2-2.0	0.8-1.4	
	Local	0.7, const.	0.3-0.7	0.8-2.6, freq. inc. spread inc.	
	Both	2.4, const.	0.4-2.1	1.2-3.4	
η	Global	2.1-1.6	1.2-1.5	1.5-3.2	
	Local	0.8-0.4	0.6-0.4	0.5-1.1	
	Both	2.2-1.7	1.1-1.6	1.8-3.7	
S	Global	0.6-1.1	0.1-1.0	0.4-1.3	
	Local	0.6-0.8	0.4-1.8	3.1-7.6	
	Both	1.0-1.4	0.6-1.6	2.4-8.1	

Table 9.3: A brief summary of spread on input power difference between source and receiver system due to different kind of uncertainty.

Part 4

A Posteriori

CHAPTER 10

Conclusions

Vibroacoustic prediction of complex structures are uncertain in nature, due to modeling difficulties of precise endogenous boundary, material and geometrical properties.

In this report two nominal system were subject to different kind and magnitude of partial endogenous uncertainty. Partial uncertainty of endogenous parameters in the nominal source system was examined in order to understand how different parameters influence the response. Effects of global uncertainty conform to the behavior of a mass-spring system at low-frequency resonances. Global uncertainty is of importance at low-frequencies where shifting or scaling of an individual mode effects the overall one-third octaveband response. Damping uncertainty had the biggest effect on the response level of individual resonances, but as no shifting occurs the overall response change was negligible. Material uncertainty which shifts the individual resonances gave the largest response spread. On the other hand, for local uncertainty, which is more pronounced at higher frequencies and primarily due to impedance mismatch, geometrical uncertainty was of main interest.

The nominal source and receiver system was chosen to represent a deterministic extreme, where power transmission between the subsystems where as good as possible. However; the results indicate that an increase of magnitude of uncertainty only conform to poorer transmission from the source to the receiver around the fundamental resonance. Considering mobility type response, the source system response level increased with the magnitude of uncertainty and large excesses was observed compared to the nominal system. Especially; for cases where global uncertainty of material or geometrical properties result in frequency shifting. The receiver subsystem response level decreased in response level.

The primary aim of the work was to investigate a generally formulated hypothesis. Nothing in the outcome of the model indicates that the hypothesis is false. The results agree with the statement that inherent uncertainty of small-scale structural details explains extremal structural response. Hence; endogenous uncertainty should be incorporated in the modeling if ensemble extremal response is of interest.

CHAPTER 11

Discussion

Worst-case structural response is a sophisticated problem. Formulated in form of a hypothesis, it was carefully investigated for the case of a beam and a beam-spring-beam system. The idea of defining a filtration with initial values, expectancy functions and perturbation functions to describe a structure resulted in a straight forward approach to incorporate various kind and amount of endogenous or exogenous uncertainty in the model. However; only aleatory phenomenon was modeled while epistemic uncertainty was neglected.

In order to properly assess the worst-case response of a dynamic system, one should consider the definition of "worst". Most likely, not only is the ensemble largest response of interest, one would also want to output the worst realization in an ensemble. In order to select the observed worst-case response in an ensemble of transfer functions proper penalty functions must be designed; here, a penalty function is a rule which rank responses from functional criteria. Depending on whether a problem is related to wideband, narrowband or tonal characteristics different penalty functions and realizations will be selected as worst. Granted a good penalty function silent or noisy realizations can be studied and the endogenous information be used to develop a theory of worst-case response. Perhaps one could even manufacture for example fluctuation of density inside a solid to increase damping or altering radiated noise in other ways; given that knowledge of a good pattern exists.

Deterministic modeling of longitudinal wave propagation in one-dimensional subsystems was done via a traveling waves approach. The subsystem properties were discretized while the vibrational field was kept continuous. The solution is therefore in some sense exact; but, the discretization was based on piecewise homogeneous partitions. It can be expected that the approach is inexact if adjacent partitions differ to much from each other. Therefore, a high spatial frequency was used; partition resonances are avoided and properties of adjacent partitions can be expected to be similar. However; in wooden beams can for example a saw cut represent a sudden and discrete change. Wooden beams represent a material where density fluctuation is expected; it could occur as inherent changes in the wood or by sudden and randomly positioned spikes.

Derivation of the deterministic model was different from other models I worked with. In reality, a freely suspended beam was derived. The homogeneous beam was then discretized and derived for the case of one, two and three endogenous junctions. In the derived matrices a pattern was seen in the position of the boundary condition elements. This knowledge allowed me to describe where an endogenous junction is applied for an arbitrary amount of partitions. The model was then extended by looking at the case of one, two and three homogeneous subsystems. Once again, a geometric pattern in the matrices could be seen and a description of where in a matrix an element belonged could be derived.

Emphasize on the numerical findings was on different properties of structures and how robust they are to uncertainty; this is the reason why I presented the overall picture of how and why a parameter uncertainty effects a nominal system rather then the precise disturbance in dB and Hz. As a first step in understanding structural uncertainty focus in this thesis was on a “nominal worst-case system”; the source and receiver subsystem is self-similar. Hence; the modes are similar and power transport should be simplified between the subsystems. This was seen in the results as the power flow between the systems went below the nominal behavior. The subsystems behavior was examined carefully as a freely suspended beam before the coupled case was presented. Therefore; an important future work would be to conclude from acquired data and to develop a theory of how and why a realization deviate from a nominal structure. A natural second step would be to run simulations with subsystems that are not similar and see how they react to uncertainty.

One of the more interesting results was the frequency shift due to local uncertainty. When material change inside of a beam, my initial thought was that the observed damping should increase; due to energy localization in local resonances. This phenomenon was not observed, but only the beam end-points was used as pick-up points. On the other hand was the frequency shift more unexpected, and a hypothesis is that it is due to a change of mode shape; however examining this effect requires further work. Another interesting observation was the high sensitivity of power flow due to low magnitude of uncertainty around the fundamental resonance. In other words is power transmission changed between 0% and 1% magnitude of uncertainty, which was not examined in this thesis.

An area of research that was not explored in this thesis is multiple sources of uncertainty, for example cross-section and density fluctuation. Perhaps, one can distinguish the different sources from the transfer functions. If a backward process is possible, one could explore eigenfrequencies of a real structural ensemble to see what kind of uncertainties are present; an experiment on wooden beams should be expected to indicate density uncertainty.

Another problem which was not discussed in this thesis is to estimate prediction confidence of the worst-case measure and the expected number of exceedences of the worst response. As the worst response is a statistical measure and not an absolute measure, there will be structures which exceed the predicted worst-case level. It would be interesting to understand the expected amount of exceedences in an ensemble given an estimated worst-case response.

Finally; structural uncertainty is not limited to endogenous properties. In modeling epistemic uncertainty is a necessity, as a model describing all phenomenon is not feasible. Validation of a model is nearly impossible as the structural filtration demands a good statistical description of material, geometrical and exogenous properties. Therefore; the model itself should be examined from a robustness perspective.

1. Suggested future work

There are at least four different areas where there is room for improvement. The deterministic model as presented in this thesis is limited to a narrow range of filtrations and utilizes piecewise homogeneous beams. The model could be extended to:

(1) Spatial sampling. The partitions could be derived with linear or higher polynomial interpolation.
(2) Excitation. Arbitrary point or line excitation of subsystems. Exogenous uncertainty such as random excitation could then be examined.
(3) Impedance junctions. Arbitrary and multiple couplings between subsystems. This would allow for a network rather than a chain of beams to be investigated.
(4) Modes. Disordered beams using Euler-Bernoulli theory or other equation of motions would allow for models with coupling between wave energies inside the same subsystem and between subsystems.

The stochastic modeling was done by uniform distributions and Markov random walks. However; the generation mechanisms were not examined in detail and there are many alternative ways to render subsystems. Hence, suggested future work would be:

(1) Evaluation of different stochastic processes and/or statistical distributions as generation mechanisms of material, geometry and boundary values.
(2) Continued evaluation of effects from and modeling of global and local endogenous structural uncertainty.

In addition to developing the model, validation is necessary. Numerical validation could be to compare SEA results with ensemble average response of the model. Experimental result would be possible on driving-point measurements of wooden beams, if the endogenous uncertainty can be described. Finally; in the long run it would be interesting to conclude on acquired data and develop a theory of when and why some structures or structural parts get increased response levels.

References

[1] W.G. Price A.J. Keane. *Statistical Energy Analysis - An Overview, With Applications in Structural Dynamics*. Cambridge University Press, 1997.

[2] F.J. Fahy. Statistical energy analysis: a critical overview. In W.G. Price A.J. Keane, editor, *Statistical Energy Analysis - An Overview, With Applications in Structural Dynamics*. Cambridge University Press, 1997.

[3] K. Marti et. al. Coping with uncertainty - modeling and policy issues. 2006.

[4] Y. Ben-Haim I. Takewaki. Info-gap robust design with load and model uncertainties. *Journal of Sound and Vibration*, 2005.

[5] S. Donders et. al. Assessment of uncertainty on structural dynamic responses with the short transformation method. *Journal of Sound and Vibration*, 2005.

[6] M.C. Lovell et. al. Physical properties of materials. 1976.

[7] J. Náprstek. Wave propagation in semi-infinite bar with random imperfections of density and elasticity module. *Journal of Sound and Vibration*, 2007.

[8] S. Russ B. Sapoval, O. Haeberlé. Acoustical properties of irregular and fractal cavities. *Acoustical Society of America*, 1997.

[9] J.F. Durand et. al. Structural-acoustic modeling of automotive vehicles in presence of uncertainties and experimental identification and validation. *Journal of Sound and Vibration*, 2008.

[10] E. Capiez-Lernout et. al. Data and model uncertainties in complex aerospace engineering systems. *Journal of Sound and Vibration*, 2006.

[11] P. Weinachter T. Loyau. Experimental study of vibration response dispersion between structures. *Journal of Sound and Vibration*, 1997.

[12] S.W. Smith. *The Scientist and Engineer's Guide to Digital Signal Processing*. California Technical Pub, 1997.

[13] F.C. Klebaner. *Introduction to Stochastic Calculus with applications, 2ED*. Imperial College Press, 2007.

[14] H.C. Tijms. *A first course in stochastic models*. John Wiley & Sons, 2003.

[15] L. Cremer M. Heckl E.E. Ungar. *Structure-Borne Sound*. Springer-Verlag Berlin Heidelberg New York, 1973.

[16] W. Kropp. Technical acoustics 1 - lecture 4. Department of Civil and Environmental Engineering, Division of Applied Acoustics, Chalmers University of Technology, 2007. Course compendium.

[17] W. Kropp. Technical acoustics 1 - lecture 7. Department of Civil and Environmental Engineering, Division of Applied Acoustics, Chalmers University of Technology, 2007. Course compendium.

[18] K.S. Peat. The acoustical impedance at the junction of an extended inlet or outlet duct. *Journal of Sound and Vibration*, 1991.

[19] E. Billauer. peakdet: Peak detection using matlab. http://www.billauer.co.il/peakdet.html, Sep 2008.

[20] B.R. Mace. Power flow between two continuous one-dimensional subsystems: A wave solution. *Journal of Sound and Vibration*, 1992.

[21] W. Kropp P. Andersson. Introduction to sound and vibration - lecture 1. Department of Civil and Environmental Engineering, Division of Applied Acoustics, Chalmers University of Technology, 2009. Course compendium.

Part 5

Appendix

APPENDIX A

Mass-spring system

Effects due to global uncertainty in a homogenous beam can be understood by comparison to a mass-spring system, see figure A.1.

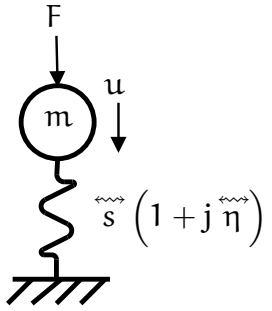

Figure A.1: A damped mass-spring system.

The motion is described by a integral-differential equation on the form

$$m\frac{\partial u}{\partial t}+\overleftrightarrow{s}\left(1+j\overleftrightarrow{\eta}\right)\int u\partial t=F, \tag{A.1}$$

which is a force balance of the system. Under an assumption of harmonic excitation $F=\underline{F}e^{+j\omega t}$, should the forced system react with a harmonic motion $u=\underline{u}e^{+j\omega t}$ where $\underline{F}$ and $\underline{u}$ is complex amplitudes. Inserting the ansatz into the equation of motion results in

$$\left(j\omega m+\frac{1}{j\omega}\overleftrightarrow{s}\left(1+j\overleftrightarrow{\eta}\right)\right)\underline{u}=\underline{F}. \tag{A.2}$$

The resonance frequency occurs at $\omega_0=\pm\sqrt{\frac{\overleftrightarrow{s}}{m}}\sqrt{\left(1+j\overleftrightarrow{\eta}\right)}$. A complex resonance frequency results in damping in the time domain; which can be seen if the expression is inserted into the velocity ansatz. To compute the mobility response level at the resonance frequency is the expression above rewritten by seperating effects of the real and imaginary part of the frequency

$$\omega_0=\pm\sqrt{\frac{\overleftrightarrow{s}}{m}}\left(\sqrt{\frac{\sqrt{1+\overleftrightarrow{\eta}^2}+1}{2}}+j\sqrt{\frac{\sqrt{1+\overleftrightarrow{\eta}^2}-1}{2}}\right). \tag{A.3}$$

	$E\uparrow$	$\rho\uparrow$	$S\uparrow$	$\eta\uparrow$	$l\uparrow$
ω_0	$\uparrow$	$\downarrow$	-	-	$\downarrow$
$\lvert Y_0\rvert$	$\downarrow$	$\downarrow$	$\downarrow$	$\downarrow$	-

Table A.1: Effects on resonance frequency and response level of a longitudinal rod when material or geometrical parameters are changed.

Normalized response magnitude of the damped system is then given by

$$|Y(\omega)|^2 = \frac{1}{\left(+\omega' m - \frac{\overleftrightarrow{s}\,\omega'}{|\omega|^2} - \frac{\overleftrightarrow{s}\,\overleftrightarrow{\eta}\,\omega''}{|\omega|^2}\right)^2 + \left(-\omega'' m - \frac{\overleftrightarrow{s}\,\omega''}{|\omega|^2} + \frac{\overleftrightarrow{s}\,\overleftrightarrow{\eta}\,\omega'}{|\omega|^2}\right)^2}. \tag{A.4}$$

Evaluated for a small loss factor $\overleftrightarrow{\eta} \ll 1$ it can be seen that the complex part of the resonance frequency is much smaller then the real part; and that the real part ω' and magnitude $|\omega|$ is close to $\sqrt{\frac{\overleftrightarrow{s}}{m}}$. The mobility can therefore be approximated as $|Y_0| = \frac{\omega_0{}'}{\overleftrightarrow{s}\,\overleftrightarrow{\eta}}$. Hence, an increased eigenfrequency $\omega_0{}'$ correspond to a increase in response level while a stiffer or more damped system reduce the response level.

The behavior at resonance of a longitudinal rod can be estimated by inserting $\overleftrightarrow{s} = \frac{ES}{l}$, $\overleftrightarrow{\eta} = \eta$ and $m = \rho S l$. The eigenfrequency is given by $\omega_0 = \frac{1}{l}\sqrt{\frac{E}{\rho}}$, and the magnitude of the driving point mobility is $|Y_0| = \frac{1}{S\sqrt{E\rho\eta}}$. Effect on the resonance due to material or geometrical change in the longitudinal rod is summarized in table A.1.

APPENDIX B

Longitudinal beam

In order to validate the model was an analytical solution for the case of an homogenous freely suspended beam derived, see figure B.1. Using a wave approach as described in the thesis, can the linear system equation $\mathbf{X}^{T}a = \underset{\sim}{B}$ be written as

$$\begin{bmatrix} Z & -Z \\ Z\,e^{-j\,kl} & -Z\,e^{+j\,kl} \end{bmatrix} \begin{bmatrix} a^{+} \\ a^{-} \end{bmatrix} = \begin{bmatrix} -\underline{F}^{in} \\ 0 \end{bmatrix}. \tag{B.1}$$

The system is excited by a time harmonic force $F^{in} = \underline{F}^{in}\,e^{+j\,\omega t}$ at the left end. Due to damping in the beam is $k, Z \in \mathbb{C}$. The first step in the solution is to find the system determinant

$$\det\left(\mathbf{X}^{T}\right) = Z^{2}\left(e^{-j\,kl} - e^{+j\,kl}\right) \tag{B.2}$$

$$= -2\,j\,Z^{2}\sin\left(kl\right) \tag{B.3}$$

System eigenfrequencies can be found by $\det\left(\mathbf{X}^{T}\right) = 0$; the equation can be formulated as

$$\sin\left(kl\right) = 0, \tag{B.4}$$

which has the solution $kl = \pi n$ which gives the eigenvalues and eigenfrequencies

$$k_{n} = n\frac{\pi}{l},\, f_{n} = n\frac{c}{2l}. \tag{B.5}$$

The modal density for longitudinal waves in beam can be expressed as

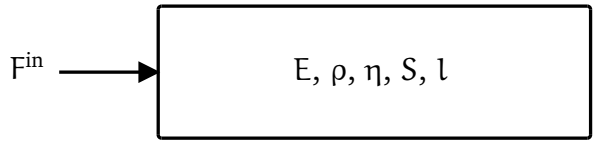

Figure B.1: A freely suspended beam.

$$\frac{\Delta n}{\Delta \omega} = \frac{l}{\pi c}. \tag{B.6}$$

Solving the system equation as described above is the forth and backward traveling wave amplitudes found to be

$$a^+ = \frac{\underline{F}^{in}}{Z} \frac{e^{+j\,kl}}{e^{-j\,kl} - e^{+j\,kl}}, a^- = \frac{\underline{F}^{in}}{Z} \frac{e^{-j\,kl}}{e^{-j\,kl} - e^{+j\,kl}}. \tag{B.7}$$

Inserting the wave amplitudes into the ansatz it is found that

$$u = j\frac{\underline{F}^{in}}{Z} \frac{\cos\left(k\left(x-l\right)\right)}{\sin\left(kl\right)}, F = \underline{F}^{in} \frac{\sin\left(k\left(x-l\right)\right)}{\sin\left(kl\right)}. \tag{B.8}$$

Driving point mobility can be written as

$$Y = \frac{j}{Z} \cot\left(k\left(x-l\right)\right). \tag{B.9}$$

Power flow at a point inside of the beam can be computed from $\Pi = 0.5\Re\{F\bar{u}\}$. An effect that can explain poor transmission at high frequencies is distance attenuation, for a wave propagating in a infinite beam can the attenuation be estimated as $\Delta L = 4.35kl\Delta x$.